ABSTRACT

A Stepwise Approach to Understanding Nanomaterial
Transformations Under Situationally Relevant Conditions

Marina Rochelle Mulenos George, Ph.D.

Mentor: Christie M. Sayes, Ph.D.

Given the increasing use of nanomaterials in various consumer products and industrial processes, it is of the utmost importance to better understand potential mechanisms of adverse effects to ensure human health and safety when developing regulations and standard operating procedure with newly developed materials, like nanomaterials. Nanomaterials are materials with one or more dimensions in the nanoscale range that are produced to advance industrial processes, used as an additive in consumer products, and produce novel drug delivery carriers. Standardized toxicological studies focus on newly produced nanomaterial products before they reach the market; however, most of these studies exclusively investigate pristine engineered nanomaterials. The issue with testing pristine engineered nanomaterials is that most environmental and/or human toxicities are induced after nanomaterials undergo transformations, e.g. release of metal ions. The goal of this dissertation was to conduct a comprehensive study of increasingly complex situationally relevant environments on organic and inorganic nanomaterials to understand important insights into nanomaterial transformations and the associated

toxicity after exposures *in vitro*. Situationally relevant conditions occur when nanomaterials are used in products or processes and interact with the surrounding environment, where they then may undergo transformations. These transformations may include distribution with biomolecules or natural organic matter, lipid membranes in cells, high ionic conditions, or changes in temperature, salt concentration, etc. In this study, important physicochemical characterization methods were established for organic and inorganic nanomaterials. Additionally, these nanomaterials were transformed under simulated conditions and examined in increasingly complex environments. Next, the transformed nanomaterials were incubated with an established *in vitro* liver model to elucidate the relationship between nanomaterial transformations and the associated toxicity after exposure. Finally, transformed nanomaterials were exposed to an *in vitro* model for steroidogenic disruption to investigate further into adverse effects nanomaterial transformations may have on human health. Ultimately, the aim of this work is to advance the field of toxicology by improving our understanding of nanomaterial transformation mechanisms and to aid in risk assessment and regulations.

A Stepwise Approach to Understanding Nanomaterial Transformations Under Situationally Relevant Conditions

by

Marina Rochelle Mulenos George, B.S.

A Dissertation

Approved by the Department of Environmental Science

_____

George Cobb, Ph.D., Chairperson

Submitted to the Graduate Faculty of
Baylor University in Partial Fulfillment of the
Requirements for the Degree
of

Doctor of Philosophy

Approved by the Dissertation Committee

_____

Christie Sayes, Ph.D., Chairperson

_____

Erica Bruce, Ph.D.

_____

George Cobb, Ph.D.

_____

Virender Sharma, Ph.D.

_____

Bernd Zechmann, Ph.D.

Accepted by the Graduate School

May 2021

_____

J. Larry Lyon, Ph.D., Dean

Page bearing signatures is kept on file in the Graduate School.

TABLE OF CONTENTS

LIST OF FIGURES

LIST OF TABLES

ACKNOWLEDGMENTS

First, I would like to thank my advisor Professor Christie Sayes for her continued support and guidance she provided throughout my time at Baylor University. All of the opportunities provided and freedom to explore my scientific curiosity have been a critical part of my scientific development today, and I would not be here without her. In addition, I would like to thank the rest of my committee: Dr. Erica Bruce, Dr. George Cobb, Dr. Virender Sharma, and Dr. Bernd Zechmann for encouragement and inspiration to push my research to new heights. My sincerest thanks also go out to Dr. Saber Hussain, the Oak Ridge Institute for Science and Education, and the Air Force Research Labs who provided me an opportunity as a summer intern and for giving access to laboratory and research facilities. I would also like to thank my fellow lab mates and undergraduate students for their camaraderie and support. Lastly, I would like to recognize the love and support from my family and friends for their unwavering support throughout my years in school.

DEDICATION

To my grandfather, Jerry Mulenos. With your love, support, and unwavering dedication and persistence, I was able to accomplish feats I never dreamed of on my own.

To my boyfriend, Henry Lujan, for his perseverance and dedication to support me and my research always.

ATTRIBUTIONS

Chapter 1:

Marina R Mulenos- Conceptualization, methodology, validation, formal analysis, investigation, writing- original draft preparation, writing- review and editing, visualization

Bernd Zechmann- Conceptualization, methodology, writing- review and editing

Christie M Sayes- Formal analysis, writing- original draft preparation, writing- review and editing, visualization, supervision, project administration

Chapter 2:

Marina R Mulenos- Methodology, formal analysis, writing- original draft preparation, writing- review and editing, visualization, supervision, project administration

Jiaqi Liu- validation, investigation, writing- original draft preparation, writing- review and editing

Henry Lujan- validation, investigation, writing- original draft preparation

Binglin Guo- validation, investigation, writing- original draft preparation

Eric Lichtfouse- writing- review and editing

Virender K Sharma- Conceptualization, formal analysis, writing- original draft preparation, writing- review and editing, visualization, supervision, project administration

Christie M Sayes- Conceptualization, formal analysis, writing- original draft preparation, writing- review and editing, visualization, supervision, project administration

Chapter 3:

Marina R Mulenos- Methodology, validation, formal analysis, investigation, writing- original draft preparation, writing- review and editing, visualization

Henry Lujan- Validation, investigation, writing- original draft preparation

Lauren R. Pitts- Validation, investigation, writing- original draft preparation

Christie M Sayes- Conceptualization, formal analysis, writing- original draft preparation, writing- review and editing, visualization, supervision, project administration

Chapter 4:

Marina R Mulenos- Conceptualization, methodology, validation, formal analysis, investigation, writing- original draft preparation, writing- review and editing, visualization

Henry Lujan- Methodology, formal analysis, validation, investigation, writing- original draft preparation

Bernd Zechmann- Methodology, investigation, visualization

Christie M Sayes- Conceptualization, formal analysis, writing- original draft preparation, writing- review and editing, visualization, supervision, project administration

CHAPTER ONE

Advanced Techniques to Characterize Notoriously Difficult Nanomaterials

This chapter published as: Mulenos, M. R., Zechmann, B., & Sayes, C. M. (2019). Sample preparation utilizing sputter coating increases contrast of cellulose nanocrystals in the transmission electron microscope. Microscopy, 68(6), 471-474.

Abstract

Cellulose Nanocrystals (CNC) are utilized due to their unique properties which advance the food industry as a food additive, are used in consumer products like cosmetics, and in the paper and mill industry. Cellulose as a bulk material is anticipated to be safe; however, there is controversy regarding CNC since it is the first manufactured nanoscale form of cellulose. When new materials are engineered, it is of utmost importance to complete full physicochemical characterizations to understand the potential mechanisms of adverse effects and to ensure health and safety when developing regulations and standard operating procedure with newly developed materials. To understand this, a complete chemical and physical assessment of CNC via a battery of analytical methods was employed. Some of the important characteristics probed in this study include CNC morphology at the micro and nano-scale, crystallinity, metal impurity, length and width survey, elemental composition, polydispersity index, hydrodynamic diameter, and surface charge. CNC are known to be difficult to complete a full physicochemical characterization due to their organic composition, so a new method for morphological characterization using transmission electron microscopy was created. To decrease artifacts and aggregation, sputter-coating at a 5 nm thickness of either carbon,

iridium, gold, or titanium was used to coat CNC before imaging. The thin layer of conductive metal atoms deposited onto the specimen surface significantly increased contrast and improved image quality. Results presented here demonstrate advantages of using sputter-coating for imaging of highly crystalline cellulose materials with TEM. We found that cellulose nanocrystals are in the nano-range with a hydrodynamic diameter of 89.4 nm, are small needle like structures, and are comprised of 84% carbon, 8% oxygen, 8% sodium, and less than 0.01% sulfur with less than 1 ppt metal impurities. The main objective was to complete a physicochemical characterization of CNC. Through that objective, a new TEM method was developed. These studies demonstrate that CNC are like conventional cellulose materials and should be generally regarded as safe.

Introduction

Nanomaterials are developed to advance processes, and consumer and industrial products through the exploitation of their novel properties and function derived from their nanometer size. For a material to be regarded as a nanomaterial, the American Society for Testing and Materials International, the American Institute of Chemical Engineers, the American Society of Mechanical Engineers, and the National Science Foundation International determined that the materials must be within the 1 and 100 nanometer size range in at least one dimension. Nanomaterials are used to advance many applications by advancing industrial processes, enhancing pharmacokinetic and targeting properties in the medical field, and the versatility of the surface functionality possibilities. The composition of nanomaterials varies from organic, inorganic, and mixtures.

The novel properties of advanced materials, such as engineered nanomaterials, thin films, and porous composites, are predominantly associated with their nanometer-

scale size, structure, and electronic configurations as well as an extremely large surface area-to-volume ratio relative to larger-sized (a.k.a. bulk) materials (Lai, Caloz, & Itoh, 2004; Shao & Jiang, 2015; Subramoney, 1998; Yin, Shi, & Yan, 2014). Particle size and surface area are important material characteristics for product development and safety assessment because as the size of a particle decreases, its surface area increases (Karakoti, Hench, & Seal, 2006). An increase in surface area allows for a greater proportion of a material's atoms to be chemically or biologically available (Borm et al., 2006; Nel, Xia, Mädler, & Li, 2006). The atoms on the surface of a material are often reactive and contribute to the unique properties that can be exploited in a new product or application. However, reactivity also contributes to the induction of adverse health effects in animals, plants, or microorganisms (Hajipour et al., 2012; Teeguarden, Hinderliter, Orr, Thrall, & Pounds, 2007). Other physical and chemical properties such as shape, surface coating, aggregation potential, and solubility may also stimulate biological effects with the possibility of amplifying or negating any associated size-related effects (Franklin et al., 2007; David B Warheit, Webb, Reed, Frerichs, & Sayes, 2007; Zhu, Chang, & Chen, 2010). To design both safe and effective nano-enabled products, each material must be accurately characterized in terms of physical and chemical properties.

Collecting complex data while simultaneously having effective methods to communicate results interpretation and data visualization is necessary. Successful results interpretation can only be completed through relating descriptive to functional analyses when understanding nanomaterial physical and chemical properties. Health effects can be determined using a battery of analytical tools, only if meaningful interpretation can be

visualized. A successful flow of information that bridges data collection, visualization, and results communication is necessary to enable a higher degree of user interaction.

As nanomaterials advance and become more widely spread, the need for materials comprised of renewable materials increase. One of the most abundant renewable resources in the world is cellulose. Cellulose is found in plants and bacteria, where it serves as a structural component of plants and is produced by invertebrates, algae, bacteria and fungi. (Moon et al., 2011). Cellulose is isolated and purified from refining wood pulp through mechanical and chemical processes. The refinement process, in addition to the bulk material source, results in diverse cellulose with varying morphological and functional properties which are utilized seamlessly in commerce (Shatkin et al., 2015). These forms of cellulose have been Generally Recognized As Safe (GRAS) by the U.S. Food and Drug Administration (SCOGS, 1973) for decades. For example, cellulose is currently used as a food additive where it can stabilize, add fiber, and aid in processing (Wustenberg 2015).

Cellulose Nanocrystals (CNC) are engineered by further processing the cellulose fibers where they release a crystalline portion. The crystalline portion of cellulose (or CNC) is utilized for its unique characteristics like enabling high tensile strength and enabling high thermal capacity where it is used as an additive in products like paper, textiles, filters, insulation, and other building materials (Moon et al., 2011). Regarding the food industry, CNC are used as additives, coatings, and in packaging of materials. (Shatkin et al., 2014). Specifically, concerning the renewable aspect of CNC, it is used as an alternative to petroleum materials in plastics, creating an environmentally friendly alternative. (Xie et al. 2018).

To verify the safety of CNC, we employed a battery of analytical techniques to fully assess the physicochemical characteristics of CNC including; size and distribution, length and width, crystallinity, surface texture, surface area, dispersion, metal impurities, elemental composition, dispersity index, hydrodynamic diameter, and surface charge. The comprehensive study generated here will inform conclusions regarding toxicological, mechanistic, and environmental fate and distribution.

Materials and Methods

Sample Preparation

Cellulose nanocrystals (CNC) were purchased from InnoTech Alberta (Edmonton, Alberta, Canada). This material is produced from wood pulp through a sulfuric acid hydrolysis process following purification and subsequent neutralization with sodium hydroxide. The CNC material was received as a dried powder (100% wt.). CNC was weighed on an analytical balance (Mettler Toledo, Columbus, OH, USA) and diluted in ultrapure water (18.2 Ohms; MilliQ Water Purification, Millipore, Burlington, Massachusetts, USA) to create a suspension with an end concentration of CNC of 2%. A Vortex Genie 2 (Scientific Industries, Bohemia, NY, USA) for 10 minutes prior to analyses to ensure complete dispersion of the aqueous suspension.

CNC Size and Surface Charge Analysis

Dynamic light scattering techniques were used to determine the Hydrodynamic Diameter (HDD), dispersity index (DI), and zeta potential (ζ potential). The Zetasizer Nanoseries Nano-ZS (Malvern Pananalytical, Almelo, Netherlands) was used to perform

all three experiments. To prepare the CNC for DLS, CNC suspensions were diluted to 0.01% with ultrapure water and loaded into a capillary cell (DTS 1060, Malvern Pananalytical, Almelo, Netherlands). Regarding replicates, CNC was scanned for 10 seconds, 11 times, and in triplicate for HDD and DI measurements. A 173° backscatter angle was used in general purpose mode. For ζ potential measurements, CNC ran 25 times, in triplicate, and data were fit to the Helmholtz-Smoluchowski model.

Light Microscopy Preparation and Imaging

CNC were diluted to a final concentration of 0.01% with ultrapure water and deposited on to a glass slide. After the droplet dried, the sample was imaged on a stereomicroscope (Stereomicroscope SZX16 Olympus Corporation, Tokyo, Japan) in brightfield mode. A 1X objective lens was used.

Transmission Electron Microscopy Preparation and Imaging

CNC powder was diluted in ultrapure water to a final concentration 3.0 %. To fully disperse the CNC before depositing, the sample was bath sonicated for 10 minutes at 37 Hz. Of the sonicated sample, approximately 10 µL was pipetted on parafilm and a copper-coated grid with a mesh width of 200 (Electron Microscopy Sciences, Hatfield, PA) was placed on top of the sample droplet for 5 minutes and allowed to air-dry for 1 hour. The sample was then placed on the edge of an SEM pin stub and coated with an ultrathin film of either iridium, carbon, gold, or titanium (Sputter Coater ACE600, Leica Microsystems, Wetzlar, Germany). Coatings were deposited at 5 nm thickness. Once completed, the grids were removed from the pin stub and samples were imaged with a

transmission electron microscope (JEM-1010, JEOL, Tokyo, Japan) at 60 kV with a spot size 2.

Quantification of contrast was performed using the Olympus CellSens (Olympus Corp. of the Americas, Center Valley, PA) software. Contrast was measured on randomly selected CNC as a value between 0 to 255, where 0 is white and 255 is black. The background contrast was then subtracted from the sample contrast and the resulting value was normalized (0 is white, 100 is black). 100 replicates were completed for the sample (CNC structure) and 100 for the background (no sample).

Scanning Electron Microscopy Preparation, Imaging, and Chemical Composition

CNC dispersions were diluted to a final concentration of 0.01% and then a 20 µL amount was mounting on to a pin stub and allowed to dry. Samples were imaged on a scanning electron microscope (SEM) Versa 3D, FEI (Field Electron and Ion Company, FEI; Hillsboro, Oregon, USA) at an accelerating voltage of 30 kV and a spot size of 5.0 with a working distance of 5 nm. Energy Dispersive X-ray Spectroscopy (EDXS, EDAX Inc, Mahwah, NJ, US) was used with the pinpoint analyses at 20kV and a spot size of 7.0 to examen the elemental composition of CNC (xT Microscope Control version 6.3.2).

Metal Impurities

Inductively coupled plasma-mass spectrometry (ICP-MS) was used to detect trace metal impurities. CNC were acid-digested via nitric and hydrochloric acids (Thermo Fisher Scientific, Waltham, MA, US) at a 1:10 ratio in a hot block set at 95ºC in a plastic digestion vessel for 2 hrs. Samples were then removed, allowed to cool at room temperature, and then spiked with additional nitric acid and put back into the hot block

for 1 hr. This was repeated until CNC looked clear to ensure complete digestion. The ICP-MS used was an ICP-MS 7900 (Agilent, Santa Clara, California, US) where a 200 ppb internal control with trace metals was used. Data was analyzed with MassHunter Software (Agilent Technologies, Santa Clara, CA, US).

Results and Discussion

Physicochemical Characterization

Light and electron micrographs (Figure 1.1) show the macroscopic and microscopic morphology of CNC. CNC is rod shaped, with individual crystals having widths below10 nm and lengths that vary from 25-250 nm. DLS measurements report an average HDD of 89.3+ 25.1 nm with a Dispersity Index (DI) of 0.51+0.02 (unitless), indicating a relatively broad size distribution (Figure 1.1 B). A negative surface charge was seen (ζ potential of -50.8+6 mV) due to the sulfuric acid hydrolysis process of isolating the CNC from cellulose wood pulp. This zeta potential value indicates that CNC is stable in aqueous solutions, where stability in indicated by a zeta potential measurement of ≥30mv or ≤-30 mv . (Figure 1.1 B) EDXS demonstrates the elemental composition of CNC, being primarily composed of carbon and oxygen (Figure 1.1 E and F). Due to the processing of CNC, there is a minute detection of sulfur. Another element detected due to the processing is sodium which comes from neutralization during production.

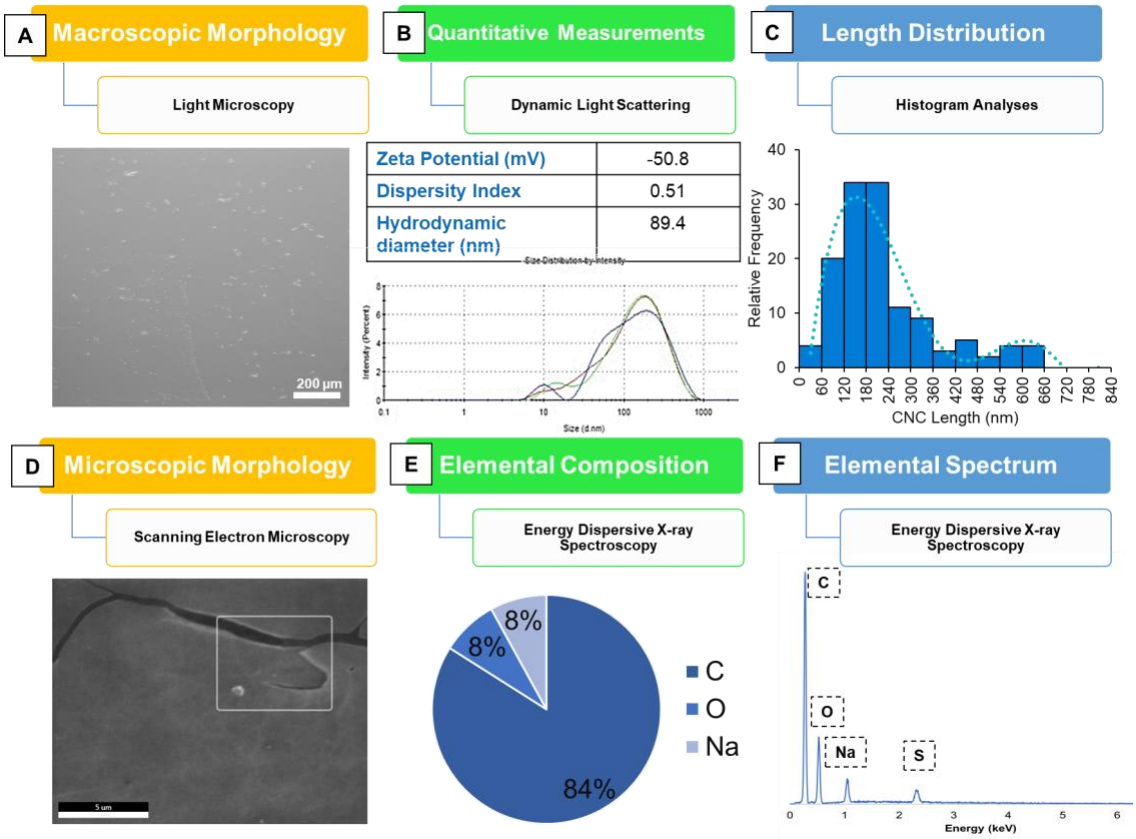

Figure 1.1 A full physicochemical characterization of CNC. Light microscopy (1.1 A) shows a macroscopic view of CNC morphology where small agglomerates can be visualized. The zeta potential, dispersity index, and hydrodynamic diameter were measured (1.1 B) where the surface charge of -50.8 mV was recorded, indicating the CNC suspension is stable and polydisperse (DI of 0.51), and the average hydrodynamic diameter was found to be 89.4 nm. A histogram of the length distribution was created (1.1 C) which indicates there is variable size, but the population is mainly in the nanorange where some agglomerates may be forming in aqueous suspensions. To characterize the microscopic morphology and elemental analyses images were acquired (1.1 D) which show sheets of CNC produced. The elemental composition was acquired with energy dispersive X-ray spectroscopy (1.1 E and F) where it was found to be comprised of 84% carbon, 8% carbon, 8% oxygen, and less than 0.01% sulfur.

New Transmission Electron Microscopy Sample Preparation Technique Analyses

The physical properties of nanomaterials are non-trivial to measure. TEM is widely used for nanoparticle characterization (Balbus et al., 2007; Sayes & Warheit, 2009; D. B. Warheit, 2008). Metal-based materials are inherently easier to image by

TEM than those composed of carbon; metals are relatively dense elements which contribute to high contrast between specimen and background (FRENS, 1972; Tao, Habas, & Yang, 2008). Carbonaceous materials are less dense and require more effort in sample preparation (Casuccio et al., 2004; IIJIMA, 1980). Specifically, cellulose nanocrystals pose a challenge with TEM imaging due to their low electron density in addition to their 3-dimensional nano structure.

For many years, carbonaceous materials have been imaged using TEM (Casuccio et al., 2004; Palotas, Rainey, Feldermann, Sarofim, & VanderSande, 1996; Wang, Li, Chen, & Huang, 2001). These materials can be either organic (composed of carbon, hydrogen, and oxygen) or inorganic (elemental carbon only); both types result in low contrast images due to low density. Stains, including lead citrate (LC), uranyl acetate (UA), and phosphotungstic acid (PTA) are three of the most common utilized to increase contrast (Brenner & Horne, 1959; Reynolds, 1963; Watson, 1958). When using these stains for cellulose nanocrystals (CNC), aggregation occurs, and significant artifacts are produced, both of which interfere with results interpretation. Some artifacts can superimpose upon parts of the specimen and consequently change the physical characterization, such as artificially increasing aggregation patterns or changing the inherent structural formations. These phenomena can be seen in Figure 1.2, where the same specimen is examined using two positive stains (Figure 1.2 B and C) and one negative stain (Figure 1.2 D) and are compared against the sample without any preparation (Figure 1.2 A). The LC and PTA stains resulted in the most severe generation of artifacts and artificial aggregation. Since the cellulose nanocrystals are difficult to differentiate with stains, another method must be developed.

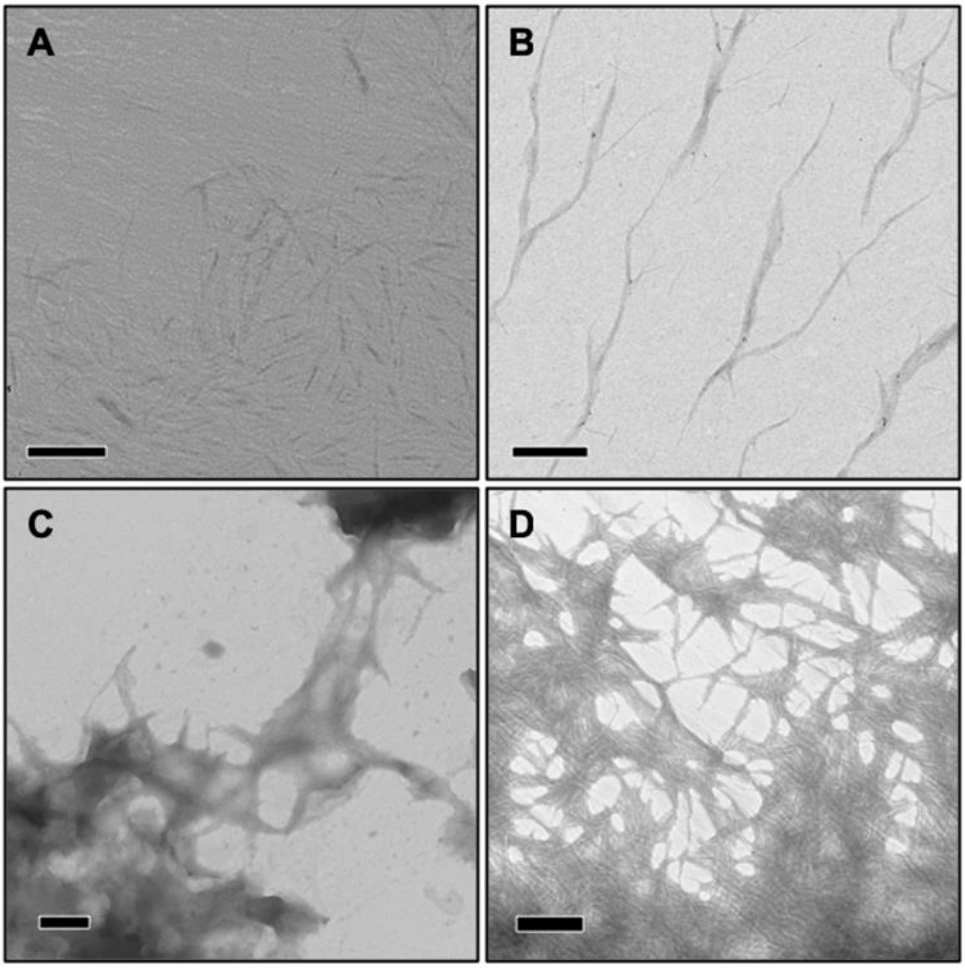

Figure 1.2. Transmission electron micrographs of CNC with various sample preparation methods (A) CNC without pre-treatment, (B) with uranyl acetate (C) lead citrate and (D) PTA stains. The images with stains illustrate artificial aggregation and/or artifact. Scale Bars: 200 nm.

Sputter-coating has been utilized in scanning electron microscopy (SEM) to increase a specimen's electron density and improve the conductivity of non-conductive samples (Lindroth, Bell, & Fredriksson, 1987). Sputter-coating samples increases image quality by decreasing sample charging. (Goldstein et al., 1992) Sample charging is when electrons are dissociated from the specimen surface and negatively interfere with signal detection. Here, we studied the effects of preparing CNC, a carbonaceous nanomaterial, for TEM analyses using sputter coating. Our results show that the electron density of

highly crystalline cellulose nanomaterials can be increased by way of layering an ultra-thin coating of electrically-conducting metal onto a sample's surface, thereby improving the resultant TEM image.

Sputter-coating CNC, to prepare specimens for TEM, increased the image quality (Figure 1.3). Sputter-coating with either iridium or gold layers produced the best results (Figure 1.3 A and C). Iridium coating had the greatest sample contrast (Figure 1.4) and induced minimal aggregation. The gold coating presented similar results. The titanium coating showed the best image quality but induced the most agglomeration (Figure 1.4 D) while the carbon coating induced the least agglomeration but yielded the worst contrast of the four coatings (Figure 1.4 B). These results were correct with our initial expectation; because iridium has the smallest mass, we hypothesized that its coating would produce the best image contrast. Overall, we conclude that iridium and gold coating not only produced the best results of all thin coatings tested, but these coatings also outperformed all the stains used in the study.

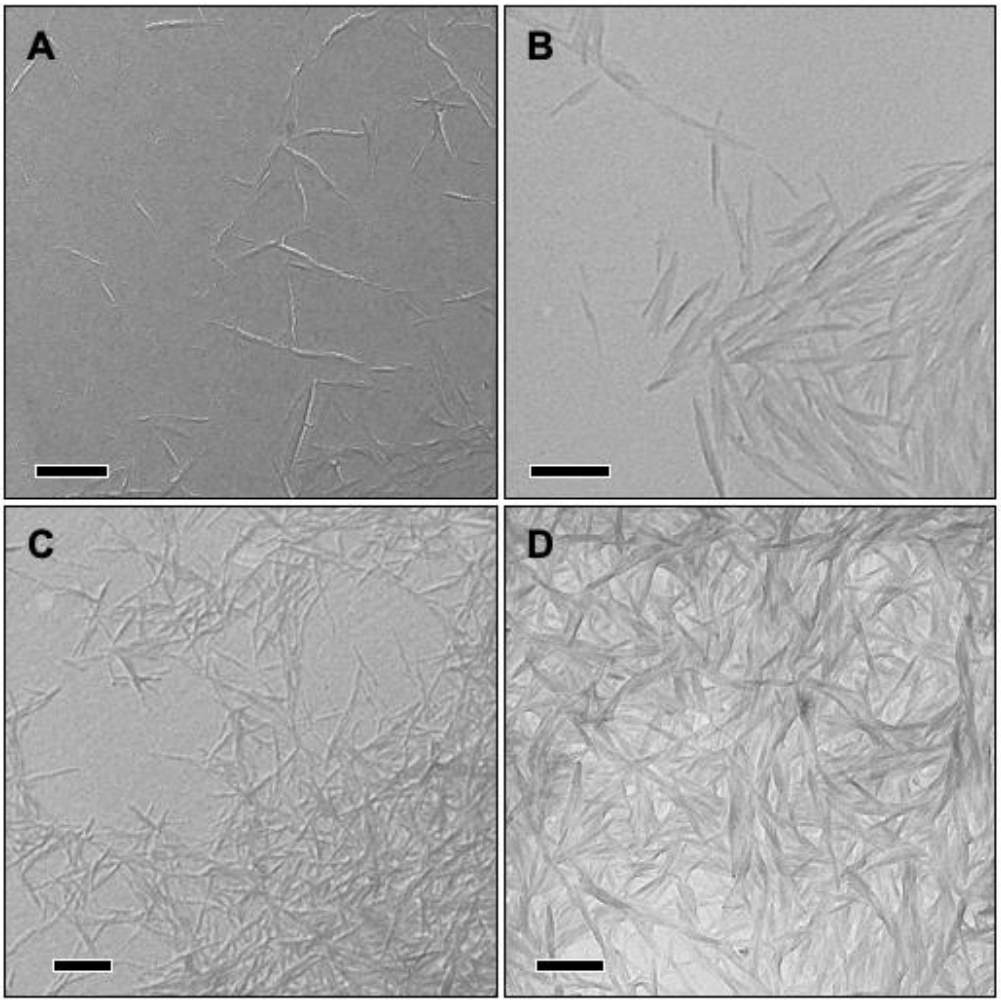

Figure 1.3. Transmission electron micrographs of sputter coated CNC. Samples were sputter coated with 5 nm of (A) iridium, (B) carbon, (C) gold, and (D) titanium. Scale bars: 200 nm.

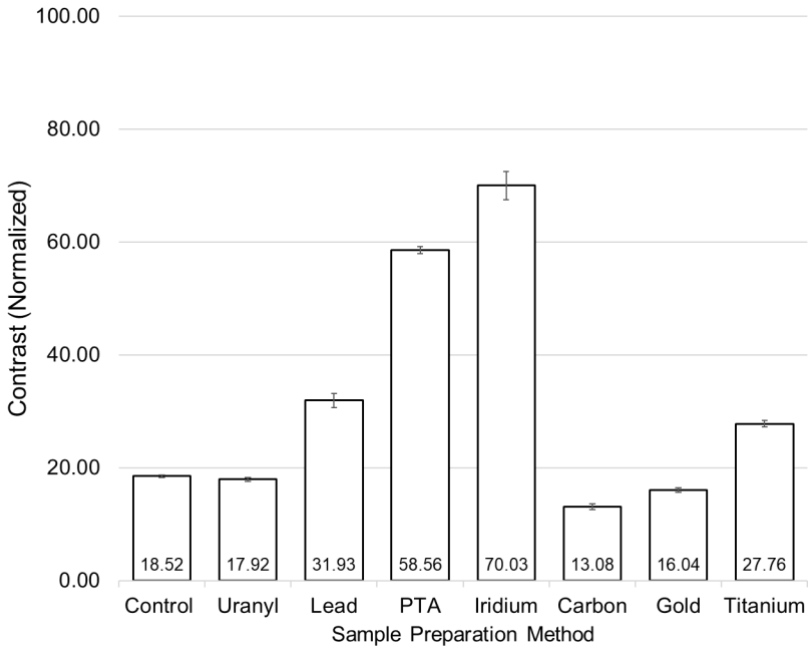

Figure 1.4. Graph of contrast for all sample preparation methods used in this study. The control is the sample not prepared with any stain or coating. Iridium and PTA are seen to show the most contrast. The y-axis displays the normalized contrast, where 0 is white, and 100 is black. N=100.

Conclusion

In conclusion, this study demonstrated that CNC pose challenges when completing physicochemical characterizations. Here we provided data that show a robust and full analytical characterization of an organic based nanomaterial to highlight the importance of comprehensive nanomaterial characterizations. With the extensive TEM analyses, the CNC needle like morphology was elucidated, as well as other important physical and chemical characteristics that can be used in future research or studies. These assessments were conducted on pristine engineered nanomaterials and give important information that can be used in toxicological studies like size, morphology, and metal impurities. To further understand the physical and chemical characteristics of

nanomaterials, the next chapters utilize these and other analytical techniques to characterize nanomaterials in complex matrices.

References

Balbus, J. M., Maynard, A. D., Colvin, V. L., Castranova, V., Daston, G. P., Denison, R. A., Wong, B. A. (2007). Meeting report: hazard assessment for nanoparticles--report from an interdisciplinary workshop. Environ Health Perspect, 115(11), 1654-1659. doi:10.1289/ehp.10327

Borm, P., Klaessig, F., Landry, T., Moudgil, B., Pauluhn, J., Thomas, K., Wood, S. (2006). Research strategies for safety evaluation of nanomaterials, Part V: Role of dissolution in biological fate and effects of nanoscale particles. Toxicological Sciences, 90(1), 23-32. doi:10.1093/toxsci/kfj084

Brenner, S., & Horne, R. (1959). A Negative Staining Method for High Resolution Electron Microscopy Of Viruses. Biochimica Et Biophysica Acta, 34(1), 103-110. Doi:10.1016/0006-3002(59)90237-9

Casuccio, G., Schlaegle, S., Lersch, T., Huffman, G., Chen, Y., & Shah, N. (2004). Measurement of fine particulate matter using electron microscopy techniques. Fuel Processing Technology, 85(6-7), 763-779. doi: 10.1016/j.fuproc.2003.11.026

Franklin, N. M., Rogers, N. J., Apte, S. C., Batley, G. E., Gadd, G. E., & Casey, P. S. (2007). Comparative toxicity of nanoparticulate ZnO, bulk ZnO, and ZnCl2 to a freshwater microalga (Pseudokirchneriella subcapitata): the importance of particle solubility. Environmental science & technology, 41(24), 8484-8490.

FRENS, G. (1972). Particle-size and sol stability in metal colloids. Kolloid-Zeitschrift and Zeitschrift Fur Polymere, 250(7), 736-+. doi:10.1007/BF01498565

Goldstein, J. I., Newbury, D. E., Echlin, P., Joy, D. C., Romig, A., Lyman, C. E., .Lifshin, E. (1992). Coating and Conductivity Techniques for SEM and Microanalysis. In Scanning Electron Microscopy and X-Ray Microanalysis (pp. 671-740): Springer.

Hajipour, M., Fromm, K., Ashkarran, A., de Aberasturi, D., de Larramendi, I., Rojo, T., Mahmoudi, M. (2012). Antibacterial properties of nanoparticles. Trends in Biotechnology, 30(10), 499-511. doi:10.1016/j.tibtech.2012.06.004

Iijima, S. (1980). High-Resolution Electron-Microscopy of Some Carbonaceous Materials. Journal of Microscopy-Oxford, 119(May), 99-111. Doi:10.1111/J.1365-2818.1980.Tb04081.X

Karakoti, A., Hench, L., & Seal, S. (2006). The potential toxicity of nanomaterials—the role of surfaces. Jom, 58(7), 77-82.

Lai, A., Caloz, C., & Itoh, T. (2004). Composite right/left-handed transmission line metamaterials. Ieee Microwave Magazine, 5(3), 34-50. doi:10.1109/MMW.2004.1337766

Lindroth, M., Bell, P. B., & Fredriksson, B. A. (1987). TEM-, SEM- and STEM- Studies of Sputter-Coated Cytoskeletons. Scanning, 9, 47-56.

Moon, R. J., Martini, A., Nairn, J., Simonsen, J., & Youngblood, J. (2011). Cellulose nanomaterials review: structure, properties and nanocomposites. Chemical Society Reviews, 40(7): 3941-3994.

Nel, A., Xia, T., Mädler, L., & Li, N. (2006). Toxic potential of materials at the nanolevel. science, 311(5761), 622-627.

Palotas, A., Rainey, L., Feldermann, C., Sarofim, A., & VanderSande, J. (1996). Soot morphology: An application of image analysis in high-resolution transmission electron microscopy. Microscopy Research and Technique, 33(3), 266-278. doi:10.1002/(SICI)1097-0029(19960215)33:3<266::AID-JEMT4>3.0.CO;2-O

Reynolds, e. (1963). Use of lead citrate at high ph as an electron-opaque stain in electron microscopy. Journal of cell biology, 17(1), 208-&. Doi:10.1083/jcb.17.1.208

Sayes, C. M., & Warheit, D. B. (2009). Characterization of nanomaterials for toxicity assessment. Wiley Interdisciplinary Reviews: Nanomedicine and Nanobiotechnology, 1(6), 660-670.

SCOGS. (1973). Select Committee on GRAS Substances (SCOGS) Report-25: Evaluation of the health aspects of cellulose and certain cellulose derivatives as food ingredients. Report Number: NTIS #PB274667; SCOGS-25.

Shao, Q., & Jiang, S. (2015). Molecular understanding and design of zwitterionic materials. Adv Mater, 27(1), 15-26. doi:10.1002/adma.201404059

Shatkin, J.A., & Kim, B. (2015). Cellulose nanomaterials: life cycle risk assessment, and environmental health and safety roadmap. Environmental Science: Nano, 2(5):477-499.

Shatkin, J.A., Wegner, T., Bilek, E., & Cowie, J. (2014). Market projections of cellulose nanomaterial-enabled products - Part 1: Applications. TAPPI Journal, 13(5):9-16.

Subramoney, S. (1998). Novel nanocarbons - Structure, properties, and potential applications. Advanced Materials, 10(15), 1157-+. doi:10.1002/(SICI)1521

Tao, A., Habas, S., & Yang, P. (2008). Shape control of colloidal metal nanocrystals. Small, 4(3), 310-325. doi:10.1002/smll.200701295

Teeguarden, J. G., Hinderliter, P. M., Orr, G., Thrall, B. D., & Pounds, J. G. (2007). Particokinetics in vitro: dosimetry considerations for in vitro nanoparticle toxicity assessments. Toxicol Sci, 95(2), 300-312. doi:10.1093/toxsci/kfl165

Wang, Q., Li, H., Chen, L., & Huang, X. (2001). Monodispersed hard carbon spherules with uniform nanopores. Carbon, 39(14), 2211-2214. doi:10.1016/S0008-6223(01)00040-9

Warheit, D. B. (2008). How meaningful are the results of nanotoxicity studies in the absence of adequate material characterization? Toxicol Sci, 101(2), 183-185.

Warheit, D. B., Webb, T. R., Reed, K. L., Frerichs, S., & Sayes, C. M. (2007). Pulmonary toxicity study in rats with three forms of ultrafine-TiO2 particles: differential responses related to surface properties. Toxicology, 230(1), 90-104.

Watson, M. (1958). Staining of Tissue Sections for Electron Microscopy with Heavy Metals. Journal of Biophysical and Biochemical Cytology, 4(4), 475-&. Doi:10.1083/Jcb.4.4.475

Xie, S., Zhang, X., Walcott, M.P., & Lin, H. (2018). Cellulose nanocrystals (CNCs) applications: a review. Eng. Sci, 2:4-16

Yin, W., Shi, T., & Yan, Y. (2014). Unique Properties of Halide Perovskites as Possible Origins of the Superior Solar Cell Performance. Advanced Materials, 26(27), 4653-+. doi:10.1002/adma.201306281

Zhu, X., Chang, Y., & Chen, Y. (2010). Toxicity and bioaccumulation of TiO2 nanoparticle aggregates in Daphnia magna. Chemosphere, 78(3), 209-215.

CHAPTER TWO

The External Environment Impacts Nanomaterial Transformation and Potential Downstream Effects

This chapter published as: Mulenos, M. R., Liu, J., Lujan, H., Guo, B., Lichtfouse, E., Sharma, V. K., & Sayes, C. M. (2020). Copper, silver, and titania nanoparticles do not release ions under anoxic conditions and release only minute ion levels under oxic conditions in water: Evidence for the low toxicity of nanoparticles. Environmental Chemistry Letters, 1-10.

Abstract

It is widely assumed that the discharge of nanoparticles into the environment may cause adverse effects on organisms. Nonetheless, most nanoparticles have demonstrated little to no observed hazards in multiple biological test systems. It isn't until nanoparticles undergo transformations, e.g. release of metal ions, that most environmental toxicities are induced. We hypothesized that in anaerobic conditions, where oxidation is absent or limited, metal nanoparticles do not release metal ions. We investigated the transformation of three commercially produced materials, i.e., copper nanoparticles, silver nanoparticles, and titania nanocrystals with an average particle size of 50 nm. The nanoparticles were subjected to different environmental conditions including oxic/anoxic suspension, natural organic matter incubation, and pH gradient and subsequently analyzed via zeta potential, hydrodynamic diameter, released metal ion concentration, and reactive oxygen species generation. Transmission electron microscopy was utilized to assess morphological changes. Results show that copper (9.4 μg/mL) and silver (6.9 μg/mL) ions were released from copper and silver nanoparticles, respectively,

when continuously stirred under oxic conditions over 48 h. An insignificant amount of copper (0.9 μg/mL) and silver (0.2 μg/mL) ions were released under stirred anoxic conditions from the same systems. Significantly, almost no (lower than 0.05 μg/mL) ion release was observed from titania nanocrystals under either oxic or anoxic conditions. The results suggest that oxygen plays an important role in releasing metal ions from the nanomaterial surfaces. We observed that copper, silver, and titania nanoparticles do not release ions under anoxic conditions.

Introduction

Engineered nanomaterials represent a wide range of advanced materials intentionally added to industrial and consumer products and processes in an effort to increase their performance (Pati, Singh et al. 2016, Ahn, Wong et al. 2018, Alivio, Fleer et al. 2018, Kim, Smith et al. 2018, Westerhoff, Atkinson et al. 2018, Vishnuvarthanan and Rajeswari 2019). Nanoparticles range from insulating to semi-conductive to conductive elemental compositions. Manufacturers generate nano-enabled products by embedding nanoparticles into a matrix or coating the surface of a product (Keller and Lazareva 2014, Bäuerlein, Emke et al. 2017, Kaur, Kaur et al. 2018). However, when nanomaterials emulsify in a gelatinous substance or suspend in a liquid, they tend to migrate from the mixture into the surrounding environment (Westesen, Bunjes et al. 1997). These embedded nanoparticles have the potential to release from products and transform under environmental conditions (Adegboyega, Sharma et al. 2014, Garner and Keller 2014, Amde, Liu et al. 2017, Joo and Zhao 2017, Ortelli, Costa et al. 2017, Zhang, Xu et al. 2018, Simeone, Blosi et al. 2019).

Metal nanoparticles are typically produced in their zerovalent forms, indicating that the outer shell of the particle has a valence value of zero. Examples of zerovalent nanoparticles are copper and silver nanoparticles (Akaighe, MacCuspie et al. 2011, Gao, Rodrigues et al. 2019, Hedberg, Blomberg et al. 2019). Similarly, metal oxide nanoparticles, e.g. titanium dioxide nanocrystals, are stable and remain intact when stored as dry powders (Sharma 2009, Li, Qian et al. 2019). Metal and metal oxide nanoparticles suspended in aqueous solutions may transform when exposed to natural organic matter, oxic/anoxic conditions, and ultraviolet light (He, Jones et al. 2011, Lowry, Espinasse et al. 2012, Yin, Liu et al. 2012, Sharma, Filip et al. 2015, Wang, Garg et al. 2017, Yin, Han et al. 2017, Yin, Xu et al. 2017, Pham, Bui et al. 2018, Hedberg, Blomberg et al. 2019). During this reaction nanoparticles may transform from their pristine engineered zerovalent state to surface-charged, ion dissociated, agglomerated/aggregated forms (Hou, Stuart et al. 2013, Sharma and Zboril 2017). These transformation processes may have negative effects on human health and ecological systems due to the possible release of toxic metal ions and reactive oxygen species (Georgantzopoulou, Almeida Carvalho et al. 2018, Rai, Kumar et al. 2018, Wang, Menzies et al. 2018, Li, Qian et al. 2019). The focus of the present paper is to understand the transformation of selected nanoparticles under different environmental conditions.

The studied nanoparticles are copper nanoparticles, silver nanoparticles, and titania nanocrystals, which have been applied in thousands of consumer products (Garner, Suh et al. 2017, Sharma, Sayes et al. 2019). The physicochemical characteristics of the nanoparticles under aqueous environment were studied with the following aims: (i) dissolution under stirring oxic and anoxic conditions to evaluate the release of toxic metal

ions, (ii) quantification of reactive oxygen species release under both oxic and anoxic conditions, (iii) the solution was exposed to natural organic matter and imaged utilizing transmission electron microscopy were determined to monitor the stability of the nanoparticles, and (iv) the pH of the aqueous solution were varied from acidic to alkaline pH and measurements of zeta potential and hydrodynamic diameters were determined to learn the change in surface charge and size. The results presented herein are expected to aid in the assessments of hazards, exposures, and risks of engineered nanomaterials that transform after entering to the aquatic environment

Experimental

Experimental Design

Copper and silver nanoparticles were purchased from Sigma Aldrich at the highest percent purity offered (St. Louis, Missouri, United States; copper nanopowder, 40 to 60 nm particle size, greater than or equal to 99.5% trace metals basis; silver nanopowder, lower than 100 nm particle size, 99.5% trace metals basis). Titania nanocrystals were purchased from Evonik (Essen, Germany; AEROXIDE® P25; lower than 100 nm particle size; 97% trace metal basis). Density reported by the manufacturers were 8.0, 10.5, and 4.2 g/cm^3 for coper nanoparticles, silver nanoparticles, and titania nanocrystals, respectively.

The experimental design, as described in Fig. 2.3., incorporates four independent studies designed to characterize surface charge and size through zeta potential and hydrodynamic size measurements, morphological information from transmission electron microscopy, metal impurities and released ion concentration using inductively coupled plasma-mass spectrometry, and generation of reactive oxygen by ultraviolet

spectroscopy. For all experiments, an incubation or exposure time period of 48 h at room temperature, i.e. 21℃, was used. 48-hour incubation time was used due to toxicological studies being 24 and/or 48 h long experiments (Lewinski, Colvin et al. 2008, Selvaraj, Bodapati et al. 2014). The particle concentration was 100 µg/mL in 18.2 mΩ Milli-Q ultrapure water, unless otherwise noted. All studies were performed in triplicate.

Nanomaterial Aqueous Suspension Stirring Under Oxic and Anoxic Conditions

Aqueous suspensions of nanomaterials were agitated via magnetic stir bar from Thermo Fischer Scientific (Waltham, Massachusetts, United States) in either oxygen-saturated water or nitrogen-purged water. Oxygen-saturated and nitrogen-purged solutions were produced by purging pressurized air and nitrogen gas into a parafilm-covered beaker throughout the agitation, respectively (Zhang, Xu et al. 2018). Every 6 h, a 10 mL aliquot was taken from the top of each suspension and underwent centrifugal ultrafiltration before preparation for analyses via digestion with a nitric and hydrochloric acid mixture, 67% and 36% respectively, at a 3:1 ratio (De Jong et al. 2008). Briefly, a particle concentrating centrifugal cartridge was used (Amicon Ultra 15, Millipore, Burlington, Massachusetts, United States). The 10 mL aliquot was added to each cartridge and centrifuged for 15 min at 5,000 rpm. After each procedure, approximately 500 µL of concentrated suspension remained in the receptacle. Both the filtrate and the concentrated sample was digested and analyzed for total metal content.

Inductively coupled plasma-mass spectrometry Agilent 7900 (Santa Clara, California, United States) instrument was used to measure metal ion concentrations from the dissolution of studied nanoparticles. Briefly, the sample digests were placed in the autosampler and ran in triplicate along with an environmental internal standard which

contained lithium, scandium, germanium, rhodium, indium, terbium, lutetium, and bismuth from Agilent (Santa Clara, California, United States). It is noted that titanium ions are difficult to analyze using inductively coupled plasma-mass spectrometry. However, to maintain consistency among nanoparticle analyses, we subjected titania to the same sample preparation process and mass spectrometry analyses as copper and silver nanoparticle samples. The concentrations of metal ions were calculated through a linear regression analysis against prepared standards from Agilent (Santa Clara, California, United States). Method blanks and acid blanks were measured as well. Data analysis was performed with Excel (Microsoft, Redmond, Washington, United States.) After data analysis, mass balance calculations verified total amount of released metal ions.

Nanomaterial Exposure to Ultraviolet Radiation and Generation of Reactive Oxygen Species

Each nanoparticle suspension was vortexed utilizing a Vortex-Genie 2 (Scientific Industries; Bohemia, New York, United States), for 30 s and then placed under shortwave ultraviolet lamp at 254 nm (Fisher Scientific, Hampton, New Hampshire, United States) for 15 min, and immediately analyzed for reaction oxygen species generation. 2′,7′-dichloro¬fluorescein diacetate (Cell Biolabs, Inc.; San Diego, California, United States) was used to measure the concentration of reactive oxygen species, described elsewhere (Romoser, Ritter et al. 2011). Briefly, a 100 μM of the diacetate solution was added to 1 mL aliquot of particle suspensions and incubated at 37°C for 15 min. 1,000 μM hydrogen peroxide (Fisher Scientific, Hampton, New Hampshire, United States) was used as a positive control for determining reactive oxygen species concentration. Ultrapure water served as a negative control. Fluorescence of the sample was measured at

an excitation of 480 nm and an emission of 530 nm using a Synergy Mx Multi-Mode Microplate Reader (BioTek Instruments, Inc.; Winooski, Vermont, United States). Analyses involved the detection and the measurement of general reactive oxygen species, i.e. super oxide anion, hydroxyl radical, and singlet oxygen.

Nanomaterial Incubation with Natural Organic Matter and Analyses by Transmission Electron Microscopy

Nanoparticle suspensions were subjected to an addition of mass equivalent concentration of Suwannee River natural organic matter (International Humic Substances Society; Denver, Colorado, United States). Suwannee River natural organic matter is used as the universal standard of natural organic matter. First, the organic matter was suspended in ultrapure water at a concentration of 100 µg/mL (Liu and Hurt 2010). After 30 s agitation on a Vortex-Genie 2 (Scientific Industries; Bohemia, New York, United States), each nanoparticle suspension was added at equal parts volume and vortexed for an additional 30 s. Samples were left to incubate at room temperature; subsequent vortex occurring for 30 s intervals every 8 h for 48 h total.

Transmission electron microscopy was performed for nanoparticles and nanoparticle-organic matter mixtures (Stebounova, Guio et al. 2011). Details of sample preparation include a 10 µL droplet of nanoparticle suspension was set on parafilm and a formvar coated copper grid from Electron Microscopy Sciences (Hatfield, Pennsylvania, United States) was placed over top for 5 minutes. The grid was then removed and dried before imaging. The samples were imaged with a JEOL 2010 microscope (JEOL Ltd.; Tokyo, Japan), operating at 60 kV. Post image analyses were performed with ImageJ software.

Change in Nanomaterial pH and Analysis via Dynamic Light Scattering

A range of nanomaterial suspensions, inclusive of 0.1 to 1000 µg/mL, were titrated using the Malvern MPT-2 Autotitrator in parallel with the Zetasizer Nano-ZS (Malvern Panalytical Ltd.; Malvern, United Kingdom). This combination allowed titration over a wide pH range and thus made it possible to determine the isoelectric point. Particles were automatically titrated from pH 12.0 to 2.0 by adding 0.25 M hydrochloric acid and 0.25 M sodium hydroxide (Fisher Scientific, Hampton, New Hampshire, United States). A folded capillary cell with electrodes (Malvern Panalytical Ltd.; Malvern, United Kingdom) was used for all measurements where 500 µL of nanoparticle suspension was loaded. At every 0.2 pH unit, the zeta potential and hydrodynamic size were determined. These experiments collected eleven measurements and the experiment was repeated in triplicate. The isoelectric point was determined using the Malvern Software Version 5.03.

Statistical Analyses

Statistical analyses were performed using SAS 9.4 software (SAS Institute Inc.; Cary, North Carolina, United States). Each experimental value was compared to the corresponding control value for each experiment. One-way ANOVA test was performed at each sampling time. When the F-test from ANOVA shows significance, the Dunnett's or Dunn's test was used to compare means from the control group. Statistical significance versus control group was established at levels corresponding to p-values lower than 0.05. Experiments were conducted with n=3 and in triplicate.

Results and Discussion

Dissolution Under Oxic and Anoxic Condition

Two orthogonal approaches, i.e. oxic and anoxic conditions, were used to measure the ion release of each investigated nanomaterial. Fig. 2.1. shows the concentrations of released metal ions over time under both conditions. Copper and silver nanoparticles released increasing amounts, 9.4 µg/mL and 6.9 µg/mL, respectively, of dissolved ions with time from the particle surfaces when stirred and aerated. Silver nanoparticles dissolved at the faster rate between 0-20 h than the rate observed between 20-48 h (Fig. 2.1.B). It is possible that an oxide shell formed on the surface of the silver nanoparticles during the dissolution in the initial phase, which would decrease the ion release rate (Akaighe, MacCuspie et al. 2011). As expected, titania nanocrystals did not produce a significant amount, lower than 0.05 µg/mL, of ions under the oxic condition (Fig. 2.1.C).

Under the anoxic conditions, i.e. stirred and purged with nitrogen gas, a significantly fewer dissolved ions were released from the nanomaterials (Fig. 2.1.). Copper nanoparticles release 0.9 µg/mL, silver nanoparticles released 0.2 µg/mL, and no measurable ions were released from titania nanocrystals. This indicates that dissolved oxygen in solution plays a pivotal role in releasing dissolved metal ions from nanomaterials. Previous investigations in the case of silver nanoparticles also showed

similar observations, e.g. $Ag^0 + O_2 \rightarrow Ag^+ + O_2^-$ (He, Jones et al. 2011, He, Garg et al. 2012, Rong, Garg et al. 2019).

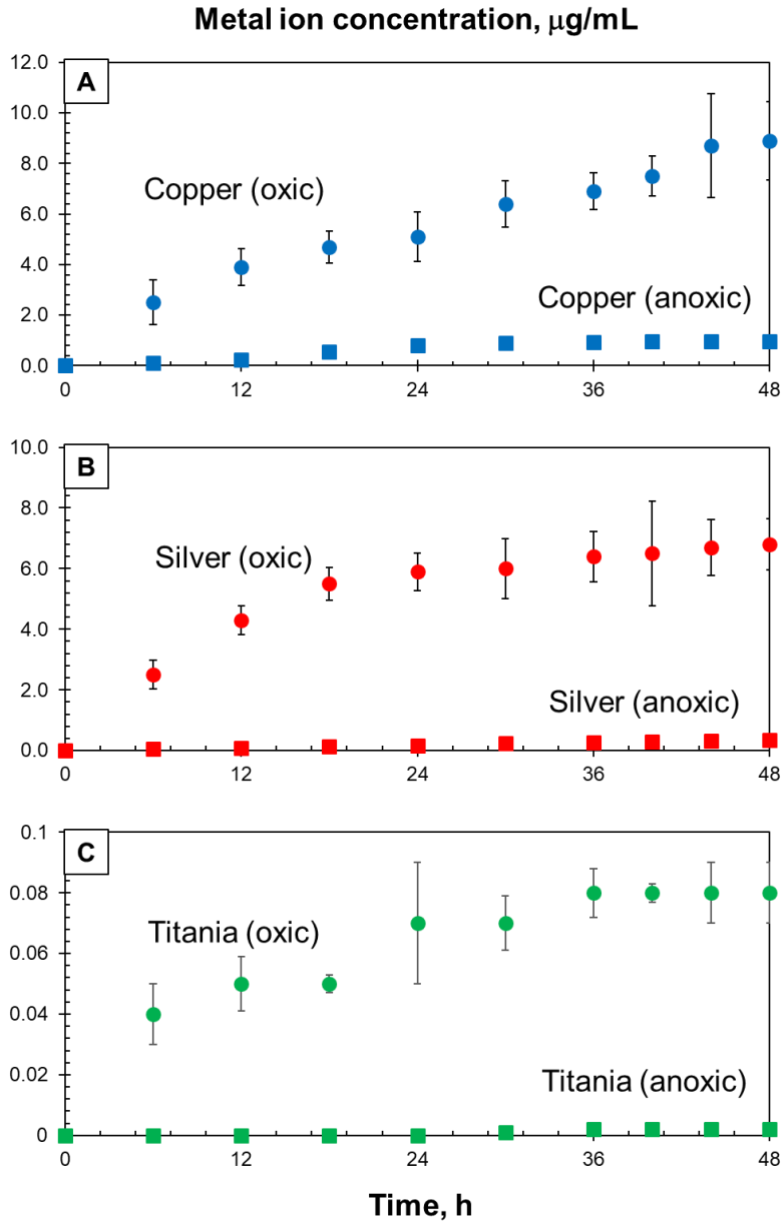

Figure 2.1. Release of metal ions from nanoparticles is dependent on oxic conditions. Metal ion concentrations under air-saturated (oxic) or nitrogen-purge (anoxic) for (A) copper, (B) silver, and (C) titania particle suspensions in water. Solid lines represent data collected from air-saturated system, while dotted lines represent data collected from nitrogen-purge system. Each data set represents the average and the standard deviation (n = 9).

Generation of Reactive Oxygen Species Under UV Irradiation

Fig. 2.2. shows the generation of reactive oxygen species from the surfaces of each nanomaterial used in the study after 15 min irradiation with ultraviolet light. In general, reactive oxygen species increases as particle concentration increases. However, the increase in reactive species production differs among the three different metal particle-types. Copper nanoparticles (2.2.A) follow a dose-response relationship, i.e. as much as 1250 ± 8% relative fluorescence units at 1000 µg/mL to as little as 800 ± 10% relative fluorescence units at 0.1 µg/mL, across all concentrations and the sample produced the most reactive oxygen species of all samples when suspended in water. The term "relative fluorescence units" is a unit of measurement used in the fluorescence detection analysis and, for this experiment, is directly proportional to the concentration of reactive oxygen species in the sample (Nasseri, Borna et al. 2018). Silver nanoparticles (2.2.B) did not follow a dose-response relationship, e.g. the highest concentration of species detected was 1,050 ± 8% relative fluorescence units at 10 µg/mL and the lowest concentration of species detected was 725 ± 9% relative fluorescence units at 1000 µg/mL. The literature has shown that silver nanoparticles can generate of reactive oxygen species with and without ultraviolet irradiation. The presence of oxygen in aerated solution upon irradiation tends to produce reactive oxygen species, e.g., O_2-● (Adegboyega, Sharma et al. 2016, Ranjan and Ramalingam 2016, Rong, Garg et al. 2019). However, the produced reactive oxygen species may interact with released metal ions to reproduce silver nanoparticles in a feedback mechanism (He, Jones et al. 2011).

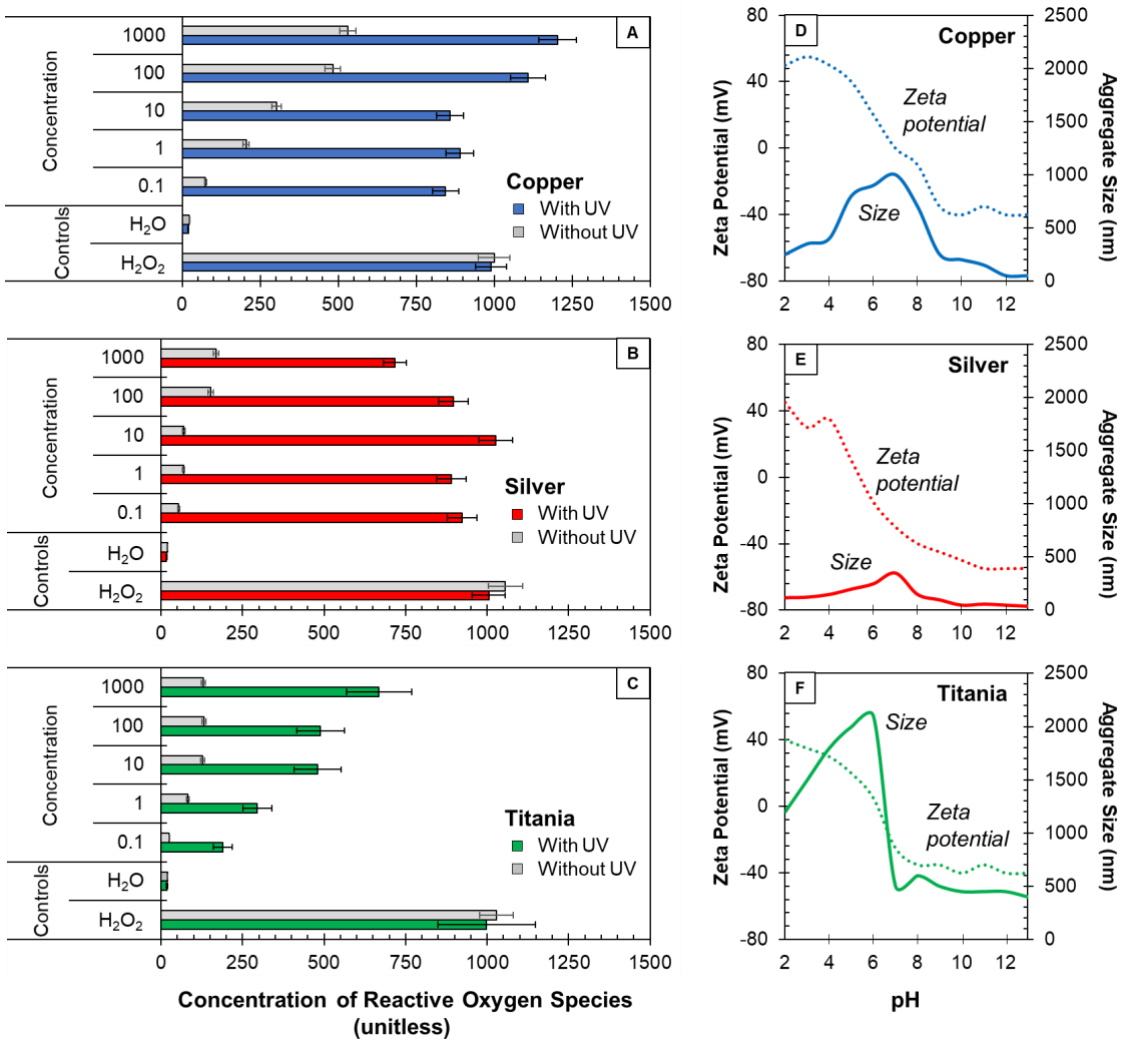

Figure 2.2. Reactive oxygen species concentration is dependent on nanoparticle concentration. (A) Copper nanoparticles follow a concentration-dependent relationship across all particle concentrations. (B) Silver nanoparticles follow a concentration-dependent relationship from 0.1-10 µg/mL, but the reactive oxygen species concentration decreases from 10-1000 µg/mL. (C) Titania nanoparticles produce the least amount of reactive oxygen species and the concentrations at statistically insignificant across all particle concentrations. All particle samples were exposed to ambient light for 1 h before analyses. Isoelectric point and hydrodynamic diameter measurements of (D) copper, (E) silver, and (F) titania nanoparticles in water over pH.

Lastly, titania nanocrystals (2.2.C) produced the least amount of reactive oxygen species over a dose-response relationship, e.g. as much as 675 ± 18% relative fluorescence units at 1,000 µg/mL to as little as 210 ± 22% relative fluorescence units at

0.1 µg/mL. Taken together, these data suggest that the cumulative effect of production and consumption of oxygen would ultimately determine the concentration of reactive oxygen species upon irradiation of nanomaterials in water (Nasseri, Borna et al. 2018, Irandost, Akbarzadeh et al. 2019, Xu, Li et al. 2019).

Effect of Natural Organic Matter

Fig. 2.3. shows the transmission electron micrographs of the three particle systems and their morphological features in absence and presence of natural organic matter in water. In water, shapes of the particles are generally spherical, triangular, and trapezoidal for copper nanoparticles, silver nanoparticles, and titania nanocrystals, respectively. In the presence of organic matter, all particles underwent dissolution to the extent where each individual particle could no longer be distinguished. The moieties of natural organic matter interact with the surface of the particle. The interaction with multiple particles may increase the overall size of the nanoparticle or possibly induce aggregation. These interactions can be physical or chemical or both (Sani-Kast, Labille et al. 2017, Huang, Qian et al. 2019). For example, silver ions, likely produced from dissolution of silver nanoparticles under oxidic conditions, would interact with sulfur-containing groups of organic matter through complexation (Ubaid, Zhang et al. 2019). The transformation of silver nanoparticles seems to be the highest in presence of natural organic matter compared to either the original sample or the absence of any organic species, where many particles agglomerated and morphed into a large agglomerated structure. In the natural environment, silver sulfide nanoparticles, thought to be reproduced from dissociated silver nanoparticles in a feedback mechanism, have been found (Sharma, Filip et al. 2015, Ubaid, Zhang et al. 2019). Similarly, copper sulfide has

also been seen in the aquatic environment (Sharma, Filip et al. 2015). Other moieties of organic matter, such as phenols and hydroquinone, may also be involved in the complexation processes. Titania nanocrystals do not dissolve into their respective metal ions and therefore, would only interact with organic species through physical phenomena, i.e. adsorption.

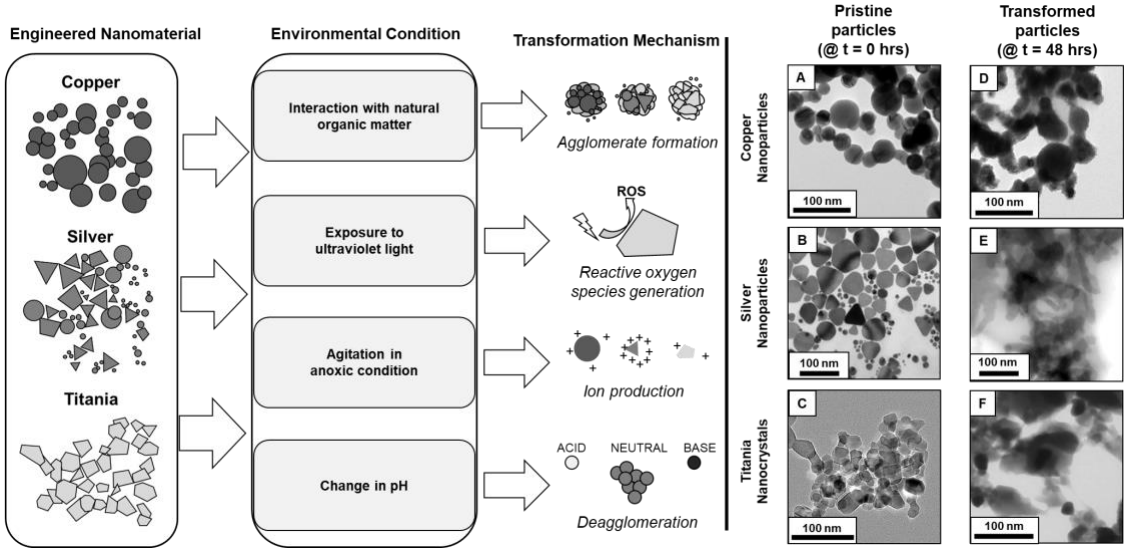

Figure 2.3. Experimental design used to observe and measure nanomaterial transformations. The conditions of each experiment are as follows: interaction with natural organic matter (room temperature, ambient light, ambient oxygen, and neutral pH); exposure to ultraviolet light (no natural organic matter, room temperature, ambient oxygen, and neutral pH); agitation with dissolved oxygen (no natural organic matter, room temperature, ambient light, and neutral pH); and change in pH (no natural organic matter, room temperature, ambient light, and ambient oxygen). (Right) Transmission electron microscopy image of (A) copper, (B) silver, and (C) titania particles taken immediately after suspension in ultrapure water. Transmission electron micrographs of (D) copper, (E) silver, and (F) titania particles taken 48 h after incubation with natural organic matter in water.

Effect of pH

Fig. 2.2. shows the variation of zeta potentials and hydrodynamic diameters with pH in the range from 2.0 to 13.0. All three samples followed the same trend; at a low pH, the zeta potentials have positive values while at a high pH, they possess negative values. The measurements of zeta potentials of the three nanomaterials over a wide pH were used to deduce the isoelectric points, a.k.a. conductometric titrations, which is the pH of the nanomaterial suspension where zeta potential is neutral. The isoelectric points are 7.0, 6.5, and 5.5 of copper nanoparticles, titania nanocrystals, and silver nanoparticles, respectively. These values suggest that the studied nanomaterials would be mostly negatively charged at environmentally pH conditions (Pham, Bui et al. 2018).

Hydrodynamic diameters of the three materials are also shown in Fig. 2.2. Titania had the largest particle size range from 200-2,200 nm, then copper with a range of 100-1,000 nm, and then silver, which did not change much, at 100-200 nm. All three samples followed similar trends with a small hydrodynamic diameter at both highly acidic and alkaline pH. The maximum sizes are at their isoelectric points.

Conclusions

The physicochemical measurements, shown in Figs. 2.1.-2.4., demonstrate the role of different environmental parameters on the transformation of the nanomaterials. The nanoparticles in natural waters are not static and their physicochemical properties would change dynamically over time and spatial coordinates. The influence of these conditions on the interactions of the nanoparticles are presented in Fig. 2.4. The investigated nanoparticles of negatively charged surfaces under environmental pH, based on isoelectric point measurements, would interact with different moieties of

organic matter. These physical and chemical interactions likely cause aggregation of the nanoparticles (Shevlin, O'Brien et al. 2018). These interactions depend on the type of metal ions. For example, titania nanocrystals do not release ions and only exhibit physical interactions; copper nanoparticles readily release ions and have both physical and chemical interactions; and silver nanoparticles also readily release ions and due to complexation processes produced the most significant physical and chemical interactions. The interaction of organic species may stabilize nanomaterials for months. In consequence, this phenomenon may promote nanomaterial intercalation within microorganisms, accumulation within aquatic organisms, or transportation through water (Quigg, Chin et al. 2013). This is important for assessing the safety of these materials because such organisms are exposed to these materials after they are released into the environment.

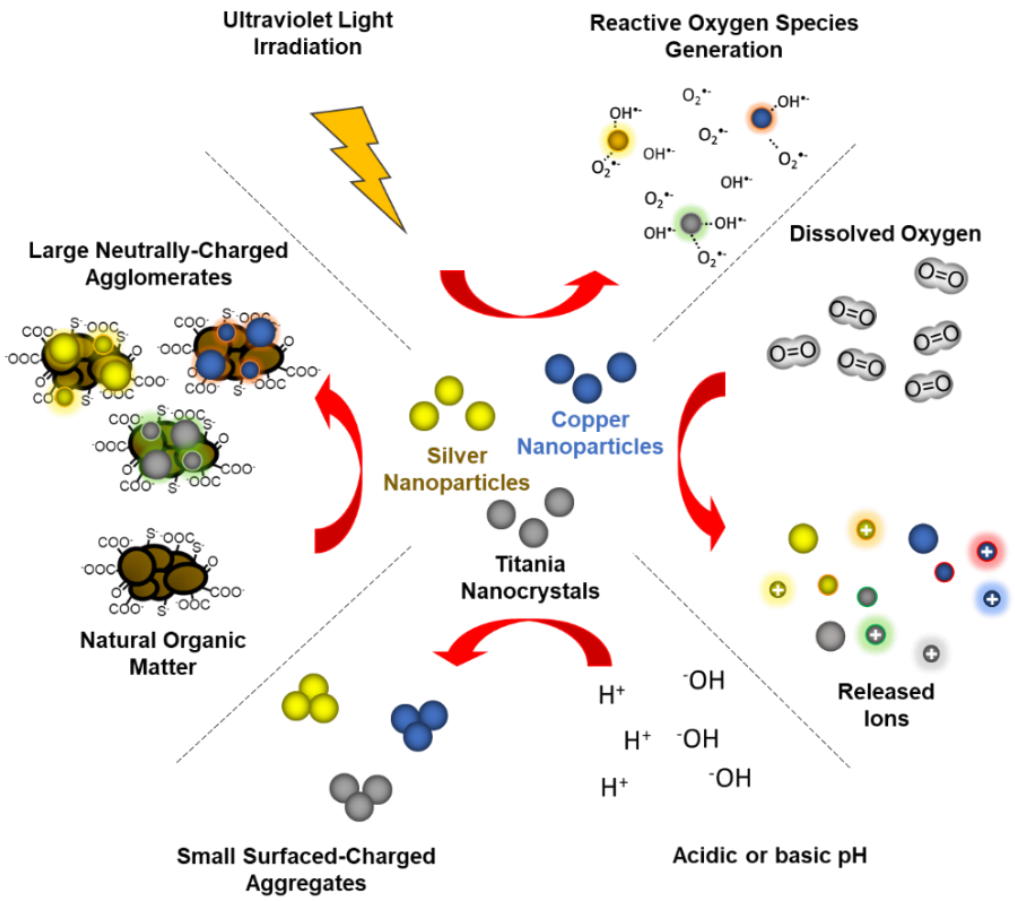

Figure 2.4. Potential mechanisms of nanoparticle transformations in environmental conditions. When irradiated with ultraviolet light, particles generate reactive oxygen species. In oxic conditions, particles release ions into surrounding matrix. In strongly acidic or basic conditions, particles are less likely to severely aggregate. In the presence of natural organic matter, particles seem to stabilize with after adsorption with organic matter. Taken together, these transformations forecast potential environmental effects.

In addition to complexation with natural organic matter, nanomaterials are exposed to ultraviolet radiation from the sun. In the natural water, organic matter can also absorb radiation and would generate reactive oxygen species, such as $^1O_2$, ●OH, and O_2●- (Zhang, Yan et al. 2014, Zhou, Lian et al. 2017). The concentrations of reactive species depend on nature and sources organic species as well as the matrices containing

metal ions (Wan, Sharma et al. 2019). Therefore, the release of metal ions from the nanomaterials is important. Titania nanocrystals did not react differently in either oxic or anoxic conditions. This contrasts with copper and silver nanoparticles, which both had nine times and seven times increase in metal ion concentration, respectively, over time. Both copper and silver nanoparticles readily produce reactive oxygen species after ultraviolet radiation while titania nanocrystals do not. Similarly, copper and silver nanoparticles readily release ions from their particle surfaces while titania nanocrystals do not. These relationships are correlative and possibly causative. It has been seen that natural light induces dissociation of ions from nanoparticle surfaces. Furthermore, surface oxidation on metal nanomaterial surfaces is inversely related to reactive oxygen species and directly proportional to metal ion generation (Albanese, Tang et al. 2012, Fu, Xia et al. 2014). Additionally, the size of the nanoparticle may also influence reactive oxygen species and metal ion generation (Carlson, Hussain et al. 2008).

The results of the study will aid in characterizing the transportation and transformation of nanomaterial predictions as well as their possible fate and effects in the aquatic environment. The transformation of metal-based nanomaterials in the environment is a culmination of pH, dissolved oxygen content, natural organic matter concentration, and light illumination. The production of reactive oxygen species in environmental systems may forecast potential toxicological effects. This research will enable the understanding of the chemical and toxicological mechanisms of metal particles and the resulting transformed products in the aquatic environment. In the previous chapters important physicochemical characterization techniques were identified in addition to understanding important toxicological mechanisms when nanomaterials

undergo environmental transformations. The next question aims to answer what important mechanisms are at play when nanomaterials are transformed and then incubated with a known *in vitro* model. Furthermore, the next chapter provides information regarding nanomaterials surface charge and the influence of transformations in physiologically relevant conditions.

References

Adegboyega, N. F., V. K. Sharma, L. Cizmas and C. M. Sayes (2016). "UV light induces Ag nanoparticle formation: roles of natural organic matter, iron, and oxygen." Environmental Chemistry Letters 14(3): 353-357.

Adegboyega, N. F., V. K. Sharma, K. M. Siskova, R. Vecerova, M. Kolar, R. Zbořil and J. L. Gardea-Torresdey (2014). "Enhanced formation of silver nanoparticles in Ag+-NOM-iron (II, III) systems and antibacterial activity studies." Environmental science & technology 48(6): 3228-3235.

Ahn, E. C., H. S. P. Wong and E. Pop (2018). "Carbon nanomaterials for non-volatile memories." Nature Reviews Materials 3(3): 1-15.

Akaighe, N., R. I. MacCuspie, D. A. Navarro, D. S. Aga, S. Banerjee, M. Sohn and V. K. Sharma (2011). "Humic acid-induced silver nanoparticle formation under environmentally relevant conditions." Environmental science & technology 45(9): 3895-3901.

Albanese, A., P. S. Tang and W. C. W. Chan (2012). "The effect of nanoparticle size, shape, and surface chemistry on biological systems." Annual review of biomedical engineering 14: 1-16.

Alivio, T. E. G., N. A. Fleer, J. Singh, G. Nadadur, M. Feng, S. Banerjee and V. K. Sharma (2018). "Stabilization of Ag–Au Bimetallic Nanocrystals in Aquatic Environments Mediated by Dissolved Organic Matter: A Mechanistic Perspective." Environmental science & technology 52(13): 7269-7278.

Amde, M., J.-f. Liu, Z.-Q. Tan and D. Bekana (2017). "Transformation and bioavailability of metal oxide nanoparticles in aquatic and terrestrial environments. A review." Environmental Pollution 230: 250-267.

Bäuerlein, P. S., E. Emke, P. Tromp, J. A. M. H. Hofman, A. Carboni, F. Schooneman, P. de Voogt and A. P. van Wezel (2017). "Is there evidence for man-made nanoparticles in the Dutch environment?" Science of the Total Environment 576: 273-283.

Carlson, C., S. M. Hussain, A. M. Schrand, L. K. Braydich-Stolle, K. L. Hess, R. L. Jones and J. J. Schlager (2008). "Unique cellular interaction of silver nanoparticles: size-dependent generation of reactive oxygen species." The journal of physical chemistry B 112(43): 13608-13619.

Fu, P. P., Q. Xia, H.-M. Hwang, P. C. Ray and H. Yu (2014). "Mechanisms of nanotoxicity: generation of reactive oxygen species." Journal of food and drug analysis 22(1): 64-75.

Gao, X., S. n. M. Rodrigues, E. Spielman-Sun, S. n. Lopes, S. Rodrigues, Y. Zhang, A. Avellan, R. M. B. O. Duarte, A. Duarte and E. A. Casman (2019). "Effect of soil organic matter, soil pH, and moisture content on solubility and dissolution rate of CuO NPs in soil." Environmental science & technology 53(9): 4959-4967.

Garner, K. L. and A. A. Keller (2014). "Emerging patterns for engineered nanomaterials in the environment: a review of fate and toxicity studies." Journal of Nanoparticle Research 16(8): 2503.

Garner, K. L., S. Suh and A. A. Keller (2017). "Assessing the Risk of Engineered Nanomaterials in the Environment: Development and Application of the nanoFate Model." Environmental Science & Technology 51(10): 5541-5551.

Georgantzopoulou, A., P. Almeida Carvalho, C. Vogelsang, M. Tilahun, K. Ndungu, A. M. Booth, K. V. Thomas and A. Macken (2018). "Ecotoxicological effects of transformed silver and titanium dioxide nanoparticles in the effluent from a lab-scale wastewater treatment system." Environmental science & technology 52(16): 9431-9441.

He, D., S. Garg and T. D. Waite (2012). "H2O2-mediated oxidation of zero-valent silver and resultant interactions among silver nanoparticles, silver ions, and reactive oxygen species." Langmuir 28(27): 10266-10275.

He, D., A. M. Jones, S. Garg, A. N. Pham and T. D. Waite (2011). "Silver nanoparticle− reactive oxygen species interactions: application of a charging− discharging model." The Journal of Physical Chemistry C 115(13): 5461-5468.

Hedberg, J., E. Blomberg and I. Odnevall Wallinder (2019). "In the search for nanospecific effects of dissolution of metallic nanoparticles at freshwater-like conditions: A critical review." Environmental science & technology 53(8): 4030-4044.

Hou, W.-C., B. Stuart, R. Howes and R. G. Zepp (2013). "Sunlight-driven reduction of silver ions by natural organic matter: formation and transformation of silver nanoparticles." Environmental science & technology 47(14): 7713-7721.

Huang, Y.-N., T.-T. Qian, F. Dang, Y.-G. Yin, M. Li and D.-M. Zhou (2019). "Significant contribution of metastable particulate organic matter to natural formation of silver nanoparticles in soils." Nature communications 10(1): 1-8.

Irandost, M., R. Akbarzadeh, M. Pirsaheb, A. Asadi, P. Mohammadi and M. Sillanpää (2019). "Fabrication of highly visible active N, S co-doped TiO2@ MoS2 heterojunction with synergistic effect for photocatalytic degradation of diclofenac: Mechanisms, modeling and degradation pathway." Journal of Molecular Liquids 291: 111342.

Joo, S. H. and D. Zhao (2017). "Environmental dynamics of metal oxide nanoparticles in heterogeneous systems: a review." Journal of hazardous materials 322: 29-47.

Kaur, M., M. Kaur and V. K. Sharma (2018). "Nitrogen-doped graphene and graphene quantum dots: A review onsynthesis and applications in energy, sensors and environment." Advances in colloid and interface science 259: 44-64.

Keller, A. A. and A. Lazareva (2014). "Predicted releases of engineered nanomaterials: from global to regional to local." Environmental Science & Technology Letters 1(1): 65-70.

Kim, Y., J. G. Smith and P. K. Jain (2018). "Harvesting multiple electron–hole pairs generated through plasmonic excitation of Au nanoparticles." Nature chemistry 10(7): 763-769.

Lewinski, N., V. Colvin and R. Drezek (2008). "Cytotoxicity of nanoparticles." small 4(1): 26-49.

Li, K., J. Qian, P. Wang, C. Wang, X. Fan, B. Lu, X. Tian, W. Jin, X. He and W. Guo (2019). "Toxicity of three crystalline TiO2 nanoparticles in activated sludge: bacterial cell death modes differentially weaken sludge dewaterability." Environmental science & technology 53(8): 4542-4555.

Liu, J. and R. H. Hurt (2010). "Ion release kinetics and particle persistence in aqueous nano-silver colloids." Environmental science & technology 44(6): 2169-2175.

Lowry, G. V., B. P. Espinasse, A. R. Badireddy, C. J. Richardson, B. C. Reinsch, L. D. Bryant, A. J. Bone, A. Deonarine, S. Chae and M. Therezien (2012). "Long-term transformation and fate of manufactured Ag nanoparticles in a simulated large scale freshwater emergent wetland." Environmental science & technology 46(13): 7027-7036.

Nasseri, S., M. O. Borna, A. Esrafili, R. R. Kalantary, B. Kakavandi, M. Sillanpää and A. Asadi (2018). "Photocatalytic degradation of malathion using Zn 2+-doped TiO 2 nanoparticles: statistical analysis and optimization of operating parameters." Applied Physics A 124(2): 175.

Ortelli, S., A. L. Costa, M. Blosi, A. Brunelli, E. Badetti, A. Bonetto, D. Hristozov and A. Marcomini (2017). "Colloidal characterization of CuO nanoparticles in biological and environmental media." Environmental Science: Nano 4(6): 1264-1272.

Pati, S. S., L. H. Singh, E. M. Guimarães, J. Mantilla, J. A. H. Coaquira, A. C. Oliveira, V. K. Sharma and V. K. Garg (2016). "Magnetic chitosan-functionalized Fe3O4@ Au nanoparticles: Synthesis and characterization." Journal of Alloys and Compounds 684: 68-74.

Pham, T. D., T. T. Bui, V. T. Nguyen, T. K. V. Bui, T. T. Tran, Q. C. Phan, T. D. Pham and T. H. Hoang (2018). "Adsorption of polyelectrolyte onto nanosilica synthesized from rice husk: characteristics, mechanisms, and application for antibiotic removal." Polymers 10(2): 220.

Quigg, A., W.-C. Chin, C.-S. Chen, S. Zhang, Y. Jiang, A.-J. Miao, K. A. Schwehr, C. Xu and P. H. Santschi (2013). "Direct and indirect toxic effects of engineered nanoparticles on algae: role of natural organic matter." ACS Sustainable Chemistry & Engineering 1(7): 686-702.

Rai, P. K., V. Kumar, S. Lee, N. Raza, K.-H. Kim, Y. S. Ok and D. C. W. Tsang (2018). "Nanoparticle-plant interaction: Implications in energy, environment, and agriculture." Environment international 119: 1-19.

Ranjan, S. and C. Ramalingam (2016). "Titanium dioxide nanoparticles induce bacterial membrane rupture by reactive oxygen species generation." Environmental Chemistry Letters 14(4): 487-494.

Romoser, A., D. Ritter, R. Majitha, K. E. Meissner, M. McShane and C. M. Sayes (2011). "Mitigation of quantum dot cytotoxicity by microencapsulation." PLoS One 6(7): e22079.

Rong, H., S. Garg and T. D. Waite (2019). "Impact of light and Suwanee River Fulvic Acid on O2 and H2O2 Mediated Oxidation of Silver Nanoparticles in Simulated Natural Waters." Environmental science & technology 53(12): 6688-6698.

Sani-Kast, N., J. Labille, P. Ollivier, D. Slomberg, K. Hungerbühler and M. Scheringer (2017). "A network perspective reveals decreasing material diversity in studies on nanoparticle interactions with dissolved organic matter." Proceedings of the National Academy of Sciences 114(10): E1756-E1765.

Selvaraj, V., S. Bodapati, E. Murray, K. M. Rice, N. Winston, T. Shokuhfar, Y. Zhao and E. Blough (2014). "Cytotoxicity and genotoxicity caused by yttrium oxide nanoparticles in HEK293 cells." International journal of nanomedicine 9:1379.

Sharma, V. K. (2009). "Aggregation and toxicity of titanium dioxide nanoparticles in aquatic environment—a review." Journal of Environmental Science and Health Part A 44(14): 1485-1495.

Sharma, V. K., J. Filip, R. Zboril and R. S. Varma (2015). "Natural inorganic nanoparticles–formation, fate, and toxicity in the environment." Chemical Society Reviews 44(23): 8410-8423.

Sharma, V. K., C. M. Sayes, B. Guo, S. Pillai, J. G. Parsons, C. Wang, B. Yan and X. Ma (2019). "Interactions between silver nanoparticles and other metal nanoparticles under environmentally relevant conditions: A review." Science of The Total Environment 653: 1042-1051.

Sharma, V. K. and R. Zboril (2017). Silver Nanoparticles in Natural Environment: Formation, Fate, and Toxicity. Bioactivity of Engineered Nanoparticles, Springer: 239-258.

Shevlin, D., N. O'Brien and E. Cummins (2018). "Silver engineered nanoparticles in freshwater systems–Likely fate and behaviour through natural attenuation processes." Science of the total environment 621: 1033-1046.

Simeone, F. C., M. Blosi, S. Ortelli and A. L. Costa (2019). "Assessing occupational risk in designs of production processes of nano-materials." NanoImpact 14: 100149.

Stebounova, L. V., E. Guio and V. H. Grassian (2011). "Silver nanoparticles in simulated biological media: a study of aggregation, sedimentation, and dissolution." Journal of Nanoparticle Research 13(1): 233-244.

Ubaid, K. A., X. Zhang, V. K. Sharma and L. Li (2019). "Fate and risk of metal sulfide nanoparticles in the environment." Environmental Chemistry Letters: 1-15.

Vishnuvarthanan, M. and N. Rajeswari (2019). "Food packaging: pectin–laponite–Ag nanoparticle bionanocomposite coated on polypropylene shows low O 2 transmission, low Ag migration and high antimicrobial activity." Environmental Chemistry Letters 17(1): 439-445.

Wan, D., V. K. Sharma, L. Liu, Y. Zuo and Y. Chen (2019). "Mechanistic insight into the effect of metal ions on photogeneration of reactive species from dissolved organic matter." Environmental science & technology 53(10): 5778-5786.

Wang, K., S. Garg and T. D. Waite (2017). "Light-mediated reactive oxygen species generation and iron redox transformations in the presence of exudate from the cyanobacterium Microcystis aeruginosa." Environmental science & technology 51(15): 8384-8395.

Wang, P., N. W. Menzies, H. Chen, X. Yang, S. P. McGrath, F.-J. Zhao and P. M. Kopittke (2018). "Risk of silver transfer from soil to the food chain is low after long-term (20 years) field applications of sewage sludge." Environmental science & technology 52(8): 4901-4909.

Westerhoff, P., A. Atkinson, J. Fortner, M. S. Wong, J. Zimmerman, J. Gardea-Torresdey, J. Ranville and P. Herckes (2018). "Low risk posed by engineered and incidental nanoparticles in drinking water." Nature nanotechnology 13(8): 661-669.

Westesen, K., H. Bunjes and M. H. J. Koch (1997). "Physicochemical characterization of lipid nanoparticles and evaluation of their drug loading capacity and sustained release potential." Journal of controlled release 48(2-3): 223-236.

Xu, J., J. Li, R. Zhang, J. He, Y. Chen, N. Bi, Y. Song, L. Wang, Q. Zhan and Z. Abliz (2019). "Development of a metabolic pathway-based pseudo-targeted metabolomics method using liquid chromatography coupled with mass spectrometry." Talanta 192: 160-168.

Yin, Y., D. Han, C. Tai, Z. Tan, X. Zhou, S. Yu, J. Liu and G. Jiang (2017). "Catalytic role of iron in the formation of silver nanoparticles in photo-irradiated Ag+-dissolved organic matter solution." Environmental Pollution 225: 66-73.

Yin, Y., J. Liu and G. Jiang (2012). "Sunlight-induced reduction of ionic Ag and Au to metallic nanoparticles by dissolved organic matter." ACS nano 6(9): 7910-7919.

Yin, Y., W. Xu, Z. Tan, Y. Li, W. Wang, X. Guo, S. Yu, J. Liu and G. Jiang (2017). "Photo-and thermo-chemical transformation of AgCl and Ag2S in environmental matrices and its implication." Environmental Pollution 220: 955-962.

Zhang, D., S. Yan and W. Song (2014). "Photochemically induced formation of reactive oxygen species (ROS) from effluent organic matter." Environmental science & technology 48(21): 12645-12653.

Zhang, X., Z. Xu, A. Wimmer, H. Zhang, J. Wang, Q. Bao, Z. Gu, M. Zhu, L. Zeng and L. Li (2018). "Mechanism for sulfidation of silver nanoparticles by copper sulfide in water under aerobic conditions." Environmental Science: Nano 5(12): 2819-2829.

Zhou, H., L. Lian, S. Yan and W. Song (2017). "Insights into the photo-induced formation of reactive intermediates from effluent organic matter: the role of chemical constituents." Water research 112: 120-128.

CHAPTER THREE

How to Determine the Toxicity of Nanomaterials at the Nexus of Nanomaterial Biotransformation, Surface Charge Influence, and Environmental Impact

This chapter published as: Mulenos, M. R., Lujan, H., Pitts, L. R., & Sayes, C. M. (2020). Silver Nanoparticles Agglomerate Intracellularly Depending on the Stabilizing Agent: Implications for Nanomedicine Efficacy. Nanomaterials, 10(10), 1953.)

Abstract

Engineered nanoparticles are utilized as drug delivery carriers in modern medicine due to the high surface area and tailorable surface functionality. After *in vivo* administration, nanoparticles distribute and interact with biomolecules, such as polar proteins in serum, lipid membranes in cells, and high ionic conditions during digestion. Electrostatic forces and steric hindrances in a nanoparticle population are disturbed and particles agglomerate in biological fluids. Little is known about the stability of nanoparticles in relation to particle surface charge. Here, we compared three different surface-stabilized silver nanoparticles (50 nm) for intracellular agglomeration in human hepatocellular carcinoma cells (HepG2). Nanoparticles stabilized with branched polyethyleneimine conferred a positive surface charge, particles stabilized with lipoic acid conferred a negative surface charge, and particles stabilized with polyethylene glycol conferred a neutral surface charge. Particles were incubated in fetal bovine serum, simulated lung surfactant fluid, and simulated stomach digestion fluid. Each nanoparticle system was characterized via microscopic (transmission electron, fluorescence, and enhanced darkfield) and spectroscopic (hyperspectral, dynamic light scattering, and

ultraviolet-visible absorption) techniques. Results showed that nanoparticle transformation included cellular internalization, agglomeration, and degradation; and that these changes were surface charge dependent. Hyperspectral analyses showed that positively charged silver nanoparticles red-shifted in spectral analysis after transformation; where, negatively charged silver nanoparticles showed a blue-shift. Neutrally charged silver nanoparticles did not demonstrate significant spectral shifts. Spectral shifting indicates de-stabilization in particle suspension, which directly affects agglomeration intracellularly. These characteristics are translatable to critical quality attributes and can be exploited when developing nano-carriers for nanomedicine.

Introduction

Silver nanoparticles (AgNPs), first used in consumer health-related products in the late 1800s, continue to be incorporated into modern medicine due to their unique properties (Medici, Peana, Nurchi, & Zoroddu, 2019). Properties such as small size and large surface area, relative low toxicity, and stability while in suspension are useful as dr3 delivery carriers (DDCs) (Araújo et al., 2015; Yih & Al-Fandi, 2006). However, information regarding agglomeration or degradation of AgNPs after *in vivo* administration is scarce. Many studies suggest that silver ions leached from AgNP surface induce significant toxicity (Choi et al., 2008; Hadrup & Lam, 2014; Mulenos et al., 2020; Sharma et al., 2019). While most studies focus on the effects of silver on microorganisms in the environment, only a few examine the effects of AgNPs in mammalian or human physiologically relevant conditions (Cortese-Krott et al., 2009; Trickler et al., 2010; Vrček et al., 2016). Given the interest in using silver and other

metal-based nanoparticles as potential DDCs, it is imperative to gain a deeper understanding of potential nanoparticle transformations in biological fluids.

Substantial attention is given to the beginning and ending stages of nano-enabled drug product development pipelines (Duvall, 2012; Zheng, Sun, Zou, & Jiang, 2017). Quality-by-design approaches in nanomaterial manufacturing, risk analyses, and hazard assessments are recommended to ensure safe and efficacious products. Physicochemical characterization (PCC) has served as in-situ critical quality attributes (CQA) enabling considerations for interactions between nano-enabled diagnostics, therapeutics, or theragnostics with different physiological fluids, such as cerebral fluids, blood and serum, lung surfactant, interstitial fluid, mucous, breast milk, digestion fluid, bile, and urine (Braydich-Stolle, Breitner, Comfort, Schlager, & Hussain, 2014; Cohen, DeLoid, Pyrgiotakis, & Demokritou, 2013). Due to the high variability of nanomaterials used in pharmaceutical research and development, CQAs are needed to improve and streamline synthesis and production methods, identify administration routes of exposure, prove efficacy in drug testing, and ensure biocompatibility during the ADME process (adsorption, distribution, metabolism, and excretion) (de Vlieger et al., 2019; Morrison et al., 2015). To-date, the most critical attributes of nano-enabled medicines are size homogeneity after production, consistent active ingredient concentration, and stability of product over time (Bobo, Robinson, Islam, Thurecht, & Corrie, 2016; Dawidczyk et al., 2014). Similar characteristics are applicable to other DDCs, such as liposomes, dendrimers, polymeric micelles, and other types of microspheres (Danaei et al., 2018; Lujan, Griffin, Taube, & Sayes, 2019; Rizvi & Saleh, 2018).

Currently, one of the most extensively studied surface coating used in nanomedicine research and development is polyethylene glycol (PEG). Other relevant surface stabilizing agents include branched polyethyleneimine (bPEI), citrate, ascorbic acid, and oleic acid. bPEI is a common cationic coating and electro-steric stabilizing agent used in drug products (Badawy et al., 2010). Studies using environmental models have found that bPEI coatings induce nanoparticle bioaccumulation and teratogenicity in aquatic organisms (Colombo et al., 2017; Gitipour, Thiel, Scheckel, & Tolaymat, 2016; Silva et al., 2014). Citrate and ascorbic acid stabilized nanoparticles have proposed use in dentistry, as these stabilizing agents have been shown to eradicate biofilm formation, while being a less toxic option relative to other types of antibiotics (Niska et al., 2016). Citrate, ascorbic acid, and oleic acid coatings create a charge barrier preventing intracellular uptake when compared to bPEI or PEG (Chandran, Riviere, & Monteiro-Riviere, 2017). Still, PEG is often the preferred choice for nanoparticle stability in nanomedicine formulations because this agent protects particles from reticuloendothelial system elimination (Kaminskas et al., 2008).

Greater focus is given to AgNP transformation in environmentally relevant conditions as compared to AgNPs subjected to physiologically relevant conditions. Of the limited information available for characteristics of AgNP in biofluids, most data focus on the nanoparticle protein corona construct (Cedervall et al., 2007; Giudice, Herda, Polo, & Dawson, 2016; Tenzer et al., 2013b). Protein corona studies are relevant to nanoparticle transformations administered through intramuscular, subcutaneous, intravenous, or intradermal injection. However, other routes of nanomedicine exposure introduce additional types of complex nanoparticle interactions, transformations, agglomeration,

and degradation (Liu, Wang, Liu, Kane, & Hurt, 2012). Other administration routes include oral, nasal, inhalation, ocular, and transmucosal including buccal, vaginal, rectal, and transdermal (H. Li et al., 2013). When nanomedicine exposure occurs orally, nanoparticles are subjected to saliva and stomach acid digestion. Through nasal, ocular, and transmucosal administrations, nanoparticles are subjected to mucosa. Through inhalation, nanoparticles are subjected to lung surfactant fluid. Through transdermal routes, nanoparticles are subjected to sebum.

Given that nanoparticles are currently used in drug delivery systems, the goal of this study was to compare the effects of surface stabilizing agents, and induced surface charge, on nanoparticle physiologically relevant transformation, including cellular internalization, agglomeration, and degradation. We utilize hyperspectral imaging coupled with a battery of analytical techniques and human hepatocellular carcinoma (HepG2) cells for this evaluation. We transformed three different AgNPs (50 nm); nanoparticles stabilized with branched polyethyleneimine (bPEI) conferred a positive surface charge, nanoparticles stabilized with lipoic acid conferred a negative surface charge, and nanoparticles stabilized with polyethylene glycol (PEG) conferred a neutral surface charge. Each nanoparticle system was incubated with polar proteins from serum, lipid membranes from surfactant fluid, and hydrochloric acid from gastric fluid. This work outlines a reproducible methodology that can be repeated when characterizing nano-enabled drug product transformations after administration. These characteristics are translatable to critical quality attributes and can be exploited to develop complex *in vitro*, *in vivo*, or *in silico* models for nanomedicine and associated risk analyses.

Methods and Materials

Silver Nanoparticles

All nanoparticles used in this study were purchased from NanoComposix (San Diego, CA, United States) at a concentration of 1 mg/mL. Per manufacturer's certificate of analysis, the three AgNPs included (1) branched polyethyleneimine polymer (1 mg/mL) at 25 kDa bound with primary amines to the silver nanoparticle surface (termed, Pos-AgNP), (2) carboxyl lipoic acid (1 mg/mL) covalently bound with a dithiol to the silver nanoparticle surface (termed Neg-AgNP), and (3) methoxy-polyethylene glycol coated silver nanoparticles (1 mg/mL) (termed Neu-AgNP).

Incubation Scenarios

Aliquots of AgNPs were incubated in three different scenarios to simulate protein adsorption, lipid interaction, and stomach acid dissolution. For Scenario 1, i.e. protein absorption simulating intravenous injection, AgNPs were separately incubated in USDA-approved fetal bovine serum (FBS; Gibco, Thermo Fischer Scientific, Waltham, MA, United States). For Scenario 2, i.e. lipid interaction simulating inhalation administration into surfactant fluid, AgNPs were incubated with a mixture of ovine cholesterol derived lipids (Avanti Polar Lipids, Alabaster, AL, United States) and didodecyldimethylammonium bromide surfactant solution (Sigma-Aldrich, St. Louis, MO, United States). For Scenario 3, i.e. stomach acid incubation simulating oral administration, AgNPs were incubated in hydrochloric acid supplemented with porcine stomach enzymes (Thermo Fischer Scientific, Waltham, MA, United States). All nanoparticle simulations were performed at 37°C after a 24-hr post-exposure time

period. The concentration of silver in all resultant samples was 0.5 mg/mL, unless otherwise indicated.

Dynamic Light Scattering

Hydrodynamic diameter, dispersity index, and zeta potential analyses were performed via DLS spectroscopy with a Zetasizer Nano ZS spectrometer (Malvern Panalytical, Malvern, United Kingdom) at 25°C (Supplemental Figure 3.1.). All measurements were performed in a 1060-folded capillary zeta cell (Malvern Panalytical, Malvern, United Kingdom) at a 1:1,000 dilution in ultrapure water (18 Ω s, MilliQ Ultrapure water purification system, GenPure-Thermo Fischer Scientific, Waltham, MA, United States). Hydrodynamic diameter and dispersity index analyses were performed with 11 replicates per sample and ran in triplicate; zeta potential measurements were performed with 50 replicates per sample and ran in triplicate. Measurements were taken before and after AgNP transformation.

Transmission Electron Microscopy

Nanoparticle morphology was assessed by TEM (JEM-1010, JEOL Inc., Akishima, Tokyo, Japan). AgNPs were collected at 24 hrs. post-incubation and deposited on a copper formvar coated grid (EMS, Hatfield, PA, United States) for 5 minutes. Once dried, loaded grids were imaged on a transmission electron microscope with a spot size of 2.0 and an acceleration voltage of 60 kV. ImageJ software was used for image analyses.

Hepatocyte Cell Culture

Human hepatocellular carcinoma cells (HepG2) were cultured in Eagle's Minimum Essential Medium (Gibco, Thermo Fisher Scientific, Waltham, MA, Unites

States) supplemented with 10% fetal bovine serum (FBS; Equitech-Bio, Inc. Kerrville, TX, United States) and a 1% penicillin/streptomycin mixture (MP Biomedical, Solon, OH, United States). Cells were cultured in an air-jacked humidified incubator at 37°C with 5% CO_2. Once cells were grown to 70% confluency, they were inoculated with a 1 μg/mL suspension of transformed AgNP systems for 24 hrs.

Fluorescent Imaging

Cellular morphology was assessed via fluorescent imaging. HepG2 cells were prepared for imaging by plating into chamber slides coated for adherent cells (Nunc, Lab-Tek Chamber Slide, Thermo Scientific, Waltham, MA, United States) and grown to 70% confluency. Cells were inoculated with a 1 μg/mL suspension of AgNP systems for 24 hrs. and then prepared with the Image-iT Fixation/Permeabilization kit (Thermo Fisher Scientific, Waltham, MA, United States.) Fluorescent dyes used were MitoTracker Red CM-H2-XRos (579/599 nm) to visualize reactive oxygen species, NucBlue LiveReadyProbes (360/430 nm) to visualize the nucleus, and ActinGreen 488 ReadyProbes (495/518 nm) Reagent (AlexaFluor 488 phalloidin) to visualize the cytoskeleton. To preserve the slides, ProLong Diamond Antifade Mountant was used. All cell slide preparation items were purchased from Thermo Fischer (Waltham, MA, United States).

Subsequently, the preserved cells were imaged using a CytoViva® Fluorescent microscope with Fluorescent excitation cubes for DAPI, FITC, and TRITC. (Auburn, AL, United States) with a 40X oil-immersion lens.

Hyperspectral Imaging Acquisition and Data Analysis

Samples were prepared as stated above in the fluorescence imaging section. Enhanced darkfield imaging was acquired using a 40X lens using the CytoViva® Hyperspectral System. (Auburn, AL, United States). Exposure time of 0.25 s was used, with high spatial resolution, and a 2.5 nm spectral resolution. The field of view was selected utilizing positioning from the fluorescent images. Intensities of each sample used were between 2000-3500 to ensure enough spectra data. Once images were collected, they were enhanced using the linear 2% function to visualize the nanoparticles intracellularly. Spectral libraries were created with nanoparticles that were taken up into cells, and spectra were averaged from 30 selected regions of interest (ROI). Data presented is the normalized mean ROI data with cellular and background corrections. Baseline samples were created with nanoparticles before incubation in physiological scenarios as well as a sample of the HepG2 cells.

Inductively Coupled Plasma-Mass Spectrometry

Samples were analyzed for dissolution as a function of time using inductively coupled plasma-mass spectrometry (ICP-MS) (Supplemental Figure 3.2.). Samples were subjected to simulated incubations for 1, 24, and 48 hrs. Silver ions were isolated from the nanoparticles and surrounding solution through centrifugation. Once centrifuged, an aliquot of the supernatant was collected for acid digestion. The metal isotope calibration standard (SPEX CertiPrep, Thermo Fischer Scientific, Waltham, MA, United States), sample aliquots, method blank (consisting of each transformation solution mentioned above), and an acid blank were placed in digestion tubes and a 1:4 mixture of hydrochloric acid to nitric acid solution was added. A watch glass was placed over top

and the digestion was prepared for 2 hrs. at 95°C in a heat block. Hydrochloric acid, nitric acid, plastic digestion tubes, and plastic watch glasses were TraceMetalGrade and purchased from Thermo Fischer Scientific (Waltham, MA, United States). After digestion, samples were filtered (0.2µm) and diluted with ultrapure water to an end acidic concentration of 2%. An internal standard mix (Agilent Technologies, Santa Clara, CA, United States) was used for drift correction. All measurements were acquired on an Agilent ICP-MS 7900 from Agilent Technologies (Santa Clara, CA, United States). Runs were performed in triplicate with isotopes 107Ag and 109Ag monitored. All data analysis was performed using MassHunter software (Agilent Technologies, Santa Clara, CA, United States).

Ultraviolet-Visible Absorption Spectroscopy

UV-Vis spectroscopy was used to assess Pos-AgNP, Neg-AgNP, and Neu-AgNP systems over time using a Lambda 35 photospectrometer (Perkin Elmer, Waltham, MA, United States) (Supplemental Figure 3.3.). Data was analyzed on UV WinLab software (PerkinElmer, Waltham, MA, United States). Ultrapure water was used as a blank and dilutant producing a 1:2 dilution of the original sample for analysis. In a quartz cuvette, scans were obtained from 200-800 nm in three separate sessions during each time point in triplicate.

Statistical Analyses

To perform statistical analysis, standard deviation and standard error were performed with Excel (Microsoft, Redmond, WA, United States). Spectral averaging and

normalization were completed with ENVI software. (Cytoviva, Auburn, AL, United States). Spectral were plotted with GraphPad Prism (San Diego, CA, United States).

Results and Discussion

Experimental Design

In this study three different potential biofluids, relevant to nanomedicine administration routes, were produced and used to study potential silver nanoparticle (AgNP) transformations. Incubation of AgNPs with fetal bovine serum, ovine cholesterol-derived lipids, and simulated gastric fluid are referred to as Scenario 1, 2, and 3, respectively. Scenario 1 represents nanoparticles administered intravenously and interactions with serum proteins. Scenario 2 represents nanoparticle inhalation and interactions with interstitial fluid. Scenario 3 represents oral administration and interaction with stomach acid. For each scenario, nanoparticle suspensions were incubated for 24 hours at 37 °C. Figure 3.1. outlines the experimental details inclusive of nanoparticle characterization, incubation parameters, and endpoint analyses. The branched polyethyleneimine-stabilized silver nanoparticles are termed ‘Pos-AgNPs’; the lipoic acid-stabilized silver nanoparticles are termed ‘Neg-AgNPs’; and the methoxy polyethylene glycol-stabilized silver nanoparticles are termed ‘Neu-AgNPs’. A comprehensive physicochemical characterization was completed prior to transformations to determine concentration and enable comparisons post-incubation.

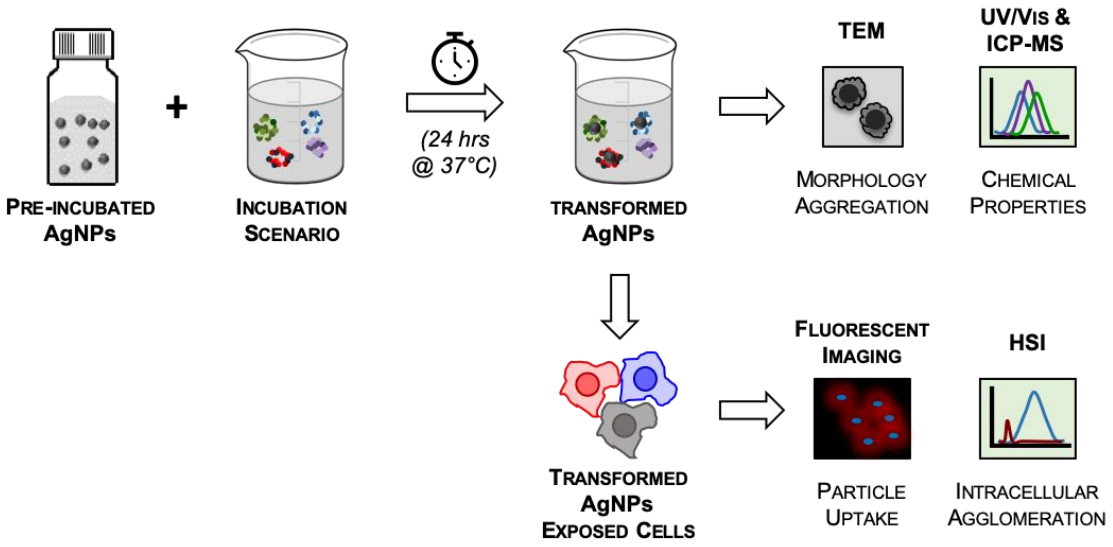

Figure 3.1. The experimental design used in this study. First, positive, negative, and neutral surface charged AgNPs were suspended in ultrapure water in separate stock suspensions. Second, each of the AgNP systems was subjected to one of three incubation scenarios for 1, 24, and 48 h. Third, analyses of transformed nanoparticles using TEM (transmission electron microscopy) and HSI (hyperspectral imaging) among other techniques.

Simulations of Scenario 1, i.e. nanoparticle interactions with polar biomolecules within the circulatory system, has been previously studied (Cedervall et al., 2007; Corbo et al., 2016; Lundqvist et al., 2008; Oh et al., 2018; Tenzer et al., 2013a). Data shows that nanoparticle size, surface charge, and stabilizing agents influence protein corona formation (Supplemental Figure 3.3.). Nanoparticle protein corona is the self-assembly of absorbed proteins on the particle surface. The nanoparticle surface and size determine the amount, identity, polarity, and arrangement of the protein corona, while also influencing downstream effects of distribution, metabolism, and excretion (Cedervall et al., 2007; Lundqvist et al., 2008; Tenzer et al., 2013a). Depending on the nanomedicine application, the formation of a protein corona could either be efficacious or produce an ineffective biological response (Corbo et al., 2016; Oh et al., 2018). Previous studies

show that the protein corona can act as a cloaking shield during targeted drug delivery; a pre-coating of proteins can reduce the particle-protein interactions *in vitro*. In contrast, the development of the protein corona on the surface of the nanomedicine may render the therapeutic agent detrimental by routing the medicine to the wrong targets (Maiolo, Del Pino, Metrangolo, Parak, & Baldelli Bombelli, 2015).

Scenario 2 represents simulated interactions between nanoparticles and interstitial fluid after inhalation and incubation. The literature indicates that nanoparticle surfaces can be exploited to promote lipid raft transport across membranes (Elder, Vidyasagar, & DeLouise, 2009; Riediker et al., 2019). Interactions with lipids induce changes in surface properties as nanoparticles pass through cytoplasmic, mitochondrial, or nuclear membranes. Kang et al (2008a and 2008b) showed that positively charged AgNPs facilitate stable transport across olefin/paraffin separation membranes (Kang, Char, & Kang, 2008; Kang, Hong, et al., 2008). However, once internalized by the cell, the metal-based nanoparticles are likely to be shuttled into lysosomes where ions dissociate and induce cellular toxicity. Recent efforts are aimed at preparing nanoparticle surface coatings to shuttle active pharmaceutical ingredients into the cytoplasmic membrane and avoid cellular internalization. Identifying the surface charge and coating that partially interacts with lipid membranes while avoiding intracellular acidification aids in reducing adverse effects of nano-enabled drug carriers (Sabella et al., 2014).

Scenario 3 represents ingestion and digestion of orally administered nanoparticles. Most studies focus on AgNPs used in food products (DeLoid et al., 2017). Cueva et al (2019) showed that nanoparticles in simulated digestion are structurally different post-digestion, but do not alter the microbiota viability (Cueva et al., 2019). Other studies

have shown that citrate-coated nanoparticle aggregation is pH-dependent in the gastrointestinal tract. At pH of 2, nanoparticles form >100 nm aggregates, and at pH of 5, nanoparticles aggregate less and often degrade (Shi, Axson, Bergin, & Ault, 2020).

Engineered Nanoparticles for Nano-enabled Drug Products

To understand the potential transformations of AgNPs under the three different scenarios, physicochemical characterization of the nanoparticles was performed before incubation. Figure 3.2. highlights key characteristics of the pre-incubated nanoparticles. In solution, Pos-AgNP was positively charged (+73 mV) as measured by zeta potential; whereas Neg-AgNP and Neu-AgNP were both negatively charged with zeta potential values of -57 and -23 mV, respectively. It is generally regarded that nanoparticle surface charge, as measured by zeta potential, greater than +30 mV or less than -30 mV, indicates a stable nanoparticle suspension (Duman & Tunç, 2009). Therefore, any neutrally charged nanoparticle system (between -30 and +30 mV) is automatically considered to be unstable.

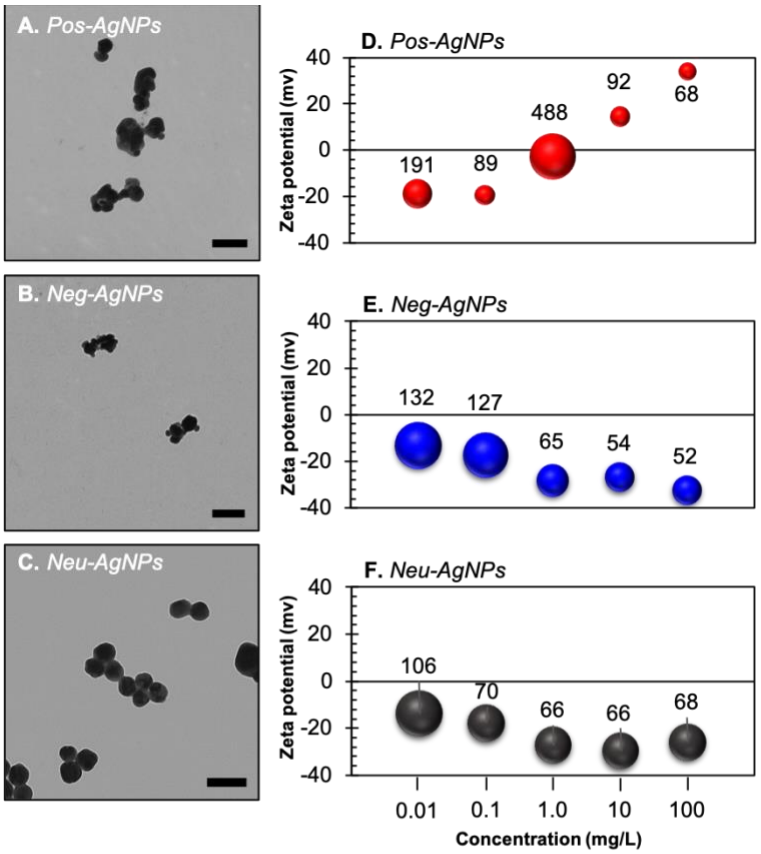

G	*Pos-AgNPs*	*Neg-AgNPs*	*Neu-AgNPs*
Surface charge *(manufacturer)*	Positive	Negative	Neutral
Particle surface *(manufacturer)*	branched Polyethylene-imine	Lipoic acid	Methoxy polyethylene glycol
Zeta potential (mV) *(in-house)*	+73.0 ± 5.90	-57 ± 3.78	-23 ± 6.09
Diameter, TEM (nm) *(in-house)*	47 ± 5	51 ± 5	49 ± 6
Hydrodynamic diameter (nm) *(in-house)*	92.0 ± 10.1	54.0 ± 4.88	66.0 ± 7.12
pH *(in-house)*	7.0	9.3	6.8
λ_{max} (nm) *(in-house)*	432	432	420

Figure 3.2. AgNPs physicochemical characterization before incubation. Representative TEM images of (A) Pos-AgNPs, (B) Neg-AgNPs, and (C) Neu-AgNPs used in this study. Scale bar indicates 50 nm. Changes in zeta potential measurements (indicated by data point) and hydrodynamic diameter (indicated by value above data point) over increasing AgNPs concentration in ultrapure water for (D) Pos-AgNPs, (E) Neg-AgNPs, and (F) Neu-AgNPs. (G) Table of properties measured in-house or provided by nanoparticle manufacturer.

Neu-AgNP with a zeta potential measurement of -23 mV indicates an unstable suspension. This observation is confirmed via transmission electron microscopy (TEM) where small nanoparticles aggregates are clearly present. Pos-AgNP and Neg-AgNP zeta potential values indicate stable suspensions. TEM analyses of pre-incubated Pos-AgNPs show slight agglomeration. Agglomeration could be due to drying effects produced during sample preparation (Dieckmann, Cölfen, Hofmann, & Petri-Fink, 2009; Michen et al., 2015). All three pre-incubated AgNP samples are spherical in shape and ~50 nm in diameter.

Nanoparticles (and nanoparticle agglomerates) below 20 nm in diameter are rapidly cleared by renal excretion. Nanoparticles (and nanoparticle agglomerates) larger than 200 nm in diameter are easily cleared by the reticuloendothelial system (Adabi et al., 2017; Moghimi, Hunter, & Murray, 2001). For these reasons, among others, nanomedicine research and development efforts have favored ~50 nm nanoparticle diameters to prolong systemic circulation and prevent unintended elimination.

Hyperspectral Imaging for Intracellular Agglomeration Analysis

Figure 3.3. shows data from enhanced darkfield hyperspectral imaging (HSI) for HepG2 cells exposed to nanoparticles. Darkfield images were collected using the Environment for Visualizing Images (ENVI) software. Corrections were performed to eliminate interferences from cell membranes, background, and lamp spectrum. A spectral library was created and only included the nanoparticles that were internalized within cells; nanoparticles on the cell surface or in the background were excluded. Regions of interest (ROIs) were obtained over an averaged spectrum of >25 nanoparticles per

sample. Data was normalized and compared to pre-incubated AgNPs where the averaged spectra are plotted in Figure 3.3.

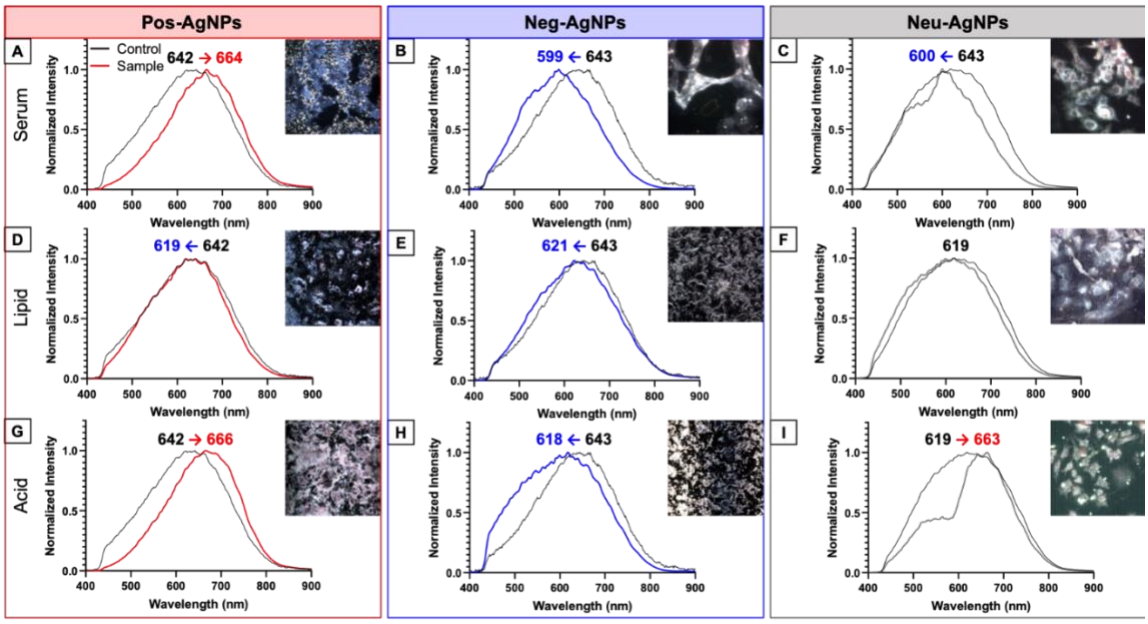

Figure 3.3. Enhanced darkfield and hyperspectral imaging of AgNPs subjected to incubation scenarios for 24 h and exposed HepG2 cells for an additional 24 h. (A) Pos-AgNPs, (B) Neg-AgNPs, and (C) Neu-AgNPs incubated in serum. (D) Pos-AgNPs, (E) Neg-AgNPs, and (F) Neu-AgNPs incubated in lipids. (G) Pos-AgNPs, (H) Neg-AgNPs, and (I) Neu-AgNPs incubated in acid. The number noted above each spectrum indicate pre-incubated λ_{max} (black font) and post-incubated λ_{max} (blue or red font).

Pos-AgNPs (Figure 3.3.A, G) showed a spectral shift to the right (i.e. an increase in wavelength), while the Neg-AgNPs (Figure 3.3.B, H) showed a spectral shift to the left (i.e. a decrease in wavelength). Neu-AgNPs showed differential spectral shifts depending on the incubation scenario. Regarding Scenario 1, a blue shift was observed (Figure 3.3.C), in contrast to Scenario 3 where a red shift was observed (Figure 3.3.I). After subjection to Scenario 2, AgNPs exhibited no shift in hyperspectral analysis (Figure 3.3.F). In fact, none of the AgNPs subjected to the lipid surfactant simulation (i.e. Scenario 2) showed a shift in hyperspectral analysis (Figure 3.3. D, E, F). Interestingly,

Scenario 2 did not have any effect on nanoparticle internalization, probably due to severe agglomeration (>500 nm) as seen in Figure 3.5.

Longer wavelengths of detected light (i.e. red shifts) observed in HSI is associated with an increase in nanoparticle size, or in this case, an increase in agglomeration. Shorter wavelengths (i.e. blue shifts) are indicative of a decrease in nanoparticle size, such as dissolution or de-aggregation, or partial degradation (Mortimer et al., 2014; Zucker, Ortenzio, Degn, Lerner, & Boyes, 2019). We show that Pos-AgNPs agglomerate intracellularly, whereas Neg-AgNPs and Neu-AgNPs tend to produce mixtures of single nanoparticles and small agglomerated nanoparticles independent of the scenarios. The transformation mechanism could involve the incomplete degradation of the AgNP surface stabilizing agent or the partial dissolution of silver cations (Ag^{+}) from nanoparticle surface. Ion dissolution was confirmed with inductively coupled plasma-mass spectrometry (ICP-MS) analyses (Supplemental Figure 3.2.). Either transformation mechanism could produce an increase in reactive oxygen species (ROS), oxidative stress, or phosphorylation of proteins, lipids, and enzymes (Lowry, Gregory, Apte, & Lead, 2012). AgNP surface charge and coating play roles in defining safety and efficacy critical attributes (Araújo et al., 2015; Yih & Al-Fandi, 2006).

Biotransformed Silver Nanoparticles used in Drug Products

Figure 3.4. shows AgNPs subjected to Scenario 1 (i.e. serum incubation). Dispersity index (a measure of polydispersity within the sample) was minimal (0.110, 0.335, and 0.154) for (Pos-AgNPs, Neg-AgNPs, and Neu-AgNPs), respectively. However, hydrodynamic diameter was large (102.8, 313.1, and 88.6 nm) for (Pos-AgNPs, Neg-AgNPs, and Neu-AgNPs), respectively. These data suggest particles

transformed to severely agglomerated entities. Agglomeration, in this scenario, is due to an abundance of proteins adsorbed on to the surface of each AgNP and subsequently creating a protein corona hindering nanoparticle stability by masking the stabilizing agent, as indicated by the similar zeta potential measurements (-25.2, -20.4, and -20.2 mV) for (Pos-AgNPs, Neg-AgNPs, and Neu-AgNPs), respectively. Neg-AgNPs had the largest change in DI, hydrodynamic diameter (HDD), and surface charge (as measured by zeta potential) compared to the Pos-AgNPs and Neu-AgNPs systems. This comparison may be the result of partial agglomeration and incomplete protein corona formation seen with TEM imaging (Figure 3.4.C-E).

All three AgNP systems underwent a significant biotransformation under Scenario 1. Agglomeration in this scenario occurs both extracellularly, i.e. when nanoparticle first interaction with serum proteins, as well as intracellularly as indicated by hyperspectral imaging. Human hepatocellular carcinoma cells (HepG2) were used for the intracellular analyses. When HepG2 cells were exposed to AgNP subjected to Scenario 1, no significant change in cell morphologies or biomarker expression was observed (Figure 3.4. F-H). This indicates that nanoparticle agglomeration may not induce unintended cellular effects but could deactivate any therapeutic activity presented by the nanoparticle carrier administered intravenously.

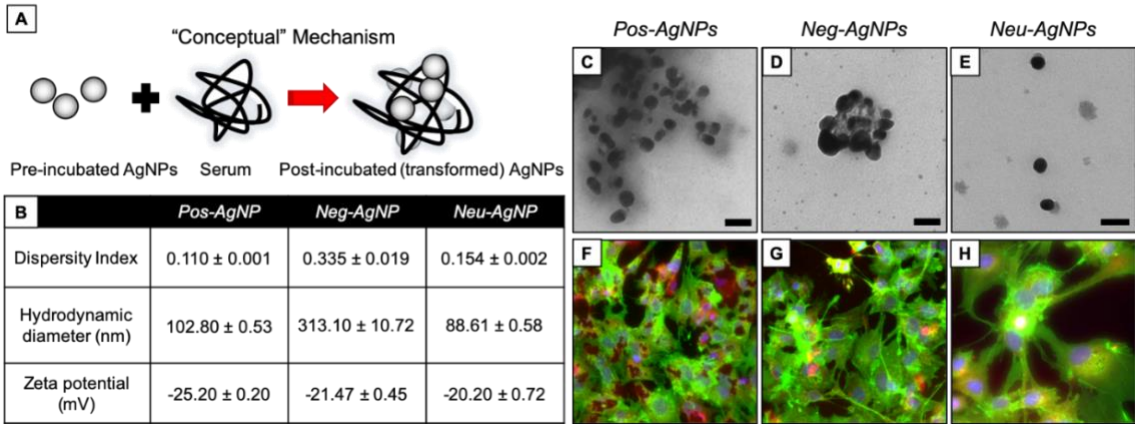

B	Pos-AgNP	Neg-AgNP	Neu-AgNP
Dispersity Index	0.110 ± 0.001	0.335 ± 0.019	0.154 ± 0.002
Hydrodynamic diameter (nm)	102.80 ± 0.53	313.10 ± 10.72	88.61 ± 0.58
Zeta potential (mV)	-25.20 ± 0.20	-21.47 ± 0.45	-20.20 ± 0.72

Figure 3.4. AgNP transformation after incubation in serum. (A) Conceptual model of transformation mechanisms. (B) Dispersity index (unitless), hydrodynamic diameter (nm), and zeta potential (mV) measurements of each particle type after simulated incubation. TEM of (C) Pos-AgNPs, (D) Neg-AgNPs, and (E) Neu-AgNPs after simulated incubation. Fluorescence microscopy of HepG2 cells after 24 h exposure to post-incubated (F) Pos-AgNPs, (G) Neg-AgNPs, and (H) Neu-AgNPs. Scale bars in (C-E) represent 50 nm. Stains in (F-H) include: DAPI (blue), F-actin (green), and MitoTracker (red).

Figure 3.5. shows AgNPs subjected to Scenario 2 (i.e. lipid surfactant incubation). In this scenario, Neg-AgNPs changed the most in DI, HDD, and zeta potential measurements compared to the Pos-AgNPs and Neu-AgNPs particle systems. The Pos-AgNP and Neu-AgNP systems became unstable as indicated by a change in zeta potential from their pre-incubated charges to unstable values of -25.43 ± 0.59 mV and -20.73 ± 1.06 mV, respectively. Neg-AgNPs, in contrast to the two other nanoparticles, had a stable zeta potential measurement at -31.40 ± 0.70mV. The Neg-AgNPs also agglomerated significantly with an HDD of 461.63 ± 61.57 nm, which is 3X and 7X greater than the size of either Pos-AgNP or Neu-AgNP systems. Neu-AgNP exhibited a lower DI and only changed -7 nm in HDD (i.e. 59.74 ± 0.64 nm), indicating subtle nanoparticle transformation. When examining the effects of Scenario 2 transformed AgNP systems to the HepG2 cells, Neg-AgNPs induced a significant amount of oxidative

stress on the cells when compared to either Pos-AgNP or Neu-AgNP systems (Figure 3.5.F-H). However, cytoskeletal degradation was observed in HepG2 cells exposed to Pos-AgNP in this scenario (Figure 3.5.F). No change is reported for the Neu-AgNP sample on HepG2 system.

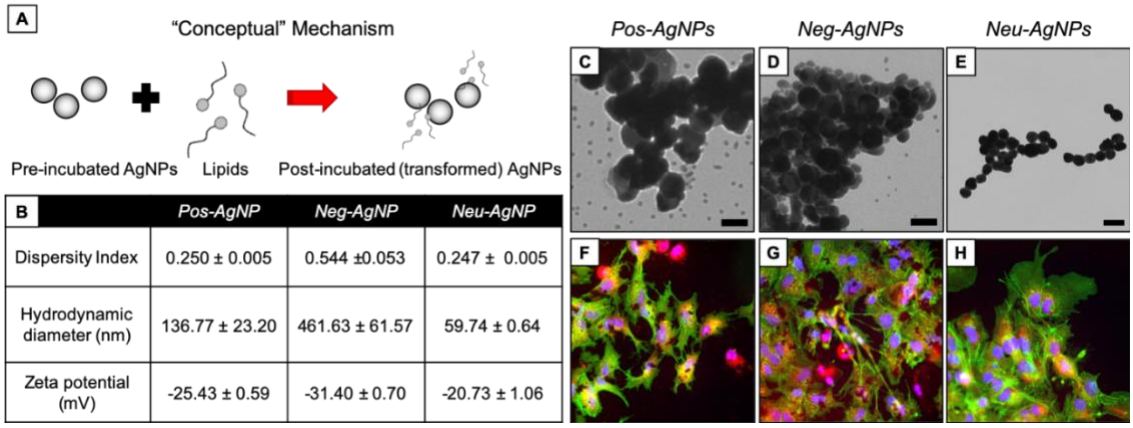

B	Pos-AgNP	Neg-AgNP	Neu-AgNP
Dispersity Index	0.250 ± 0.005	0.544 ±0.053	0.247 ± 0.005
Hydrodynamic diameter (nm)	136.77 ± 23.20	461.63 ± 61.57	59.74 ± 0.64
Zeta potential (mV)	-25.43 ± 0.59	-31.40 ± 0.70	-20.73 ± 1.06

Figure 3.5. AgNP transformation after incubation in lipids. (A) Conceptual model of transformation mechanisms. (B) Dispersity index (unitless), hydrodynamic diameter (nm), and zeta potential (mV) measurements of each particle type after simulated incubation. TEM of (C) Pos-AgNPs, (D) Neg-AgNPs, and (E) Neu-AgNPs after simulated incubation. Fluorescence microscopy of HepG2 cells after 24-hr exposure to post-incubated (F) Pos-AgNPs, (G) Neg-AgNPs, and (H) Neu-AgNPs. Scale bars in (C-E) represent 50 nm. Stains in (F-H) include: DAPI (blue), F-actin (green), and MitoTracker (red).

Figure 3.6. shows AgNPs subjected to Scenario 3 (i.e. stomach acid incubation). Like Scenario 1, the Pos-AgNP, Neg-AgNP, and Neu-AgNP systems became unstable as indicated by a change in zeta potential from their pre-incubated charges to unstable values of -16.63, -28.07, and -17.23, respectively. In this scenario, Neg-AgNPs and Pos-AgNPs agglomerated, where Neu-AgNPs decreased in HDD. This observation could be due to the increased likelihood of charged particles interacting with surrounding biomolecules and the high ionic concentration present in the scenario. In short, Neu-AgNPs simply degraded in the acidic environment. When examining the effects of

Scenario 3 transformed AgNP systems to the HepG2 cells, Pos-AgNPs induced a significant amount of oxidative stress and cytoskeleton damage on the cells when compared to either Neg-AgNP or Neu-AgNP systems (Figure 3.6.F-H).

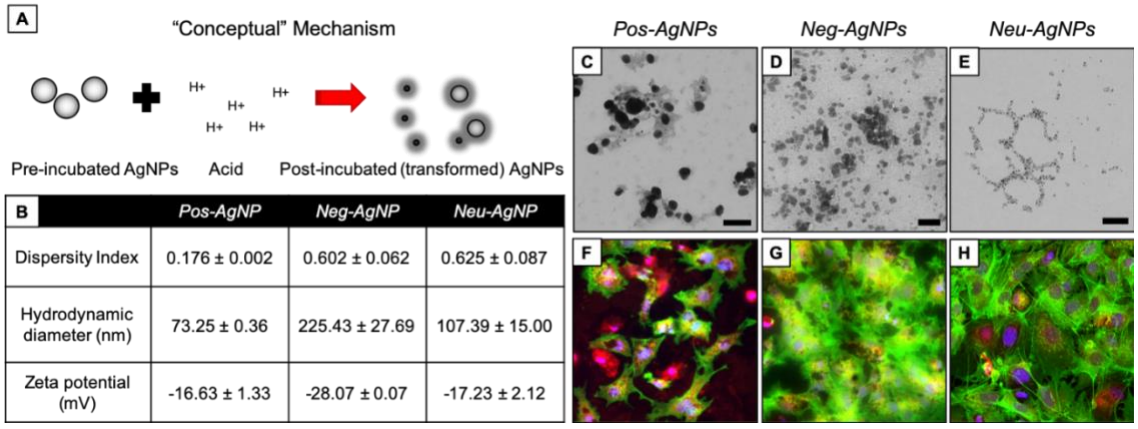

B	*Pos-AgNP*	*Neg-AgNP*	*Neu-AgNP*
Dispersity Index	0.176 ± 0.002	0.602 ± 0.062	0.625 ± 0.087
Hydrodynamic diameter (nm)	73.25 ± 0.36	225.43 ± 27.69	107.39 ± 15.00
Zeta potential (mV)	-16.63 ± 1.33	-28.07 ± 0.07	-17.23 ± 2.12

Figure 3.6. AgNP transformation after incubation in acid. (A) Conceptual model of transformation mechanisms. (B) Dispersity index (unitless), hydrodynamic diameter (nm), and zeta potential (mV) measurements of each particle type after simulated incubation. TEM of (C) Pos-AgNPs, (D) Neg-AgNPs, and (E) Neu-AgNPs after simulated incubation. Fluorescence microscopy of HepG2 cells after 24 h exposure to post-incubated (F) Pos-AgNPs, (G) Neg-AgNPs, and (H) Neu-AgNPs. Scale bars in (C-E) represent 50 nm. Stains in (F-H) include: DAPI (blue), F-actin (green), and MitoTracker (red).

Taken together, Pos-AgNP, Neg-AgNP, and Neu-AgNP systems] transformed under all scenario conditions. The transformation products can be related to the pre-incubation zeta potential measurements. Not only are strongly surface-charged nanoparticle able to enter cells more readily, they also interactive to biomolecular constituents in the complex microenvironment and accumulate intracellularly differently (Hirn et al., 2011). Thus, cellular effects induced by these particle-types are likely to be caused by the increased oxidative stress, which is consistent to what has been extensively studied with AgNP behavior in the environment (Li, Zhang, Niu, & Chen, 2013).

Neutrally charged nanoparticle surfaces readily dissolve in acidic conditions. Therefore, effects induced by these particle-types are more likely to be caused by metal ion dissociation and subsequent ionic interferences with normal cellular processes.

Negatively-Charged Silver Nanoparticle Influences Nanoparticle Biotransformation

Neg-AgNPs subjected to incubation in all three scenarios used in this study produced significantly transformed product in terms of large shift in dispersity index, increased hydrodynamic diameter, weakened zeta potential, severe agglomeration, and induced cytoskeletal damage. Neu-AgNPs were not transformed as much as Neg-AgNPs due to the neutral surface being ineffective at interacting with the surrounding environment.

Pos-AgNPs transformations were more noticeable than the Neu-AgNPs results but were still minor when compared to those of Neg-AgNPs. Evidence of this was observed in the blue shift in Neg-AgNPs hyperspectral imaging. A blue shift is indicative of the nanoparticle de-aggregation or degradation, indicating that nano-enabled drug products with positively charged surfaces have more surface area available to interact with the complex mixtures. In comparison the Pos-AgNPs, which had red shifts indicating severe agglomeration, decrease in surface area, and decrease in biomolecular interactions. The Neu-AgNPs having slight red shift in Scenario 1, no shift in Scenario 2, and slight blue shift in Scenario 3 is indicative of neutrality and these particle transformations are largely influenced by the surrounding environment. These results indicate that there are charge-dependent nanoparticle biotransformation mechanisms at play. Agglomeration, cellular internalization, and degradation transformations of nano-enabled drug products may increase efficacy by transporting through the surrounding

environment easily. Alternatively, transformation products may decrease effectiveness by modifying flux between biological compartments. Nanoparticle surface stabilizing agents can impact the therapeutic efficacy of nano-enabled drug products by not only altering stability, but also dictating transformation after administration. The mechanisms of transformations observed in this study are summarized in Figure 3.7.

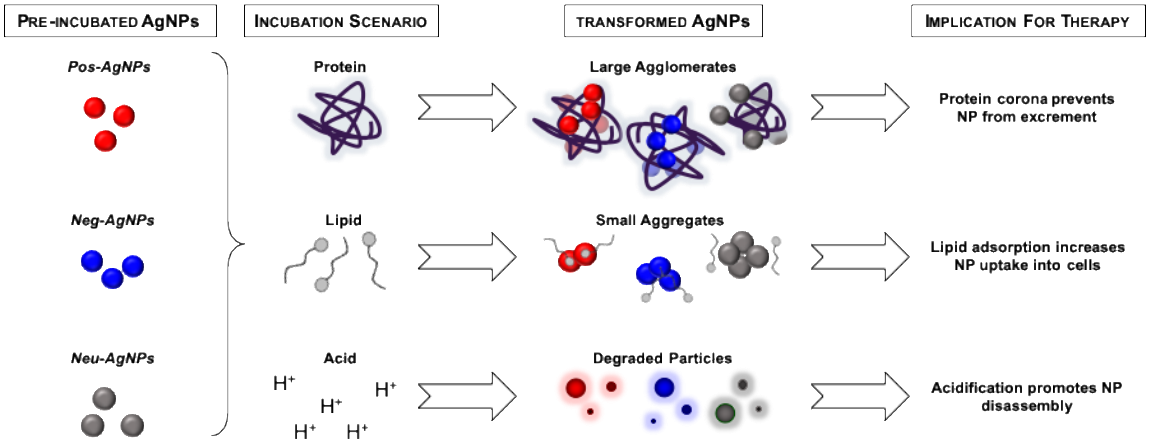

Figure 3.7. Summary of transformation mechanisms revealed by this study.

Conclusions

In summary, we studied three uniquely stabilized silver nanoparticles, each with a different surface charge, and subjected to three separate physiologically relevant incubation scenarios. The surface charges included positive (conferred by bPEI), negative (conferred by lipoic acid), and neutral (conferred by PEG). The incubation scenarios included serum which represented intravenous administration, lipid surfactant fluid representing inhalation administration, and stomach acid that representing oral administration. AgNP system transformation products after subjection to each incubation scenario are strikingly different than their pre-incubated engineered structure. Changes in

nanoparticle size and agglomeration (measured by hydrodynamic diameter), surface charge (measured by zeta potential), and agglomeration (measured by hyperspectral imaging and transmission electron microscopy) are evident and ought to be considered in nanomedicine research and development. In this study, we showed that the surface charge plays a substantial role in predicting agglomeration and intercellular uptake. A one size fits all characterization approach for nano-enabled drug products is not enough; multiple physicochemical properties are translatable to critical quality attributes. In the next chapter, we take important information here regarding the biological influence on nanomaterial transformations and go one step deeper into molecular mechanisms and ultrastructural morphological changes after nanomaterial exposure. Furthermore, understandings of nanomaterial physicochemical properties as well as the environmental impact on biotransformation are used to understand the endocrine disruption potential of nanomaterials.

Supplemental Figures:

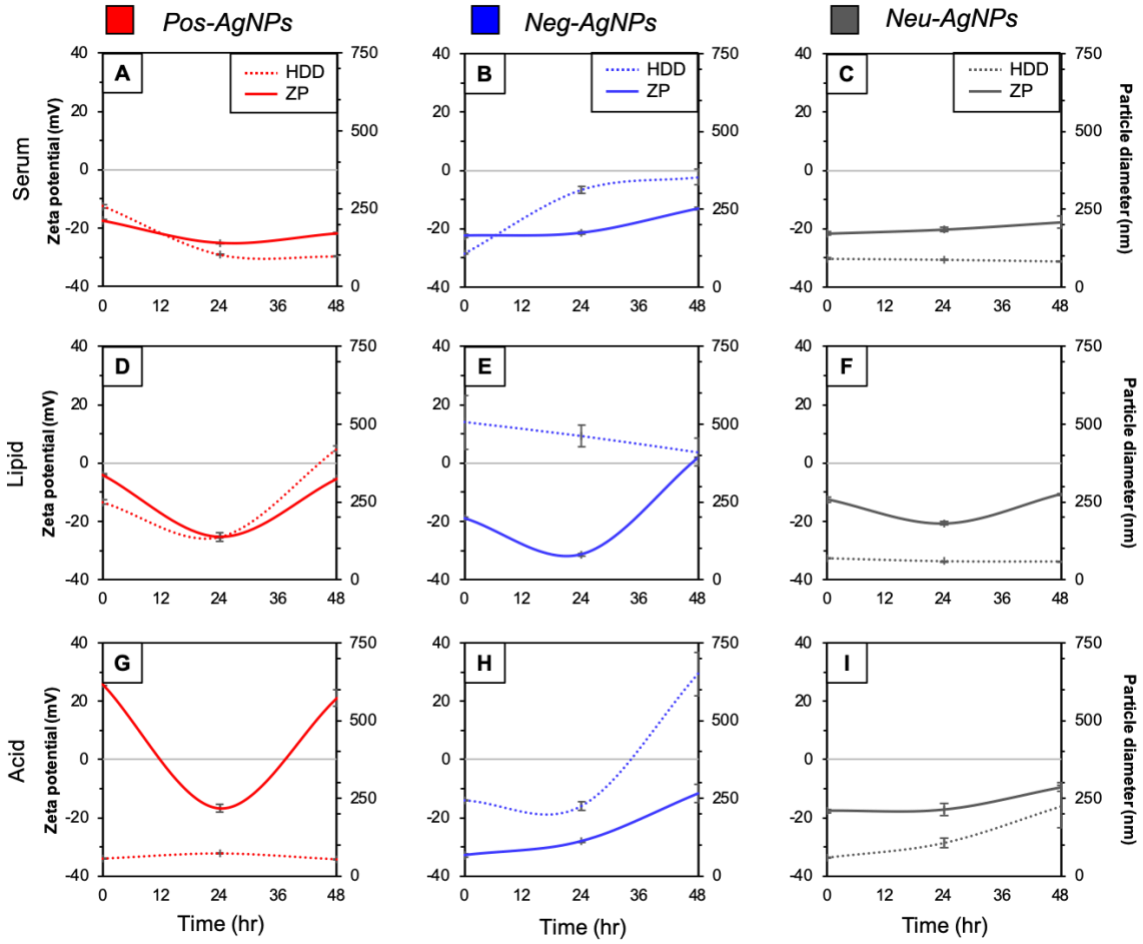

Supplemental Figure 3.1. Trends in AgNP HDD and ZP over time. Data shows significant changes among stabilizing agents charge, but not incubation scenario. No trends were found in the Neg-AgNPs (B, E, H) plots.

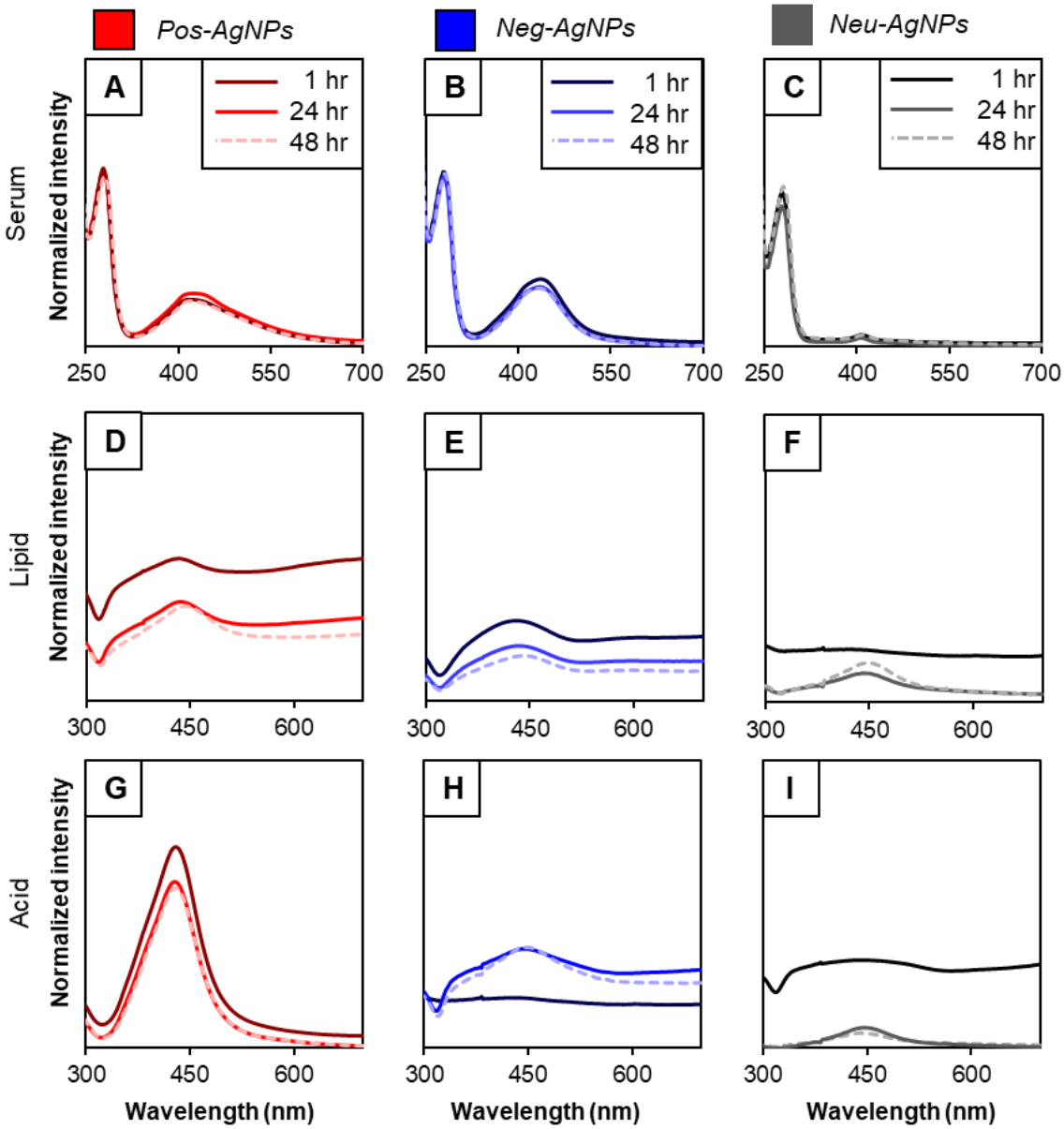

Supplemental Figure 3.2 Absorbance spectra was monitored over 1 24 and 48 hr time periods. AgNPs transformed with protein had increased absorption compared to all other simulations(D-I) which could be due to proteins on the surface of nanoparticles. A significant finding was the decrease in absorption for the lipid transformed Neu-AgNPs (F) and digested Neg-AgNPs (H) which had minimal absorption. This could be due to severe agglomeration where they fell out of solution.

References

Adabi, M., Naghibzadeh, M., Adabi, M., Zarrinfard, M. A., Esnaashari, S. S., Seifalian, A. M., . . . Ghanbari, H. (2017). Biocompatibility and nanostructured materials: applications in nanomedicine. Artificial cells, nanomedicine, and biotechnology, 45(4), 833-842.

Araújo, F., Shrestha, N., Granja, P. L., Hirvonen, J., Santos, H. A., & Sarmento, B. (2015). Safety and toxicity concerns of orally delivered nanoparticles as drug carriers. Expert opinion on drug metabolism & toxicology, 11(3), 381-393.

Badawy, A. M. E., Luxton, T. P., Silva, R. G., Scheckel, K. G., Suidan, M. T., & Tolaymat, T. M. (2010). Impact of environmental conditions (pH, ionic strength, and electrolyte type) on the surface charge and aggregation of silver nanoparticles suspensions. Environmental science & technology, 44(4), 1260-1266.

Bobo, D., Robinson, K. J., Islam, J., Thurecht, K. J., & Corrie, S. R. (2016). Nanoparticle-based medicines: a review of FDA-approved materials and clinical trials to date. Pharmaceutical research, 33(10), 2373-2387.

Braydich-Stolle, L. K., Breitner, E. K., Comfort, K. K., Schlager, J. J., & Hussain, S. M. (2014). Dynamic characteristics of silver nanoparticles in physiological fluids: toxicological implications. Langmuir, 30(50), 15309-15316.

Cedervall, T., Lynch, I., Lindman, S., Berggård, T., Thulin, E., Nilsson, H., . . . Linse, S. (2007). Understanding the nanoparticle–protein corona using methods to quantify exchange rates and affinities of proteins for nanoparticles. Proceedings of the National Academy of Sciences, 104(7), 2050-2055.

Chandran, P., Riviere, J. E., & Monteiro-Riviere, N. A. (2017). Surface chemistry of gold nanoparticles determines the biocorona composition impacting cellular uptake, toxicity and gene expression profiles in human endothelial cells. Nanotoxicology, 11(4), 507-519.

Choi, O., Deng, K. K., Kim, N.-J., Ross Jr, L., Surampalli, R. Y., & Hu, Z. (2008). The inhibitory effects of silver nanoparticles, silver ions, and silver chloride colloids on microbial growth. Water research, 42(12), 3066-3074.

Cohen, J., DeLoid, G., Pyrgiotakis, G., & Demokritou, P. (2013). Interactions of engineered nanomaterials in physiological media and implications for in vitro dosimetry. Nanotoxicology, 7(4), 417-431.

Colombo, A., Saibene, M., Moschini, E., Bonfanti, P., Collini, M., Kasemets, K., & Mantecca, P. (2017). Teratogenic hazard of BPEI-coated silver nanoparticles to Xenopus laevis. Nanotoxicology, 11(3), 405-418.

Corbo, C., Molinaro, R., Parodi, A., Toledano Furman, N. E., Salvatore, F., & Tasciotti, E. (2016). The impact of nanoparticle protein corona on cytotoxicity, immunotoxicity and target drug delivery. Nanomedicine, 11(1), 81-100.

Cortese-Krott, M. M., Münchow, M., Pirev, E., Heβner, F., Bozkurt, A., Uciechowski, P., . . . Suschek, C. V. (2009). Silver ions induce oxidative stress and intracellular zinc release in human skin fibroblasts. Free Radical Biology and Medicine, 47(11), 1570-1577.

Cueva, C., Gil-Sánchez, I., Tamargo, A., Miralles, B., Crespo, J., Bartolomé, B., & Moreno-Arribas, M. V. (2019). Gastrointestinal digestion of food-use silver nanoparticles in the dynamic SIMulator of the GastroIntestinal tract (simgi®). Impact on human gut microbiota. Food and Chemical Toxicology, 132, 110657.

Danaei, M., Dehghankhold, M., Ataei, S., Hasanzadeh Davarani, F., Javanmard, R., Dokhani, A., . . . Mozafari, M. (2018). Impact of particle size and polydispersity index on the clinical applications of lipidic nanocarrier systems. Pharmaceutics, 10(2), 57.

Dawidczyk, C. M., Kim, C., Park, J. H., Russell, L. M., Lee, K. H., Pomper, M. G., & Searson, P. C. (2014). State-of-the-art in design rules for drug delivery platforms: lessons learned from FDA-approved nanomedicines. Journal of Controlled Release, 187, 133-144.

de Vlieger, J. S., Crommelin, D. J., Tyner, K., Drummond, D. C., Jiang, W., McNeil, S. E., . . . Shah, V. P. (2019). Report of the AAPS Guidance Forum on the FDA draft guidance for industry:“drug products, including biological products, that contain nanomaterials”. In: Springer.

DeLoid, G. M., Wang, Y., Kapronezai, K., Lorente, L. R., Zhang, R., Pyrgiotakis, G., . . . De La Torre-Roche, R. (2017). An integrated methodology for assessing the impact of food matrix and gastrointestinal effects on the biokinetics and cellular toxicity of ingested engineered nanomaterials. Particle and fibre toxicology, 14(1), 40.

Dieckmann, Y., Cölfen, H., Hofmann, H., & Petri-Fink, A. (2009). Particle size distribution measurements of manganese-doped ZnS nanoparticles. Analytical Chemistry, 81(10), 3889-3895.

Duman, O., & Tunç, S. (2009). Electrokinetic and rheological properties of Na-bentonite in some electrolyte solutions. Microporous and Mesoporous Materials, 117(1-2), 331-338.

Duvall, M. N. (2012). FDA regulation of nanotechnology. Washington, DC, USA: Beveridge & Diamond, PG.

Elder, A., Vidyasagar, S., & DeLouise, L. (2009). Physicochemical factors that affect metal and metal oxide nanoparticle passage across epithelial barriers. Wiley Interdisciplinary Reviews: Nanomedicine and Nanobiotechnology, 1(4), 434-450.

Gitipour, A., Thiel, S. W., Scheckel, K. G., & Tolaymat, T. (2016). Anaerobic toxicity of cationic silver nanoparticles. Science of the total Environment, 557, 363-368.

Giudice, M. C. L., Herda, L. M., Polo, E., & Dawson, K. A. (2016). In situ characterization of nanoparticle biomolecular interactions in complex biological media by flow cytometry. Nature communications, 7(1), 1-10.

Hadrup, N., & Lam, H. R. (2014). Oral toxicity of silver ions, silver nanoparticles and colloidal silver–a review. Regulatory Toxicology and Pharmacology, 68(1), 1-7.

Hirn, S., Semmler-Behnke, M., Schleh, C., Wenk, A., Lipka, J., Schäffler, M., . . . Kreyling, W. G. (2011). Particle size-dependent and surface charge-dependent biodistribution of gold nanoparticles after intravenous administration. European Journal of Pharmaceutics and Biopharmaceutics, 77(3), 407-416. doi:10.1016/j.ejpb.2010.12.029

Kaminskas, L. M., Boyd, B. J., Karellas, P., Krippner, G. Y., Lessene, R., Kelly, B., & Porter, C. J. (2008). The impact of molecular weight and PEG chain length on the systemic pharmacokinetics of PEGylated poly l-lysine dendrimers. Molecular pharmaceutics, 5(3), 449-463.

Kang, S. W., Char, K., & Kang, Y. S. (2008). Novel application of partially positively charged silver nanoparticles for facilitated transport in olefin/paraffin separation membranes. Chemistry of Materials, 20(4), 1308-1311.

Kang, S. W., Hong, J., Park, J. H., Mun, S. H., Kim, J. H., Cho, J., . . . Kang, Y. S. (2008). Nanocomposite membranes containing positively polarized gold nanoparticles for facilitated olefin transport. Journal of Membrane Science, 321(1), 90-93.

Li, H., Yu, Y., Faraji Dana, S., Li, B., Lee, C.-Y., & Kang, L. (2013). Novel engineered systems for oral, mucosal and transdermal drug delivery. Journal of drug targeting, 21(7), 611-629.

Li, Y., Zhang, W., Niu, J., & Chen, Y. (2013). Surface-coating-dependent dissolution, aggregation, and reactive oxygen species (ROS) generation of silver nanoparticles under different irradiation conditions. Environmental Science and Technology, 47(18), 10293-10301. doi:10.1021/es400945v

Liu, J., Wang, Z., Liu, F. D., Kane, A. B., & Hurt, R. H. (2012). Chemical transformations of nanosilver in biological environments. ACS nano, 6(11), 9887-9899.

Lowry, G. V., Gregory, K. B., Apte, S. C., & Lead, J. R. (2012). Transformations of nanomaterials in the environment. In: ACS Publications.

Lujan, H., Griffin, W. C., Taube, J. H., & Sayes, C. M. (2019). Synthesis and characterization of nanometer-sized liposomes for encapsulation and microRNA transfer to breast cancer cells. International journal of nanomedicine, 14, 5159.

Lundqvist, M., Stigler, J., Elia, G., Lynch, I., Cedervall, T., & Dawson, K. A. (2008). Nanoparticle size and surface properties determine the protein corona with possible implications for biological impacts. Proceedings of the National Academy of Sciences, 105(38), 14265-14270.

Maiolo, D., Del Pino, P., Metrangolo, P., Parak, W. J., & Baldelli Bombelli, F. (2015). Nanomedicine delivery: does protein corona route to the target or off road? Nanomedicine, 10(21), 3231-3247.

Medici, S., Peana, M., Nurchi, V. M., & Zoroddu, M. A. (2019). Medical uses of silver: history, myths, and scientific evidence. Journal of medicinal chemistry, 62(13), 5923-5943.

Michen, B., Geers, C., Vanhecke, D., Endes, C., Rothen-Rutishauser, B., Balog, S., & Petri-Fink, A. (2015). Avoiding drying-artifacts in transmission electron microscopy: Characterizing the size and colloidal state of nanoparticles. Scientific reports, 5, 9793.

Moghimi, S. M., Hunter, A. C., & Murray, J. C. (2001). Long-circulating and target-specific nanoparticles: theory to practice. Pharmacological reviews, 53(2), 283-318.

Morrison, H. G., Tao, W., Trieu, W., Walker, S. D., Cui, S., Huggins, S., & Nagapudi, K. (2015). Correlation of Drug Substance Particle Size Distribution with Other Bulk Properties to Predict Critical Quality Attributes. Organic Process Research & Development, 19(9), 1076-1081.

Mortimer, M., Gogos, A., Bartolomé, N., Kahru, A., Bucheli, T. D., & Slaveykova, V. I. (2014). Potential of hyperspectral imaging microscopy for semi-quantitative analysis of nanoparticle uptake by protozoa. Environmental science & technology, 48(15), 8760-8767.

Mulenos, M. R., Liu, J., Lujan, H., Guo, B., Lichtfouse, E., Sharma, V. K., & Sayes, C. M. (2020). Copper, silver, and titania nanoparticles do not release ions under anoxic conditions and release only minute ion levels under oxic conditions in water: Evidence for the low toxicity of nanoparticles. Environmental Chemistry Letters, 1-10.

Niska, K., Knap, N., Kędzia, A., Jaskiewicz, M., Kamysz, W., & Inkielewicz-Stepniak, I. (2016). Capping agent-dependent toxicity and antimicrobial activity of silver nanoparticles: an in vitro study. Concerns about potential application in dental practice. International journal of medical sciences, 13(10), 772.

Oh, J. Y., Kim, H. S., Palanikumar, L., Go, E. M., Jana, B., Park, S. A., . . . Kwak, S. K. (2018). Cloaking nanoparticles with protein corona shield for targeted drug delivery. Nature communications, 9(1), 1-9.

Riediker, M., Zink, D., Kreyling, W., Oberdörster, G., Elder, A., Graham, U., . . . Ichihara, S. (2019). Particle toxicology and health-where are we? Particle and fibre toxicology, 16(1), 19.

Rizvi, S. A., & Saleh, A. M. (2018). Applications of nanoparticle systems in drug delivery technology. Saudi Pharmaceutical Journal, 26(1), 64-70.

Sabella, S., Carney, R. P., Brunetti, V., Malvindi, M. A., Al-Juffali, N., Vecchio, G., . . . Stellacci, F. (2014). A general mechanism for intracellular toxicity of metal-containing nanoparticles. Nanoscale, 6(12), 7052-7061.

Sharma, V. K., Sayes, C. M., Guo, B., Pillai, S., Parsons, J. G., Wang, C., . . . Ma, X. (2019). Interactions between silver nanoparticles and other metal nanoparticles under environmentally relevant conditions: A review. Science of the Total Environment, 653, 1042-1051.

Shi, J. H., Axson, J. L., Bergin, I. L., & Ault, A. P. (2020). Nanoparticle Digestion Simulator Reveals pH-dependent Aggregation in the Gastrointestinal Tract. Analytical Chemistry.

Silva, T., Pokhrel, L. R., Dubey, B., Tolaymat, T. M., Maier, K. J., & Liu, X. (2014). Particle size, surface charge and concentration dependent ecotoxicity of three organo-coated silver nanoparticles: comparison between general linear model-predicted and observed toxicity. Science of the total Environment, 468, 968-976.

Tenzer, S., Docter, D., Kuharev, J., Musyanovych, A., Fetz, V., Hecht, R., . . . Reinhardt, C. (2013a). Rapid formation of plasma protein corona critically affects nanoparticle pathophysiology. Nature nanotechnology, 8(10), 772-781.

Tenzer, S., Docter, D., Kuharev, J., Musyanovych, A., Fetz, V., Hecht, R., Reinhardt, C. (2013b). Rapid formation of plasma protein corona critically affects nanoparticle pathophysiology. Nature nanotechnology, 8(10), 772.

Trickler, W. J., Lantz, S. M., Murdock, R. C., Schrand, A. M., Robinson, B. L., Newport, G. D., . . . Slikker Jr, W. (2010). Silver nanoparticle induced blood-brain barrier inflammation and increased permeability in primary rat brain microvessel endothelial cells. Toxicological Sciences, 118(1), 160-170.

Vrček, I. V., Žuntar, I., Petlevski, R., Pavičić, I., Dutour Sikirić, M., Ćurlin, M., & Goessler, W. (2016). Comparison of in vitro toxicity of silver ions and silver nanoparticles on human hepatoma cells. Environmental toxicology, 31(6), 679-692.

Yih, T., & Al-Fandi, M. (2006). Engineered nanoparticles as precise drug delivery systems. Journal of cellular biochemistry, 97(6), 1184-1190.

Zheng, N., Sun, D. D., Zou, P., & Jiang, W. (2017). Scientific and regulatory considerations for generic complex drug products containing nanomaterials. The AAPS journal, 19(3), 619-631.

Zucker, R. M., Ortenzio, J., Degn, L. L., Lerner, J. M., & Boyes, W. K. (2019). Biophysical comparison of four silver nanoparticles coatings using microscopy, hyperspectral imaging and flow cytometry. PloS one, 14(7), e0219078.

CHAPTER FOUR

Advancing Human Health and Nanomaterial Safety Assessments: Identifying Endocrine Disruption Potential after Nanocellulose Exposure

Effects of Renewable Nanomaterials *In Vitro*: Studies on Cytotoxicity, Endocrine Disruption Potential and Antioxidant Markers

Abstract

Recent efforts by industry and universities alike are focused on incorporating renewable resources in technological advances. One of the most abundant renewable resources on earth is cellulose, which is derived from trees, plants, or microorganisms. Cellulose can be modified into the crystalline form, termed cellulose nanocrystals (CNC), and is utilized in many different industries like paper and mill, food packaging, and cosmetics. However, with the incorporation of CNC in an immense number of products and processes, there is a high exposure potential to consumers, occupational workers, and the environment. The goal of this study was to understand the effects CNC exposure has with *in vitro* models regarding cytotoxicity, endocrine disruption potential and with antioxidant defense. In this study, we used the H295R human cell line to understand the potential cytotoxicity, endocrine disrupting effects, and antioxidant capacity of CNC exposure at three concentrations 0.5, 5.0, and 50.0 mg/m^3 for 48 hours. Specifically, cellular viability, ultrastructure analyses, and gene expression of important antioxidant and steroidogenic biomarkers were monitored by viability, metabolic activity, ultrastructural analysis, and qRT-PCR. analyses. The results showed that CNC at the OECD daily allowable limit (5.0 mg/m^3) had no to undetectable endocrine disrupting

potential, but induced minute metabolic activity and cellular stress. CNC at the overload concentration (50 mg/m^3) had irreversible cellular damage and potential steroidogenic pathway perturbations through the up-regulation of CYP19A1, CYP21A1P, and STAR genes which are directly involved in determining endocrine disruption potential. This study is significance because it offers deeper insight into testing the endocrine disruption potential of nanomaterial exposures which can be used to implement proper testing and safety regulations and mitigate potential adverse effects.

Introduction

Over the past decade, the chemical industry has made strides to transition from using environmentally damaging substances to using renewable resources. (Chen, Li, Grätzel, Kostecki, & Mao, 2012; Teo & Wahab, 2020) This movement is of high importance to industry, government agencies, and academia, alike. Renewable resources are biodegradable, safer for the environment, and, in some cases, cost-effective compared to non-renewable resources currently used. (Dincer, 2000) One example of sustainability adoption is the use of cellulosic materials in product formulations. Industries that utilize cellulose technologies include paper/packaging, cosmetics, food/drug, concrete, and rubber/plastics (Belgacem & Gandini, 2011). With the abundant amount of hydroxyl (-OH) surface functional groups on a chain of cellulose monomers, modifications are easy, making cellulose ideal for a multitude of advanced manufacturing processes. Specifically, modified cellulose nanocrystals (CNC; natural cellulose fibers spun down into the nanometer size range) have been shown to be stronger than conventional cellulose, generally regarded as safe, and renewable from a wide range of plant species. Some characteristics of CNC that are commonly exploited in advanced material processing

include stability, decreased weight, electrical properties, and others (Habibi, Lucia, & Rojas, 2010).

The use of CNC in many industrial processes and consumer products result in a significant and measurable human health exposure (Martinez, Eastlake, Rudie, & Geraci, 2013). The unique size and shape of CNC resembles other materials in the nanometer size range, (Joseph et al., 2021) otherwise known as nanomaterials, like carbon nanotubes (used in electronics) (Paradise & Goswami, 2007) and asbestos (used in insulation) (Selikoff, Churg, & Hammond, 1964). However, because both asbestos and carbon nanotubes have been shown to induce toxicological effects in humans, (Donaldson et al., 2013; Kamp & Weitzman, 1999; Kane, Hurt, & Gao, 2018)) there is a need to assess the potential toxicological responses after CNC exposure. In fact, a recent study by Shedova et. al. from NIOSH implicated CNC as a potential immunological trigger. Their study demonstrated that the extent of immunotoxicological responses was dependent upon gender, i.e. female mice are more susceptible to CNC-induced toxicities (Catalán et al., 2015; Shvedova et al., 2015). However, the study did not evaluate the endocrine disrupting potential after exposure. Additionally, it is important to study sex hormone imbalances from nanomaterials derived from anthropogenic sources, especially since new materials are being produced every day. Even though many new materials being produced are "green" to the environment, the potential toxicity of these environmentally sustainable materials has not been studied extensively in humans (Poliakoff & Licence, 2007).

Different methods have been established to monitor chemical and pharmaceutical effects on the steroidogenic pathway (Gracia et al., 2006; He et al., 2010; Zhang et al., 2011) , but hormone specific adverse effects of nanomaterials, specifically induced through cellulose nanocrystal exposures, remain unknown. Therefore, the objective of this study is the first of its kind in asking if cellulose nanocrystals exhibit an endocrine disrupting response over three concentrations of cellulose nanocrystals (0.5, 5, and 50 mg/m^3) after exposure to the H295R cell line for 48 hours. These concentrations of CNC were used to understand low, acceptable, and overload concentration exposure scenarios. The Occupational Safety & Health Administration (OSHA) determined the human equivalent workplace exposure to be a cumulative dose of 5 mg/m^3 (240 µg) of CNC during 42 working days. The experimental concentrations of 0.5, 5, and 50 mg/ m^3 CNC represent one order of magnitude below the acceptable limit termed ”Low”, the exact allowable limit termed “Medium”, and the “High” concentration was one order of magnitude above the allowable limit. Additionally, the H295R cell line was used due to its innate ability to express key genes related to steroidogenesis and extensive use in the literature as an animal alternative test method. (Hilscherova et al., 2004) (Zhang et al., 2005) (Hecker et al., 2006) (He et al., 2008) The overall cytotoxicity, metabolic activity, ultrastructure analyses and key biosignatures including 5 antioxidant genes and 10 steroidogenic specific genes were measured to help elucidate CNC nanomaterial endocrine disrupting potential. Overall, this work may be used as the basis for future testing the endocrine disrupting potential of newly created renewable nanomaterial technologies.

Results and Discussion

Cytotoxicity

Results showed (Figure 4.1A) that there was a significant decrease in viability after CNC exposure at the low and high concentrations. ($p=0.033$ and 0.023 respectively). Mechanistically, our hypothesis is that when CNC is at a low concentration, the cell experiences exposure to the 'nano' portion of the sample, and as the sample increases in concentration, more aggregates form. This has been published in the literature previously where at low concentrations CNC suspension create chiral liquid crystalline structures, and at higher concentrations the suspension becomes like a gel (Shafiei-Sabet, Hamad, & Hatzikiriakos, 2014). At the medium concentration, there is not a significant decrease in viability due to the agglomeration of CNC in aqueous suspension, causing no reaction between the cells and CNC. At the high concentration, the CNC severely agglomerated in the media, potentially causing a gel like layer above the cells which we hypothesize that this caused the cells to undergo nutrient deficiency due to the CNC sequestering the water molecules in the media (Mendes et al., 2020).

The metabolic activity assay (MTS) was used as an additional method alongside the PrestoBlue assay to capture the metabolic activity and cytotoxicity of the cells. While MTS is commonly used for measuring viable cells, the assay functions through the bioreduction of the dye from dehydrogenase enzymes in metabolically active cells. Therefore, this assay allows researchers to probe the metabolic health of the cell after exposure to different toxicants. Compared to the baseline (unexposed control) sample, the metabolic activity of the low and medium concentration groups did not significantly change. (Figure 4.1B) The highest concentration caused a significant ($p=0.015$) decrease

in the metabolic activity of the cell, however the exposure only caused a small decrease in metabolic activity. Overall, there is little to no decrease in metabolic activity or viability between each concentration of CNC exposure as seen in the PrestoBlue and MTS *assays.*

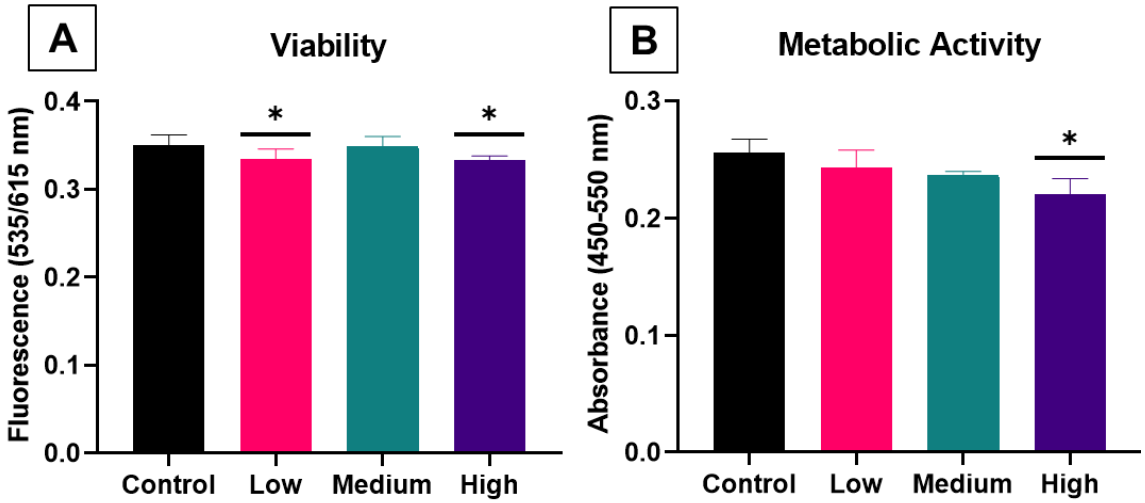

Figure 4.1. H295R potential cytotoxicity from CNC. H295R cells were dosed at low, medium and high concentrations of CNC (0.5, 5, and 50 mg/m3 respectively.) The control sample is untreated H295R cells. There was seen to be a significant decrease in viability after CNC exposure at the low and high concentrations. (B) The metabolic activity of the H295R cells followed a dose-dependent response where the metabolic activity declined as the concentration of CNC increased. The high concentration had a statistically significant($p=0.015$) decrease in metabolic activity.

Ultrastructural Analyses

Ultrastructure analyses of H295R cells which were unexposed or exposed to three increasing concentrations of CNC were imaged using transmission electron microscopy. Samples include baseline and CNC exposures at low, medium, and high concentrations (Figure 4.2). The baseline (Figure 4.2A) shows organelles typical of a healthy secretory cell where there are many mitochondria with intact cristae structure, an abundance of

rough endoplasmic reticulum, and a healthy nucleus. The low concentration sample (Figure 4.2B) display early stages of cellular stress where the mitochondria are swelling and becoming elongated. (Bhatia, Capili, & Choi, 2020; Bosc et al., 2020)The medium concentration (Figure 4.2C) indicates early stages of mitophagy where there is a decrease in the number of mitochondria and these mitochondria have decreased in size (area). The decrease in the number and size of mitochondria is indicative of stress induced fission and increase in mitophagy as the cell is responding to the CNC exposure. (Youle & Van Der Bliek, 2012) Furthermore, fission is a critical process of the cell in regard to mitigating stress occurring within the cell either from metabolic or external stressors. (Vincent et al., 2016, Ahmadi, Ghanbarinejad, Ommati, Jamshidzadeh, & Heidari, 2018) Additionally, degraded nuclear plasma was seen in the micrographs. The sample with the high CNC concentration (Figure 4.2D) shows the most severe stress where (1) multivesicular bodies have formed which are indicative of fusion and downstream degradation, (2) the endoplasmic reticulum is becoming swollen indicating autophagy, and (3) the degradation of various organelles and their membranes including the cristae structure within the mitochondria. Overall, the CNC exposure is causing slight cellular stress at the structural level at lower concentrations, and irreversible damage at the highest concentration.

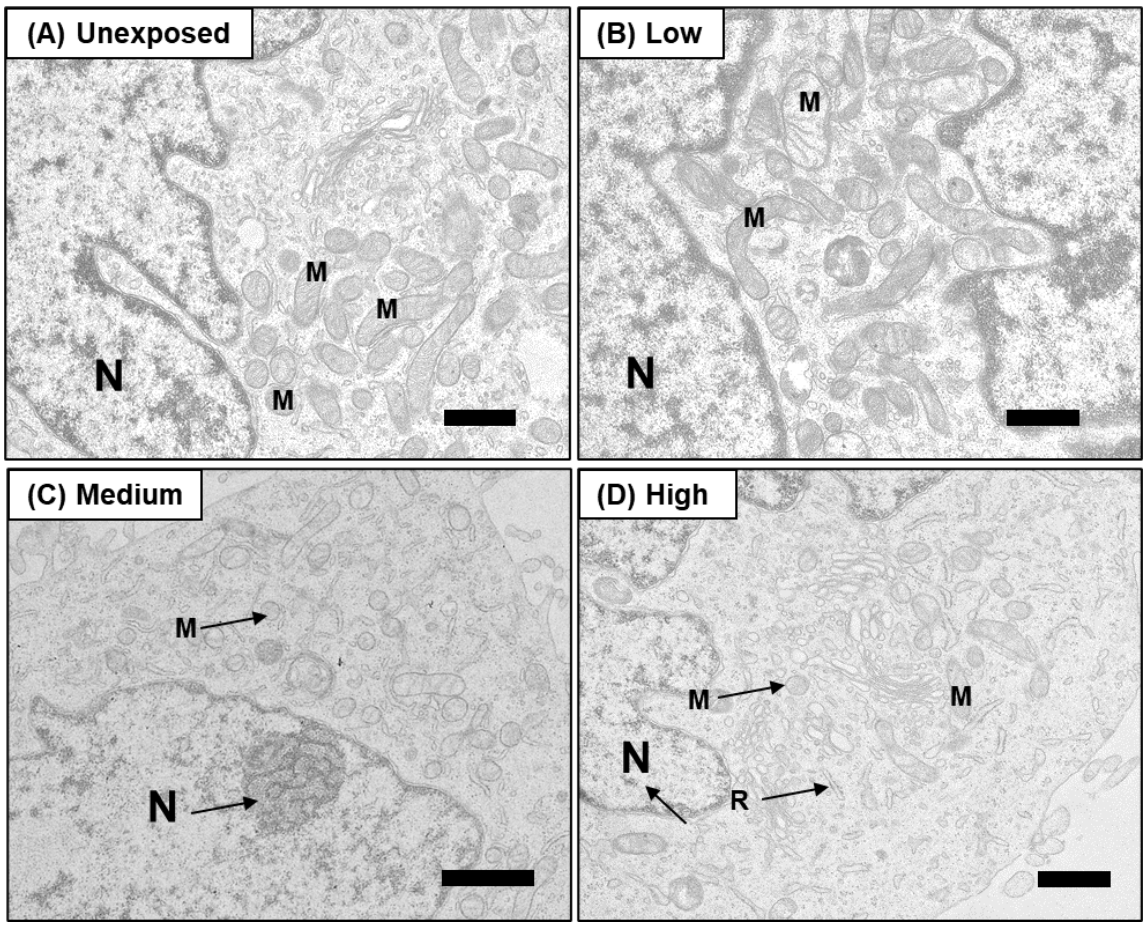

Figure 4.2. Transmission electron micrographs showing the ultrastructure of H295R cells. Samples are of the control (A) and CNC exposures at low (B) medium (C) and high concentrations (D). The control sample (A) shows organelles typical of a healthy secretory cell where there are many mitochondria with intact cristae structure, an abundance of rough endoplasmic reticulum, and a healthy nucleus. The low CNC exposure sample (B) displays early stages of cellular stress where the mitochondria are swelling and elongating. The medium concentration (C) indicates early stages of mitophagy where there is a decrease in the number of mitochondria and the mitochondria have decreased in area, indicating increased fission. The high concentration sample (D) shows severe stress where there is formation of multivesicular bodies indicative of fusion, swollen endoplasmic reticulum around the mitophagy indicating autophagy, and degradation of various membranes including decreased cristae structure in the mitochondria as well as decreased number of mitochondria. Micrographs show- nuclei (N), mitochondria (M), rough endoplasmic reticulum (R). Scale bars represent 800 nm.

The mitochondria from the H295R cells were imaged using TEM. Mitochondrial length and width were measured using ImageJ software to understand the changes in

mitochondrial morphology. Equation 1 (in methods) was used which incorporated $R_{Mitochondria}$ to represent the average roundness, $L_{Mitochondria}$ is the average length, and $W_{Mitochondria}$ is the average width of each mitochondria within an analyzed cell gives insight into the mitochondrial health of the cell. Figure 4.3A the mitochondrial roundness distributions are represented in violin plots where a value of "0" is a perfectly round mitochondria and values greater than 0 are of increasing elongation or swelling, indicative of mitochondrial stress. Here, in Figure 4.3A we utilized a violin plot, which shows the full distribution of mitochondrial roundness. The distribution of the violin plots, specifically the higher values in the third and fourth quartile, increase in outliers (where the violin plot decreases in width) as the concentration of CNC increase in comparison to the baseline. It can also be seen that as the concentration of CNC increase, the values drift farther away from "0" which is indicative of mitochondria elongating or swelling. Specifically, the baseline concentration has the fourth quartile under a value of 5, in comparison to the low, medium, and high, which all have increasing values, up to over 7 with the high concentration. Additionally, the shapes of the distributions vary, and a multimodal distribution is elucidated. These changes in distribution were not statistically significant. However, we note that there was cellular stress, but this may not be related to endocrine disruption.

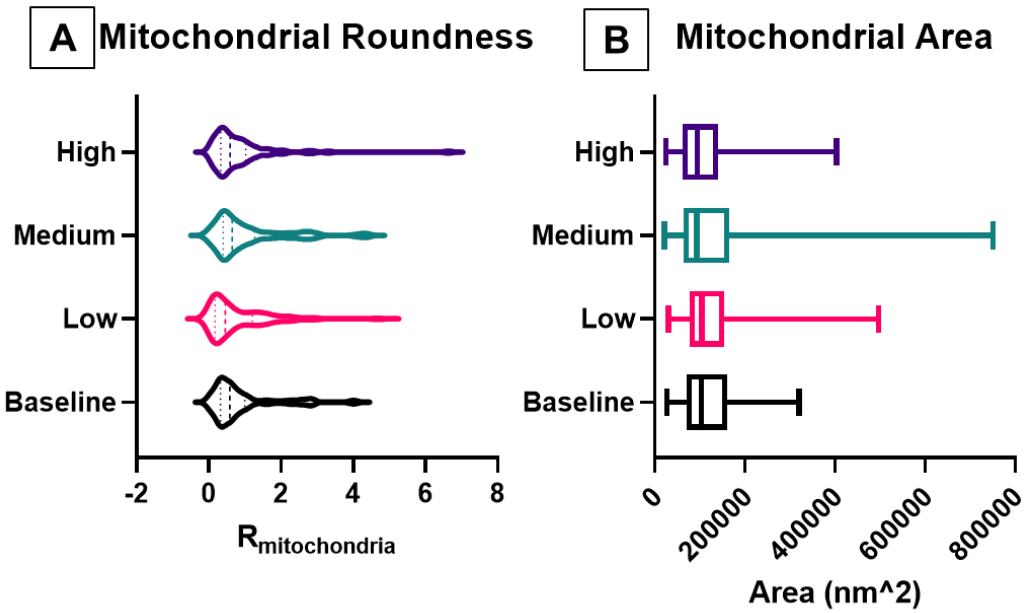

Figure 4.3. Mitochondria roundness and area. The mitochondrial length and width were measured using ImageJ software to understand the mitochondrial roundness. A "round" mitochondrial is indicated by a value of 0. As the values increase, the more severe the elongation and swelling of the mitochondria is. The mitochondria roundness distributions were plotted using a violin plot (A) which shows the dose-dependent response of mitochondria swelling and elongation as CNC concentration increases. All samples were seen to change distribution shape, but not significantly. The average mitochondria area is also plotted (B) using a box plot. The maximum mitochondria area is seen to increase in area as CNC concentration increases, until the high concentration where the maximum mitochondria area decreases in comparison to the medium CNC concentration. However, compared to the baseline, the maximum area of all samples has increased.

In addition to mitochondrial roundness, the mitochondrial area was also measured using the equation $(L_{Mitochondria} \times 0.5)\ (W_{Mitochondria} \times 0.5)\pi$. In Figure 4.3B all average areas are plotted for each treatment. There is no significant difference between the exposed samples to the baseline, however there are trends in the data indicating that the maximum mitochondrial area is increasing slightly at a dose response. After this, the mitochondrial maximum area decreases with the highest sample. This may be due to the mitochondria undergoing some slight swelling or an increase in fusion from the low to medium concentrations causing mild stress, while the high concentration shows

mitochondria with decreased maximum area potentially due to mitochondrial fission and mitophagy due to higher levels of stress related to high CNC exposure. (Gao et al., 2020)

Expression of Antioxidant Genes

Real-time quantitative polymerase chain reaction (RT-qPCR) was used to monitor the expression levels of 5 antioxidant genes seen in Table 4.1. H295R cells were exposed to CNC for 48 hours and harvested for qRT-PCR. Experiments were performed in triplicate with β-actin as the endogenous control. Genes probed were heme oxygenase 1 (HMOX1) , nuclear factor erythroid 2 like 2 (NERF2), superoxide dismutase 1 (SOD1), 2 (SOD2), and 3 (SOD3). Each gene expression was normalized to the endogenous control and then normalized to the baseline H295R cell gene expression level, creating the $2^{-\Delta\Delta CT}$ value. A positive value indicates decreased gene expression and negative values indicate an increase in gene expression levels. Table 4.1 shows expression changes represented by arrows. A ↑ arrow is indicative of the gene being up-regulated compared to the controls, and a ↓ arrow is indicative of down-regulation. 1 arrow indicates a 2 fold or more change, 2 arrows indicate a 5 fold or more change, and 3 arrows indicate a 120 fold or more change. All others are less than a 2 fold change. Also indicated on Table 4.1 is the subcellular location where the gene is expressed. At the low and medium CNC concentrations (Table 4.1) there are no change in expression levels for any of the antioxidant genes for the low and medium concentration. At the highest concentration, HMOX1, SOD1, and SOD2 were significantly down-regulated (fold change greater than -10) compared to the control sample. This may indicate that the higher concentration of CNC exposure did not illicit a NFE2L2 dependent antioxidant response, however the exposure did cause a cellular stress response. There was no significant induction or

reduction in NERF2 or SOD3 at any concentration. Regarding the SOD expression levels, there was seen to be slight mitophagy in the ultrastructural analyses which is in agreement with the significant downregulation of SOD1 and SOD2, which is known in the literature to increase oxidative stress (Scott et al., 2010) and eventually cell death through apoptosis triggered by the down-regulation. (Troy, Derossi, Prochiantz, Greene, & Shelanski, 1996)

Table 4.1. Antioxidant Genes are down-regulated at the high CNC concentration. This table indicates the antioxidant genes probed after CNC exposure to H295R cells and their subcellular location. Symbols represent the fold change in relation to the endogenous control and the baseline expression of H295R cells. ↓↓↓ arrows indicate a 10 or more-fold change, now arrows indicate now change. Down arrows represent down-regulation. Significant down-regulation of HMOX1, SOD1, and SOD2 were reported following RT-qPCR analyses.

	HMOX1	NERF2	SOD1	SOD2	SOD3
Subcellular location	Endoplasmic reticulum	Nucleus, cytoskeleton	Mitochondria, nucleus, cytoskeleton	Mitochondria	Extracellular matrix
Low					
Medium					
High	↓↓↓		↓↓↓	↓↓↓	

Expression of Steroidogenic Genes

The genes analyzed include: CYP11A, CYP11B1, CYP17, CYP19, CYP21, HMGR 17βHSD1, 3βHSD1, 3βHSD2, and StAR. Each concentration was normalized to the baseline concentration of actin beta, and then normalized to the control sample, displaying the $2^{-\Delta\Delta Ct}$ value. At the low concentration CYP11A was up-regulated by a

factor of 2 or less and CYP19 and 3βHSD2 were down-regulated at a factor of 2 or less as well. At the medium concentration CYP11A, CYP11B1, CYP19, CYP21, and StAR were all significantly down-regulated. At the high concentration, CYP19, CYP21, and StAR were significantly down-regulated at a factor of 10 or more. No changes were seen with the gene expression from CYP17, HMGR, 17βHSD1, and 3βHSD1. Regarding the significant down-regulation of CYP19 (aromatase), CYP21, and StAR (steroidogenic acute regulatory protein) a significant biotransformation in the steroidogenic pathway was noticed in the high concentration. However, at the allowable concentration (medium) and low concentration there was no significant indication that CNC elicited endocrine disrupting potential. It is also interesting to note that many of the genes here which were perturbed after exposure directly interact with genes that were not perturbed. There is no statistically significant change in the mitochondrial area between the baseline and exposed samples. Therefore, at the genomic level there are the beginnings of changes, however, the structural changes are not detrimental. None of the methods used showed no drastic changes in overall cellular health.

Table 4.2. Steroidogenic Genes are down-regulated at the high CNC concentration. This table indicates steroidogenic genes probed after CNC exposure to H295R cells and their subcellular location. Symbols represent the fold change in relation to the endogenous control and the baseline expression of H295R cells. ↓ indicates a 2 or more-fold change, ↓↓ indicate a 5 or more-fold change, and ↓↓↓ arrows indicate a 10 or more-fold change. All others are less than 2-fold change. Down arrows represent down-regulation and up arrows represent up-regulation.

	CYP11A	CYP11B1	CYP17	CYP19	CYP21	HMGR	17βHSD1	3βHSD1	3βHSD2	StAR
Subcellular location	Mitochondria	Mitochondria	Endoplasmic reticulum	Endoplasmic reticulum	Endoplasmic reticulum	Endoplasmic reticulum	Cytoplasm	Endoplasmic reticulum	Endoplasmic reticulum	Mitochondria
Low	↑			↓					↓	
Medium	↓↓↓	↓↓↓		↓↓↓	↓					↓↓
High				↓↓↓	↓↓↓					↓↓↓

Future Implications

Conclusion

In this study we exposed H295R cells to CNC to understand potential cytotoxic, antioxidant, and endocrine disruption effects after exposure. Here we found that there was only a significant decline in cellular viability at the high exposure concentration of CNC, which is an order of magnitude above the allowable exposure limit determined by OSHA. Additionally, there was indication of mitophagy at the medium and high concentrations, but these findings were not statistically significant. The high concentration was the only treatment to have significant fold changes in HMOX1, SOD1, and SOD2 expression levels which is consistent with the steroidogenic fold change in the high CNC concentration sample where CYP19, CYP21, and StAR were significantly down-regulated (greater than 10 fold). Here we integrated nanomaterial transformation while understanding the potential adverse effects after exposure scenarios through

advanced molecular biology techniques. We also gained the understanding of potential toxicities after nanomaterial transformation in biological fluids and the effects on the steroidogenic pathway. These findings are the first to demonstrate endocrine disruption potential of a nanomaterial exposure. We hope that this study will serve as an outline of how future renewable nanomaterials can be tested. These studies can be used to inform regulators regarding exposure concentration limits and impact occupational health and safety precautions.

Materials and Methods

Physicochemical Characterization of CNC

The CNC powder used in this study was acquired from InnoTech Alberta (Vegreville, AB, Canada). The CNC powder was fully characterized for important physical and chemical properties including morphology, length, size, and width, elemental composition, metal impurities, surface charge, dispersity index, and the hydrodynamic diameter. Before exposure, CNC was inoculated with cell culture media and serum as a relevant exposure condition.

Maintaining Cell Culture

Human adrenocortical carcinoma cells (H295R CRL-2128) were purchased from American Type Culture Collection (ATCC, Manassas, Virginia, US) and cultured in a humidified incubator with 5% CO_2 at 37 °C (NuAire Laboratory Equipment, Plymouth, MN, US). The cells were cultured as a monolayer in Dulbecco's modified eagle medium:F12 (Thermo Fisher Scientific, Waltham, MA, US) which was supplemented with Nu-serum I 2.5% and ITS+ Premix (Corning Inc., Corning, NY, US), and 0.01%

penicillin and streptomycin antibiotics (Thermo Fisher Scientific, Waltham, MA, US)). Media was replenished every 2-3 days and cells were subcultured with trypsin-EDTA at 0.05% and trypsin neutralizing solution. (Thermo Fisher Scientific, Waltham, MA, US). During experimentation, cells were all utilized at a low and consistent passage (8) and each cell culture assay represent 6 independent sample replicates. Cells were assayed at 80% confluency.

Exposure of CNC to H295R Cells

Once H295R cells were grown to 80% confluency, cultures were inoculated with 0.5, 5.0, and 50.0 mg/m^3 CNC previously suspended in cell culture media. These samples are termed low, medium, and high exposure concentration samples, respectively. Exposure duration was 48 hours as guided by OCSPP Guideline 890.1550 provided by the EPA.

Cytotoxicity

The PrestoBlue Cell Viability Reagent Assay (ThermoFisher Scientific) was used to measure cellular proliferation. Briefly, the H295R cells were exposed to the three low, medium, and high concentrations of CNC for 48 hours and then rinsed with PBS and supplemented with fresh media. A 1:10 volume of PrestoBlue reagent was added to the H295R cells and the assay incubated at 37 °C with 5% CO_2 for 2 hours. The absorbance was measured at 570 nm with a reference wavelength of 600 nm on a Synergy H1 plate reader (BioTek, Winooski, VT, US). Untreated (control) and media only controls were measured as well. The PrestoBlue assay was used to monitor cellular proliferation and viability after CNC exposure. For metabolic activity the MTS Assay Kit (Abcam,

Cambridge, United Kingdom) was utilized. In summary, the rinsed exposed H295R cells were incubated at 37 °C with 5% CO_2 for 2 hours with a 1:5 volume of the MTS reagent. The MTS assay absorbance was read at 490 nm on the Synergy H1 plate reader. This assay was used to measure the cell proliferation in response to CNC exposure.

H295R Preparation for Ultrastructure Analysis

H295R cells were treated with 0.5, 5.0, and 50.0 mg/m^3 CNC suspensions for 48 hours. Note, all microscopy preparation reagents were purchased from Electron Microscopy Sciences (EMS; Hatfield, PA, US) unless otherwise stated. The inoculated cell culture media was removed, and the cells were rinsed with phosphate buffered saline (PBS, Thermo Fisher Scientific, Waltham, MA, US) to ensure removal of excess CNC. The samples were then removed from the cell culture dish by incubating with trypsin for 5 minutes at 37℃. Once cells began to detach from the plate, the trypsin was neutralized with the addition of equal parts media. This solution was collected into a microcentrifuge tube and centrifuged at 200 x g for 5 minutes to create a pellet. The supernatant was discarded and then replaced with 2.5% glutaraldehyde solution was suspended in a 0.1 M sodium cacodylate buffer (EMS) with the pH adjusted to 7.2. The cells were fixed for 30 minutes in the solution, and then the supernatant was removed. The pellet of cells was washed with cacodylate buffer for 10 minutes in triplicate.

The cells were then secondary fixed for 30 minutes. The secondary fixation solution contained 1% osmium tetroxide, 0.1 M cacodylate buffer, 3mM calcium chloride, and 0.8% potassium ferrocyanide (EMS). After 30 minutes, the secondary fixation solution was removed, and the cells were washed with cacodylate buffer for 10 minutes in triplicate. Next, to achieve post-fixation staining, a 1% uranyl acetate solution was added

for 30 minutes. The samples were washed and dehydrated in a series of increasing concentrations of acetone. The dehydration series consisted of two incubations in 50% acetone in de-ionized water for 10 min, two incubations in 70% acetone in de-ionized water for 10 min, two incubations in 90% acetone in de-ionized water for 15 min, and two incubations in 100% acetone for 15 min.

An Embed 812 epoxy resin was then prepared using Embed 812, dodecenylsuccinic anhydride (DDSA), methyl nadic anhydride (MNA), and benzyldimethylamine (BDMA) (Electron Microscopy Sciences) as the accelerant. The samples were then infiltrated with increasing concentrations (1:2, 1:1, 2:1) of the Embed 812 resin and acetone. The samples were then placed in 100 % Embed 812 resin and pelleted in preparation of polymerization (incubation in 60℃ oven for 48 h). Following polymerization, the blocks were trimmed, ultrathin sectioned to 70 nm, and placed on copper mesh grids. Post-staining was performed with lead citrate (Electron Microscopy Sciences) for 5 min, and 1% uranyl acetate for 15 min. The grids were then imaged with a transmission electron microscope (JEM-1010; JEOL Inc., Tokyo, Japan) at 60kV with a spot size of 2.0.

Mitochondria Ultrastructural Analyses

Mitochondria in each pictured were numbered and the length and widths were measured with ImageJ software. (NIH) The measurements recorded were exported into GraphPad Prism for analyses. The following equation was used to determine mitochondrial roundness.

$$R_{Mitochondria}=|1-L_{Mitochondria}/W_{Mitochondria}| \quad [1]$$

The average roundness is $R_{Mitochondria}$, the average length is $L_{Mitochondria}$, and the average width is represented by $W_{Mitochondria}$. The absolute value of the ratio represents the "roundness" of the mitochondria. A perfectly round mitochondrial is represented as a value of "0", where values greater than 0 represent mitochondrial elongation. The sample size per treatment was N=100 to ensure accurate depiction of sample. The mitochondrial area was quantified using ImageJ software. The average mitochondrial area was calculated with the following equation.

$$(L_{Mitochondria} \times 0.5)\,(W_{Mitochondria} \times 0.5)\pi \quad [2]$$

The mitochondrial sample size was N=100, where mitochondria probed were the same for the roundness and area calculations.

Gene Expression

H295R cells with no treatment and the low, medium, and high CNC exposure concentrations were harvested after 48 hours. The PureLink RNA Mini Kit (Invitrogen, Waltham, MA, US) was used to isolate RNA from the harvested cells. To remove genomic DNA and complete reverse transcription from RNA to cDNA, the SuperScript IV VILO Master Mix with ezDNase Enzyme (Invitrogen) was used. The Qubit RNA HS Assay kit in conjunction with the Qubit 3 (Invitrogen) was utilized to quantify the RNA and cDNA used in this experiment. The TaqMan Fast Advanced Master mix kit was used with selected primers to perform qPCR measurements on a StepOne Real-Time PCR System (Applied Biosystems, Foster City, CA, US) using 48 well plates. TaqMan primer assays were selected for the steroidogenic and antioxidant genes probed here. The $2^{-\Delta\Delta CT}$

values are used to express the fold change which has been normalized to the endogenous control, βactin, and then the expression levels were normalized to the unexposed H295R cell sample.

Statistical Analysis

All statistical analyses were completed with GraphPad Prism software version 8.4.3. for windows (San Diego, CA, US.) A violin plot of the average mitochondrial roundness as well as the average mitochondrial area was plotted to show the probability density of the data across the values. This method was used to visualize trends in the data. Sample size for all mitochondrial analyses was N=100. Statistical analyses completed for viability, mitochondrial roundness and area, and the gene expression analyses were assessed using one-way ANOVA, where a significant value was represented having a p-value <0.05. When a value was considered as significant, the Dunnett's post-hoc test was used. The gene expression data was completed with 3 biological replicates and 3 technical replicates.

References

Ahmadi, N., Ghanbarinejad, V., Ommati, M. M., Jamshidzadeh, A., & Heidari, R. (2018). Taurine prevents mitochondrial membrane permeabilization and swelling upon interaction with manganese: Implication in the treatment of cirrhosis-associated central nervous system complications. Journal of biochemical and molecular toxicology, 32(11), e22216.

Belgacem, M. N., & Gandini, A. (2011). Monomers, polymers and composites from renewable resources: Elsevier.

Bhatia, D., Capili, A., & Choi, M. E. (2020). Mitochondrial dysfunction in kidney injury, inflammation, and disease: potential therapeutic approaches. Kidney Research and Clinical Practice, 39(3), 244.

Bosc, C., Broin, N., Fanjul, M., Saland, E., Farge, T., Courdy, C., . . . Skuli, S. (2020). Autophagy regulates fatty acid availability for oxidative phosphorylation through mitochondria-endoplasmic reticulum contact sites. Nature communications, 11(1), 1-14.

Catalán, J., Ilves, M., Järventaus, H., Hannukainen, K. S., Kontturi, E., Vanhala, E., . . . Norppa, H. (2015). Genotoxic and immunotoxic effects of cellulose nanocrystals in vitro. Environmental and molecular mutagenesis, 56(2), 171-182.

Chen, X., Li, C., Grätzel, M., Kostecki, R., & Mao, S. S. (2012). Nanomaterials for renewable energy production and storage. Chemical Society Reviews, 41(23), 7909-7937.

Dincer, I. (2000). Renewable energy and sustainable development: a crucial review. Renewable and sustainable energy reviews, 4(2), 157-175.

Donaldson, K., Poland, C. A., Murphy, F. A., MacFarlane, M., Chernova, T., & Schinwald, A. (2013). Pulmonary toxicity of carbon nanotubes and asbestos—similarities and differences. Advanced drug delivery reviews, 65(15), 2078-2086.

Gao, K., Zhang, C., Tian, Y., Naeem, S., Zhang, Y., & Qi, Y. (2020). The role of endoplasmic reticulum stress in lead (Pb)-induced mitophagy of HEK293 cells. Toxicology and Industrial Health, 36(12), 1002-1009.

Gracia, T., Hilscherova, K., Jones, P. D., Newsted, J. L., Zhang, X., Hecker, M., . . . Wu, R. S. (2006). The H295R system for evaluation of endocrine-disrupting effects. Ecotoxicology and environmental safety, 65(3), 293-305.

Habibi, Y., Lucia, L. A., & Rojas, O. J. (2010). Cellulose nanocrystals: chemistry, self-assembly, and applications. Chemical reviews, 110(6), 3479-3500.

He, Y., Murphy, M. B., Richard, M., Lam, M. H., Hecker, M., Giesy, J. P., . . . Lam, P. K. (2008). Effects of 20 PBDE metabolites on steroidogenesis in the H295R cell line. Toxicology Letters, 176(3), 230-238.

He, Y., Wiseman, S. B., Zhang, X., Hecker, M., Jones, P. D., El-Din, M. G., . . . Giesy, J. P. (2010). Ozonation attenuates the steroidogenic disruptive effects of sediment free oil sands process water in the H295R cell line. Chemosphere, 80(5), 578-584.

Hecker, M., Newsted, J. L., Murphy, M. B., Higley, E. B., Jones, P. D., Wu, R., & Giesy, J. P. (2006). Human adrenocarcinoma (H295R) cells for rapid in vitro determination of effects on steroidogenesis: hormone production. Toxicology and applied pharmacology, 217(1), 114-124.

Hilscherova, K., Jones, P. D., Gracia, T., Newsted, J. L., Zhang, X., Sanderson, J., . . . Giesy, J. P. (2004). Assessment of the effects of chemicals on the expression of ten steroidogenic genes in the H295R cell line using real-time PCR. Toxicological Sciences, 81(1), 78-89.

Joseph, P., Umbright, C. M., Roberts, J. R., Cumpston, J. L., Orandle, M. S., McKinney, W. G., & Sager, T. M. (2021). Lung toxicity and gene expression changes in response to whole-body inhalation exposure to cellulose nanocrystal in rats. Inhalation Toxicology, 1-15.

Kamp, D. W., & Weitzman, S. A. (1999). The molecular basis of asbestos induced lung injury. Thorax, 54(7), 638-652.

Kane, A. B., Hurt, R. H., & Gao, H. (2018). The asbestos-carbon nanotube analogy: an update. Toxicology and applied pharmacology, 361, 68-80.

Martinez, K. F., Eastlake, A., Rudie, A., & Geraci, C. (2013). Occupational exposure characterization during the manufacture of cellulose nanomaterials. In: Production and applications of Cellulose Nanomaterials, TAPPI Press, Chapter 1.2, 2013; pp. 61-64., 1, 61-64.

Mendes, B. B., Gómez-Florit, M., Osório, H., Vilaça, A., Domingues, R. M., Reis, R. L., & Gomes, M. E. (2020). Cellulose nanocrystals of variable sulfation degrees can sequester specific platelet lysate-derived biomolecules to modulate stem cell response. Chemical Communications, 56(50), 6882-6885.

Paradise, M., & Goswami, T. (2007). Carbon nanotubes–production and industrial applications. Materials & design, 28(5), 1477-1489.

Poliakoff, M., & Licence, P. (2007). Green chemistry. Nature, 450(7171), 810-812.

Scott, J. L., Gabrielides, C., Davidson, R. K., Swingler, T. E., Clark, I. M., Wallis, G. A., . . . Young, D. A. (2010). Superoxide dismutase downregulation in osteoarthritis progression and end-stage disease. Annals of the rheumatic diseases, 69(8), 1502-1510.

Selikoff, I. J., Churg, J., & Hammond, E. C. (1964). Asbestos exposure and neoplasia. Jama, 188(1), 22-26.

Shafiei-Sabet, S., Hamad, W., & Hatzikiriakos, S. (2014). Ionic strength effects on the microstructure and shear rheology of cellulose nanocrystal suspensions. Cellulose, 21(5), 3347-3359.

Shvedova, A. A., Kisin, E. R., Yanamala, N., Farcas, M. T., Menas, A. L., Williams, A., . . . Star, A. (2015). Gender differences in murine pulmonary responses elicited by cellulose nanocrystals. Particle and fibre toxicology, 13(1), 1-20.

Teo, H. L., & Wahab, R. A. (2020). Towards an eco-friendly deconstruction of agro-industrial biomass and preparation of renewable cellulose nanomaterials: A review. International journal of biological macromolecules.

Troy, C. M., Derossi, D., Prochiantz, A., Greene, L. A., & Shelanski, M. L. (1996). Downregulation of Cu/Zn superoxide dismutase leads to cell death via the nitric oxide-peroxynitrite pathway. Journal of Neuroscience, 16(1), 253-261.

Vincent, A. E., Ng, Y. S., White, K., Davey, T., Mannella, C., Falkous, G., . . . Gorman, G. S. (2016). The spectrum of mitochondrial ultrastructural defects in mitochondrial myopathy. Scientific reports, 6(1), 1-12.

Youle, R. J., & Van Der Bliek, A. M. (2012). Mitochondrial fission, fusion, and stress. Science, 337(6098), 1062-1065.

Zhang, X., Chang, H., Wiseman, S., He, Y., Higley, E., Jones, P., . . . Hecker, M. (2011). Bisphenol A disrupts steroidogenesis in human H295R cells. Toxicological Sciences, 121(2), 320-327.

Zhang, X., Yu, R. M., Jones, P. D., Lam, G. K., Newsted, J. L., Gracia, T., . . . Wu, R. S. (2005). Quantitative RT-PCR methods for evaluating toxicant-induced effects on steroidogenesis using the H295R cell line. Environmental science & technology, 39(8), 2777-2785.

CHAPTER FIVE

General Discussion and Conclusions

In this dissertation, critical research questions were answered regarding how to complete a step-wise approach in understanding nanomaterials transformations under situationally relevant conditions. Here, different ways to characterize nanomaterials, the associated toxicity with changing external environments, the toxicity of nanomaterial biotransformation and environmental impact, as well as the biological environment influence on physiological health and potential adverse outcomes were addressed. Some major findings elucidated that a full physicochemical characterization of nanomaterials may help understand the associated toxicities with nanomaterial transformations under different environmentally or physiologically relevant conditions. Additionally, nanomaterial transformations have a direct influence on the release of ions or reactive oxygen species, agglomeration or aggregation, and the dissolution properties of nanomaterials. These morphological changes are directly related to the potential adverse effects in both environmental and physiological conditions where the release of ions may cause an increase in cytotoxicity, agglomeration or aggregation may decrease cytotoxicity, and dissolution is situationally dependent.

The work described here aims to improve and impact the field of nanotoxicology through the diverse use of numerous techniques and mechanistic understanding of the impact of nanomaterial transformations on physiological health and potential adverse outcomes. Specifically, the work is directly linked to the Toxicology Testing in the 21st

century (Tox21). (Thomas, 2018) The Tox21 Consortium was developed in 2008 as a memorandum of understanding and now includes the Environmental Protection Agency (EPA), the National Toxicology Program (NTP) at the National Institute of Environmental Health Sciences (NIEHS), and National Human Genome Research Institute's National Chemical Genomics Center (NCGC) which is now National Center for Advancing Translational Sciences (NCATS), and the Food and Drug Administration (FDA). The consortium was created to advance the field of toxicology to create quick and efficient methods to test chemicals with potential to disrupt homeostasis and cause adverse effects. Through this, thousands of data on chemicals and pharmaceuticals have been generated and is applied to regulatory decisions. The specific goals include to (1) identify mechanisms of chemically-induced biological activity, (2) prioritize chemicals for more extensive testing, and (3) to develop more relevant and predictive models of *in vivo* toxicological response. Recently published in December 2020, Tox21 discussed its strategic direction for the next five years to improve the field of toxicology.

The first strategic direction in the Tox21 five year plan that correlated with this dissertation work is cell line selection for high throughput transcriptomics (HTT). The specific goal described is to develop a strategy for selecting maximally-diverse cell types/lines to robustly cover biological targets and pathways for high-throughput chemical screening using gene expression. Described in Chapter Four, we utilized an OECD approved *in vitro* method using the H295R cell line to rapidly screen key genes related to the steroidogenic pathway to further understand endocrine disruption potential. We found that using this cell line was very high throughput and gave maximal information related to most genes expressed in the steroidogenic pathway.

Another Tox21 strategic direction that this work focused on was its goal regarding the 'Expansion of Pathway Coverage by Tox21 High-Throughput Screening Assay for Better Prediction of Adverse Drug Effects'. Specifically, this goal aims to improve prediction of adverse drug effects by using additional assays to probe toxicologically important targets and pathways. This goal is directly addressed in Chapter Three where we performed hyperspectral imaging techniques (HSI) to understand the biotransformation of nanomaterials which are used in nanomedicines. This technique allows for the investigation of important mechanistic analyses of nanomedicine interactions in the body, where the transformation of the nanomaterial is indicative of potential toxicities from the release of ions, aggregation and agglomeration, and dissolution. By understanding what happens to the transformation of the nanomedicine *in vitro*, key insights to predict adverse drug effects, which are not currently captured in Tox21, or in the field of toxicology, can be ascertained.

The Tox21 goal of generating chemical reactivity information to understand which chemicals have electrophilic properties was also addressed in this dissertation, where nanomaterials of different capping agents were tested in Chapter Three. Many nanomaterials contain capping agents, including thiol-mediated capping agents. (Subramanian, Ganapathy, Rajaram, & Ayyaswamy, 2020; Zhou et al., 2019) In this study positive (electrophile) , negative (nucleophile) and neutral nanomaterials were tested. Some underwent aggregation, dissolution, and/or released ions. The rapid and detailed methods utilized here give insight to the understanding of nanomaterials and if they are strong electrophiles (oxidants) or if they are neutrophiles.

In Chapter Four, we investigated CNC steroidogenic gene expression after an *in vitro* exposure. Another Tox21 goal is to investigate environmental determinants of pubertal timing in girls through the activation or inhibition of gonadotropin-releasing hormone (GnRH). GnRH controls pubertal timing in girls and is also in direct correlation with the steroidogenic pathway, where previous publications indicate that CYP17A, HSD3B1, and HSDB2 (among other genes and hormone release) are directly related to GnRH signaling pathways. (Lin et al., 2008; Njar & Brodie, 1999) In this body of work, we showed how to monitor gene expression levels after toxicological exposures, which can be easily translated to inducing exposures related to environmental determinants.

Lastly, the future work will incorporate the knowledge gained from these studies to develop an *in vitro* ocular model to understand mechanisms of environmental stressors and to understand cellular irritation and damage through the developing high-throughput assays to testing nanomaterial mixtures. This work will serve as a continuation of the direct correlation through the Tox21 program where one of the five year strategic goals include developing a high-throughput assay to detect chemicals with the potential to induce skin sensitization, eye irritation, or serious eye damage. Not only is this dissertation work a basis for assessing nanomaterials, but it is also a steppingstone for continuing the advancement of the field of toxicology through complex models in situationally relevant conditions.

This body of work serves as a toxicity testing framework to be tailored to specific conditions or materials alike. The use of testing materials of varying compositions in different environments in this work was crucial in understanding the effects the surrounding environment has on nanomaterial transformations. An improvement that can

be made to this work would be the addition of full physicochemical characterizations on the transformation products *in situ* and *in vitro*. Additionally, this study highlighted the critical influence that surface charge has in nanomedicine transformation mechanisms. The understanding of surface charge influence is important in the field of nanomedicine because it allows us to predict potential transformation mechanisms *in vitro*. Furthermore, transformation changes regarding nanomaterial size and agglomeration (measured by hydrodynamic diameter), surface charge (measured by zeta potential), and agglomeration (measured by hyperspectral imaging and transmission electron microscopy) are evident and ought to be considered in nanomedicine research and development. In this study, we showed that the surface charge plays a substantial role in predicting agglomeration and intercellular uptake. A "one size fits all" characterization approach for nano-enabled drug products is not enough to make predictive and insightful conclusions; multiple physicochemical properties are translatable to critical quality attributes.

To further this line of inquiry, mixture exposure scenarios along with more advanced *in vitro* or *in vivo* models should be utilized. More specifically, three-dimensional cell culture models (organoids) can be used to have a more sophisticated approach to monitoring adverse effects through the incorporation of multiple cell types. Organoids are a cost-effective and rapid analog to *in vivo* models which could be used for nanomaterial transformation assessments. These advancements offer further insight into crucial mechanisms via multiple cell lineages where monocultures cannot. Organoids are currently used for drug testing, absorption distribution metabolism and excretion (ADME) studies, and drug development studies, to name a few (Hedrich et al., 2020; Qin

et al., 2020; Weeber, Ooft, Dijkstra, & Voest, 2017). The models can resemble the brain, kidney, intestine, lung, stomach, eye, and many other types of body systems or organ functions. One example of relevant organoids that can be used to study situationally relevant conditions is the use of an eye surface organoid. (Lu, Yin, Grant, & Elisseeff, 2017) The organoid can be exposed to situationally relevant conditions and probed for changes in gene, protein, cellular and ultrastructural changes to understand the effects of nanomaterials in the air and how they transform when interacting with tear fluid. Additionally, the mechanistic effects of the nanomaterial transformations in tear fluid could elucidate mechanisms of tissue damage or irreversible repair. (Weber et al., 2010)

Another way the toxicological studies in this work could be advanced is the integration of a mixture or chronic transformation simulations. The studies included in this work were limited to one type of nanomaterial for one time point. It would be of interest to elucidate findings regarding nanomaterial transformations over an extended period. Chronic simulations could include increasing the time the nanomaterial would be in various conditions and allow for understanding the transformation life cycle (i.e. release into waterways and uptake into wildlife or metabolized in the body and excreted). These transformations would elucidate a more advanced understanding of the potential toxicities of the nanomaterial at each stage of its life cycle.

Given the increasing use of nanomaterials in various consumer products and industrial processes, it is of the utmost importance to better understand potential mechanisms of adverse effects. This work serves as a stepwise approach to understand nanomaterial transformations under situationally relevant conditions to ensure human health and safety when developing regulations and standard operating procedure with

newly developed materials. The goal of this dissertation was to conduct a comprehensive study of increasingly complex situationally relevant environments on organic and inorganic nanomaterials to understand nanomaterial transformations and the associated toxicity after exposures. We were specifically interested in determining ways to characterize nanomaterials within situationally relevant conditions, how the external environment impacts nanomaterial transformation, how the toxicity of nanomaterial biotransformation is impacted by situationally relevant conditions, and finally, how this may impact health and cause potential adverse outcomes. Ultimately, the significance of this dissertation is to increase the understanding of nanomaterial transformation mechanisms in more detail to advance the field of toxicology. This work will aid in risk assessments and regulatory considerations of potential adverse or favorable effects that nanomaterial transformations may have in drug delivery or new product formation scenarios.

References

Hedrich, W. D., Panzica-Kelly, J. M., Chen, S.-J., Strassle, B., Hasson, C., Lecureux, L., . . . Gan, J. (2020). Development and characterization of rat duodenal organoids for ADME and toxicology applications. Toxicology, 446, 152614.

Lin, Y. M., Poon, S. L., Choi, J. H., Lin, J. S. N., Leung, P. C., & Huang, B. M. (2008). Transcripts of testicular gonadotropin-releasing hormone, steroidogenic enzymes, and intratesticular testosterone levels in infertile men. Fertility and sterility, 90(5), 1761-1768.

Lu, Q., Yin, H., Grant, M. P., & Elisseeff, J. H. (2017). An in vitro model for the ocular surface and tear film system. Scientific reports, 7(1), 1-11.

Njar, V., & Brodie, A. (1999). Inhibitors of 170-Hydroxylase/17, 20-Lyase (CYP17): Potential Agents for. Current pharmaceutical design, 5(3), 163.

Qin, X., Sufi, J., Vlckova, P., Kyriakidou, P., Acton, S. E., Li, V. S., . . . Tape, C. J. (2020). Cell-type-specific signaling networks in heterocellular organoids. Nature methods, 17(3), 335-342.

Subramanian, S., Ganapathy, S., Rajaram, M., & Ayyaswamy, A. (2020). Tuning the optical properties of colloidal Quantum Dots using thiol group capping agents and its comparison. Materials Chemistry and Physics, 249, 123127.

Thomas, R.T, Paules, R.S, Simeonov, A, Fitzpatrick, S, Crofton, K, Casey, W and Mendrick, D. The US Federal Tox21 Program: A Strategic and Operational Plan for Continued Leadership. ALTEX. (2018). doi:10.14573/altex.1803011

Weber, J. A., Baxter, D. H., Zhang, S., Huang, D. Y., How Huang, K., Jen Lee, M., . . . Wang, K. (2010). The microRNA spectrum in 12 body fluids. Clinical chemistry, 56(11), 1733-1741.

Weeber, F., Ooft, S. N., Dijkstra, K. K., & Voest, E. E. (2017). Tumor organoids as a pre-clinical cancer model for drug discovery. Cell chemical biology, 24(9), 1092-1100.

Zhou, W., Ling, L., Du, Y., He, W., Xia, Q., Yao, C., & Li, X. (2019). Thiol-Mediated Multidentate Phosphorylcholine as a Zwitterionic Ligand for Stabilizing Biocompatible Gold Nanoparticles. Langmuir, 35(40), 13031-13039.

APPENDIX

APPENDIX A

Supporting Chapter Three

Excerpt From: Stewart, M., Mulenos, M. R., Steele, L. R., & Sayes, C. M. (2018). Differences among unique nanoparticle protein corona constructs: a case study using data analytics and multi-variant visualization to describe physicochemical characteristics. Applied Sciences, 8(12), 2669.

The published paper “Differences Among Unique Nanoparticle Protein Corona Constructs: A Case Study Using Data Analytics and Multi-Variant Visualization To Describe Physicochemical Characteristics " expands upon themes from Chapter 3 in this dissertation. The paper highlights the importance of data analytics and multi-variate visualization in addition to the relation between data analyses and the correlation between nanomaterial properties to adverse effects. This appendix will discuss why the results and results interpretation are essential to understanding downstream effects.

The field of nanotoxicology strives to correlate nanoparticle properties to adverse health effects. Currently in the literature there is no consensus to which physicochemical properties predict toxicological responses. For example, crystal structure, nanomaterial size, and surface charge are all indicators of different important toxicological endpoints (i.e.) increased cytotoxicity in mammalian cell populations (Braydich-Stolle et al., 2009; Kobayashi et al., 2009; Sayes et al., 2006; Warheit, Webb, Reed, Frerichs, & Sayes, 2007), drivers in systemic distribution (Fujiwara et al., 2008; Powers, Palazuelos, Moudgil, & Roberts, 2007) (Warheit, Webb, Sayes, Colvin, & Reed, 2006) , and cellular uptake mechanisms (Berg, Romoser, Banerjee, Zebda, & Sayes, 2009; Chithrani, Ghazani, & Chan, 2006; Fröhlich, 2012; He, Hu, Yin, Tang, & Yin, 2010), respectively. However, each paper discussing the relationship between nanomaterial physical and

chemical properties to induced biological effects is opposed with reports which lack association. (Christensen et al., 2010; Fischer & Chan, 2007; Huk et al., 2014; Warheit, Webb, Colvin, Reed, & Sayes, 2007)

Nanomaterial studies in complex mixtures are studied to decipher physical and chemical properties that induce mechanisms of toxic action. The data required for these studies requires multi-level analyses which include multiple parameters. Specifically related to the nanomaterial transformation research, important parameters studied include the nanomaterial composition, size, charge, corona composition, source, and mass. Advanced techniques are required for most or all the analyses. Data visualization is critical in the interpretation of complex data and applying the knowledge gained to the next set of research questions. (Docherty, Vorderstrasse, Brandon, & Johnson, 2017)

Chapter 3 utilizes a battery of complex techniques to identify nanomaterial physical and chemical properties to understand physiological effects related to nanomedicines. Techniques used in that study included enhanced dark field imaging with hyperspectral imaging, transmission electron microscopy, fluorescent microcopy, dynamic light scattering, UV-Vis absorbance, to identify how nanomaterials agglomerate intracellularly. Results showed de-stabilization and/or agglomeration of nanomaterial systems intracellularly. Data collection, visualization, and results communication directly influenced conclusions made regarding health effects of nanomaterials. Results are directly translated to critical quality attributes and are exploited when developing nano-carries for nanomedicine.

References

Berg, J. M., Romoser, A., Banerjee, N., Zebda, R., & Sayes, C. M. (2009). The relationship between pH and zeta potential of∼ 30 nm metal oxide nanoparticle suspensions relevant to in vitro toxicological evaluations. Nanotoxicology, 3(4), 276-283.

Braydich-Stolle, L. K., Schaeublin, N. M., Murdock, R. C., Jiang, J., Biswas, P., Schlager, J. J., & Hussain, S. M. (2009). Crystal structure mediates mode of cell death in TiO 2 nanotoxicity. Journal of Nanoparticle Research, 11(6), 1361-1374.

Chithrani, B. D., Ghazani, A. A., & Chan, W. C. (2006). Determining the size and shape dependence of gold nanoparticle uptake into mammalian cells. Nano letters, 6(4), 662-668.

Christensen, F. M., Johnston, H. J., Stone, V., Aitken, R. J., Hankin, S., Peters, S., & Aschberger, K. (2010). Nano-silver–feasibility and challenges for human health risk assessment based on open literature. Nanotoxicology, 4(3), 284-295.

Docherty, S. L., Vorderstrasse, A., Brandon, D., & Johnson, C. (2017). Visualization of multidimensional data in nursing science. Western journal of nursing research, 39(1), 112-126.

Fischer, H. C., & Chan, W. C. (2007). Nanotoxicity: the growing need for in vivo study. Current opinion in biotechnology, 18(6), 565-571.

Fröhlich, E. (2012). The role of surface charge in cellular uptake and cytotoxicity of medical nanoparticles. International journal of nanomedicine, 7, 5577.

Fujiwara, K., Suematsu, H., Kiyomiya, E., Aoki, M., Sato, M., & Moritoki, N. (2008). Size-dependent toxicity of silica nano-particles to Chlorella kessleri. Journal of Environmental Science and Health, Part A, 43(10), 1167-1173.

He, C., Hu, Y., Yin, L., Tang, C., & Yin, C. (2010). Effects of particle size and surface charge on cellular uptake and biodistribution of polymeric nanoparticles. Biomaterials, 31(13), 3657-3666.

Huk, A., Izak-Nau, E., Reidy, B., Boyles, M., Duschl, A., Lynch, I., & Dušinska, M. (2014). Is the toxic potential of nanosilver dependent on its size? Particle and fibre toxicology, 11(1), 1-16.

Kobayashi, N., Naya, M., Endoh, S., Maru, J., Yamamoto, K., & Nakanishi, J. (2009). Comparative pulmonary toxicity study of nano-TiO2 particles of different sizes and agglomerations in rats: different short-and long-term post-instillation results. Toxicology, 264(1-2), 110-118.

Powers, K. W., Palazuelos, M., Moudgil, B. M., & Roberts, S. M. (2007). Characterization of the size, shape, and state of dispersion of nanoparticles for toxicological studies. Nanotoxicology, 1(1), 42-51.

Sayes, C. M., Wahi, R., Kurian, P. A., Liu, Y., West, J. L., Ausman, K. D., . . . Colvin, V. L. (2006). Correlating nanoscale titania structure with toxicity: a cytotoxicity and inflammatory response study with human dermal fibroblasts and human lung epithelial cells. Toxicological Sciences, 92(1), 174-185.

Warheit, D. B., Webb, T. R., Colvin, V. L., Reed, K. L., & Sayes, C. M. (2007). Pulmonary bioassay studies with nanoscale and fine-quartz particles in rats: toxicity is not dependent upon particle size but on surface characteristics. Toxicological Sciences, 95(1), 270-280.

Warheit, D. B., Webb, T. R., Reed, K. L., Frerichs, S., & Sayes, C. M. (2007). Pulmonary toxicity study in rats with three forms of ultrafine-TiO2 particles: differential responses related to surface properties. Toxicology, 230(1), 90-104.

Warheit, D. B., Webb, T. R., Sayes, C. M., Colvin, V. L., & Reed, K. L. (2006). Pulmonary instillation studies with nanoscale TiO2 rods and dots in rats: toxicity is not dependent upon particle size and surface area. Toxicological Sciences, 91(1), 227-236.

BIBLIOGRAPHY

Adabi, M., Naghibzadeh, M., Adabi, M., Zarrinfard, M. A., Esnaashari, S. S., Seifalian, A. M., . . . Ghanbari, H. (2017). Biocompatibility and nanostructured materials: applications in nanomedicine. Artificial cells, nanomedicine, and biotechnology, 45(4), 833-842.

Adegboyega, N. F., V. K. Sharma, K. M. Siskova, R. Vecerova, M. Kolar, R. Zbořil and J. L. Gardea-Torresdey (2014). "Enhanced formation of silver nanoparticles in Ag+-NOM-iron (II, III) systems and antibacterial activity studies." Environmental science & technology 48(6): 3228-3235.

Adegboyega, N. F., V. K. Sharma, L. Cizmas and C. M. Sayes (2016). "UV light induces Ag nanoparticle formation: roles of natural organic matter, iron, and oxygen." Environmental Chemistry Letters 14(3): 353-357.

Ahmadi, N., Ghanbarinejad, V., Ommati, M. M., Jamshidzadeh, A., & Heidari, R. (2018). Taurine prevents mitochondrial membrane permeabilization and swelling upon interaction with manganese: Implication in the treatment of cirrhosis-associated central nervous system complications. Journal of biochemical and molecular toxicology, 32(11), e22216.

Ahn, E. C., H. S. P. Wong and E. Pop (2018). "Carbon nanomaterials for non-volatile memories." Nature Reviews Materials 3(3): 1-15.

Akaighe, N., R. I. MacCuspie, D. A. Navarro, D. S. Aga, S. Banerjee, M. Sohn and V. K. Sharma (2011). "Humic acid-induced silver nanoparticle formation under environmentally relevant conditions." Environmental science & technology 45(9): 3895-3901.

Albanese, A., P. S. Tang and W. C. W. Chan (2012). "The effect of nanoparticle size, shape, and surface chemistry on biological systems." Annual review of biomedical engineering 14: 1-16.

Alivio, T. E. G., N. A. Fleer, J. Singh, G. Nadadur, M. Feng, S. Banerjee and V. K. Sharma (2018). "Stabilization of Ag–Au Bimetallic Nanocrystals in Aquatic Environments Mediated by Dissolved Organic Matter: A Mechanistic Perspective." Environmental science & technology 52(13): 7269-7278.

Amde, M., J.-f. Liu, Z.-Q. Tan and D. Bekana (2017). "Transformation and bioavailability of metal oxide nanoparticles in aquatic and terrestrial environments. A review." Environmental Pollution 230: 250-267.

Araújo, F., Shrestha, N., Granja, P. L., Hirvonen, J., Santos, H. A., & Sarmento, B. (2015). Safety and toxicity concerns of orally delivered nanoparticles as drug carriers. Expert opinion on drug metabolism & toxicology, 11(3), 381-393.

Badawy, A. M. E., Luxton, T. P., Silva, R. G., Scheckel, K. G., Suidan, M. T., & Tolaymat, T. M. (2010). Impact of environmental conditions (pH, ionic strength, and electrolyte type) on the surface charge and aggregation of silver nanoparticles suspensions. Environmental science & technology, 44(4), 1260-1266.

Balbus, J. M., Maynard, A. D., Colvin, V. L., Castranova, V., Daston, G. P., Denison, R. A., . . . Wong, B. A. (2007). Meeting report: hazard assessment for nanoparticles--report from an interdisciplinary workshop. Environ Health Perspect, 115(11), 1654-1659. doi:10.1289/ehp.10327

Bäuerlein, P. S., E. Emke, P. Tromp, J. A. M. H. Hofman, A. Carboni, F. Schooneman, P. de Voogt and A. P. van Wezel (2017). "Is there evidence for man-made nanoparticles in the Dutch environment?" Science of the Total Environment 576: 273-283.

Belgacem, M. N., & Gandini, A. (2011). Monomers, polymers and composites from renewable resources: Elsevier.

Berg, J. M., Romoser, A., Banerjee, N., Zebda, R., & Sayes, C. M. (2009). The relationship between pH and zeta potential of∼ 30 nm metal oxide nanoparticle suspensions relevant to in vitro toxicological evaluations. Nanotoxicology, 3(4), 276-283.

Bhatia, D., Capili, A., & Choi, M. E. (2020). Mitochondrial dysfunction in kidney injury, inflammation, and disease: potential therapeutic approaches. Kidney Research and Clinical Practice, 39(3), 244.

Bobo, D., Robinson, K. J., Islam, J., Thurecht, K. J., & Corrie, S. R. (2016). Nanoparticle-based medicines: a review of FDA-approved materials and clinical trials to date. Pharmaceutical research, 33(10), 2373-2387.

Borm, P., Klaessig, F., Landry, T., Moudgil, B., Pauluhn, J., Thomas, K., . . . Wood, S. (2006). Research strategies for safety evaluation of nanomaterials, Part V: Role of dissolution in biological fate and effects of nanoscale particles. Toxicological Sciences, 90(1), 23-32. doi:10.1093/toxsci/kfj084

Bosc, C., Broin, N., Fanjul, M., Saland, E., Farge, T., Courdy, C., . . . Skuli, S. (2020). Autophagy regulates fatty acid availability for oxidative phosphorylation through mitochondria-endoplasmic reticulum contact sites. Nature communications, 11(1), 1-14.

Braydich-Stolle, L. K., Breitner, E. K., Comfort, K. K., Schlager, J. J., & Hussain, S. M. (2014). Dynamic characteristics of silver nanoparticles in physiological fluids: toxicological implications. Langmuir, 30(50), 15309-15316.

Braydich-Stolle, L. K., Schaeublin, N. M., Murdock, R. C., Jiang, J., Biswas, P., Schlager, J. J., & Hussain, S. M. (2009). Crystal structure mediates mode of cell death in TiO 2 nanotoxicity. Journal of Nanoparticle Research, 11(6), 1361-1374.

Brenner, S., & Horne, R. (1959). A Negative Staining Method for High Resolution Electron Microscopy Of Viruses. Biochimica Et Biophysica Acta, 34(1), 103-110. Doi:10.1016/0006-3002(59)90237-9

Carlson, C., S. M. Hussain, A. M. Schrand, L. K. Braydich-Stolle, K. L. Hess, R. L. Jones and J. J. Schlager (2008). "Unique cellular interaction of silver nanoparticles: size-dependent generation of reactive oxygen species." The journal of physical chemistry B 112(43): 13608-13619.

Casuccio, G., Schlaegle, S., Lersch, T., Huffman, G., Chen, Y., & Shah, N. (2004). Measurement of fine particulate matter using electron microscopy techniques. Fuel Processing Technology, 85(6-7), 763-779. doi: 10.1016/j.fuproc.2003.11.026

Catalán, J., Ilves, M., Järventaus, H., Hannukainen, K. S., Kontturi, E., Vanhala, E., . . . Norppa, H. (2015). Genotoxic and immunotoxic effects of cellulose nanocrystals in vitro. Environmental and molecular mutagenesis, 56(2), 171-182.

Cedervall, T., Lynch, I., Lindman, S., Berggård, T., Thulin, E., Nilsson, H., . . . Linse, S. (2007). Understanding the nanoparticle–protein corona using methods to quantify exchange rates and affinities of proteins for nanoparticles. Proceedings of the National Academy of Sciences, 104(7), 2050-2055.

Chandran, P., Riviere, J. E., & Monteiro-Riviere, N. A. (2017). Surface chemistry of gold nanoparticles determines the biocorona composition impacting cellular uptake, toxicity and gene expression profiles in human endothelial cells. Nanotoxicology, 11(4), 507-519.

Chen, X., Li, C., Grätzel, M., Kostecki, R., & Mao, S. S. (2012). Nanomaterials for renewable energy production and storage. Chemical Society Reviews, 41(23), 7909-7937.

Chithrani, B. D., Ghazani, A. A., & Chan, W. C. (2006). Determining the size and shape dependence of gold nanoparticle uptake into mammalian cells. Nano letters, 6(4), 662-668.

Choi, O., Deng, K. K., Kim, N.-J., Ross Jr, L., Surampalli, R. Y., & Hu, Z. (2008). The inhibitory effects of silver nanoparticles, silver ions, and silver chloride colloids on microbial growth. Water research, 42(12), 3066-3074.

Christensen, F. M., Johnston, H. J., Stone, V., Aitken, R. J., Hankin, S., Peters, S., & Aschberger, K. (2010). Nano-silver–feasibility and challenges for human health risk assessment based on open literature. Nanotoxicology, 4(3), 284-295.

Cohen, J., DeLoid, G., Pyrgiotakis, G., & Demokritou, P. (2013). Interactions of engineered nanomaterials in physiological media and implications for in vitro dosimetry. Nanotoxicology, 7(4), 417-431.

Colombo, A., Saibene, M., Moschini, E., Bonfanti, P., Collini, M., Kasemets, K., & Mantecca, P. (2017). Teratogenic hazard of BPEI-coated silver nanoparticles to Xenopus laevis. Nanotoxicology, 11(3), 405-418.

Corbo, C., Molinaro, R., Parodi, A., Toledano Furman, N. E., Salvatore, F., & Tasciotti, E. (2016). The impact of nanoparticle protein corona on cytotoxicity, immunotoxicity and target drug delivery. Nanomedicine, 11(1), 81-100.

Cortese-Krott, M. M., Münchow, M., Pirev, E., Heβner, F., Bozkurt, A., Uciechowski, P., . . . Suschek, C. V. (2009). Silver ions induce oxidative stress and intracellular zinc release in human skin fibroblasts. Free Radical Biology and Medicine, 47(11), 1570-1577.

Cueva, C., Gil-Sánchez, I., Tamargo, A., Miralles, B., Crespo, J., Bartolomé, B., & Moreno-Arribas, M. V. (2019). Gastrointestinal digestion of food-use silver nanoparticles in the dynamic SIMulator of the GastroIntestinal tract (simgi®). Impact on human gut microbiota. Food and Chemical Toxicology, 132, 110657.

Danaei, M., Dehghankhold, M., Ataei, S., Hasanzadeh Davarani, F., Javanmard, R., Dokhani, A., . . . Mozafari, M. (2018). Impact of particle size and polydispersity index on the clinical applications of lipidic nanocarrier systems. Pharmaceutics, 10(2), 57.

Dawidczyk, C. M., Kim, C., Park, J. H., Russell, L. M., Lee, K. H., Pomper, M. G., & Searson, P. C. (2014). State-of-the-art in design rules for drug delivery platforms: lessons learned from FDA-approved nanomedicines. Journal of Controlled Release, 187, 133-144.

de Vlieger, J. S., Crommelin, D. J., Tyner, K., Drummond, D. C., Jiang, W., McNeil, S. E., . . . Shah, V. P. (2019). Report of the AAPS Guidance Forum on the FDA draft guidance for industry:“drug products, including biological products, that contain nanomaterials”. In: Springer.

DeLoid, G. M., Wang, Y., Kapronezai, K., Lorente, L. R., Zhang, R., Pyrgiotakis, G., . . . De La Torre-Roche, R. (2017). An integrated methodology for assessing the impact of food matrix and gastrointestinal effects on the biokinetics and cellular toxicity of ingested engineered nanomaterials. Particle and fibre toxicology, 14(1), 40.

Dieckmann, Y., Cölfen, H., Hofmann, H., & Petri-Fink, A. (2009). Particle size distribution measurements of manganese-doped ZnS nanoparticles. Analytical Chemistry, 81(10), 3889-3895.

Dincer, I. (2000). Renewable energy and sustainable development: a crucial review. Renewable and sustainable energy reviews, 4(2), 157-175.

Docherty, S. L., Vorderstrasse, A., Brandon, D., & Johnson, C. (2017). Visualization of multidimensional data in nursing science. Western journal of nursing research, 39(1), 112-126.

Donaldson, K., Poland, C. A., Murphy, F. A., MacFarlane, M., Chernova, T., & Schinwald, A. (2013). Pulmonary toxicity of carbon nanotubes and asbestos—similarities and differences. Advanced drug delivery reviews, 65(15), 2078-2086.

Duman, O., & Tunç, S. (2009). Electrokinetic and rheological properties of Na-bentonite in some electrolyte solutions. Microporous and Mesoporous Materials, 117(1-2), 331-338.

Duvall, M. N. (2012). FDA regulation of nanotechnology. Washington, DC, USA: Beveridge & Diamond, PG.

Elder, A., Vidyasagar, S., & DeLouise, L. (2009). Physicochemical factors that affect metal and metal oxide nanoparticle passage across epithelial barriers. Wiley Interdisciplinary Reviews: Nanomedicine and Nanobiotechnology, 1(4), 434-450.

Fischer, H. C., & Chan, W. C. (2007). Nanotoxicity: the growing need for in vivo study. Current opinion in biotechnology, 18(6), 565-571.

Franklin, N. M., Rogers, N. J., Apte, S. C., Batley, G. E., Gadd, G. E., & Casey, P. S. (2007). Comparative toxicity of nanoparticulate ZnO, bulk ZnO, and ZnCl2 to a freshwater microalga (Pseudokirchneriella subcapitata): the importance of particle solubility. Environmental science & technology, 41(24), 8484-8490.

FRENS, G. (1972). Particle-size and sol stability in metal colloids. Kolloid-Zeitschrift and Zeitschrift Fur Polymere, 250(7), 736-+. doi:10.1007/BF01498565

Fröhlich, E. (2012). The role of surface charge in cellular uptake and cytotoxicity of medical nanoparticles. International journal of nanomedicine, 7, 5577.

Fu, P. P., Q. Xia, H.-M. Hwang, P. C. Ray and H. Yu (2014). "Mechanisms of nanotoxicity: generation of reactive oxygen species." Journal of food and drug analysis 22(1): 64-75.

Fujiwara, K., Suematsu, H., Kiyomiya, E., Aoki, M., Sato, M., & Moritoki, N. (2008). Size-dependent toxicity of silica nano-particles to Chlorella kessleri. Journal of Environmental Science and Health, Part A, 43(10), 1167-1173.

Gao, K., Zhang, C., Tian, Y., Naeem, S., Zhang, Y., & Qi, Y. (2020). The role of endoplasmic reticulum stress in lead (Pb)-induced mitophagy of HEK293 cells. Toxicology and Industrial Health, 36(12), 1002-1009.

Gao, X., S. n. M. Rodrigues, E. Spielman-Sun, S. n. Lopes, S. Rodrigues, Y. Zhang, A. Avellan, R. M. B. O. Duarte, A. Duarte and E. A. Casman (2019). "Effect of soil organic matter, soil pH, and moisture content on solubility and dissolution rate of CuO NPs in soil." Environmental science & technology 53(9): 4959-4967.

Garner, K. L. and A. A. Keller (2014). "Emerging patterns for engineered nanomaterials in the environment: a review of fate and toxicity studies." Journal of Nanoparticle Research 16(8): 2503.

Garner, K. L., S. Suh and A. A. Keller (2017). "Assessing the Risk of Engineered Nanomaterials in the Environment: Development and Application of the nanoFate Model." Environmental Science & Technology 51(10): 5541-5551.

Georgantzopoulou, A., P. Almeida Carvalho, C. Vogelsang, M. Tilahun, K. Ndungu, A. M. Booth, K. V. Thomas and A. Macken (2018). "Ecotoxicological effects of transformed silver and titanium dioxide nanoparticles in the effluent from a lab-scale wastewater treatment system." Environmental science & technology 52(16): 9431-9441.

Gitipour, A., Thiel, S. W., Scheckel, K. G., & Tolaymat, T. (2016). Anaerobic toxicity of cationic silver nanoparticles. Science of the total Environment, 557, 363-368.

Giudice, M. C. L., Herda, L. M., Polo, E., & Dawson, K. A. (2016). In situ characterization of nanoparticle biomolecular interactions in complex biological media by flow cytometry. Nature communications, 7(1), 1-10.

Goldstein, J. I., Newbury, D. E., Echlin, P., Joy, D. C., Romig, A., Lyman, C. E., . . . Lifshin, E. (1992). Coating and Conductivity Techniques for SEM and Microanalysis. In Scanning Electron Microscopy and X-Ray Microanalysis (pp. 671-740): Springer.

Gracia, T., Hilscherova, K., Jones, P. D., Newsted, J. L., Zhang, X., Hecker, M., . . . Wu, R. S. (2006). The H295R system for evaluation of endocrine-disrupting effects. Ecotoxicology and environmental safety, 65(3), 293-305.

Habibi, Y., Lucia, L. A., & Rojas, O. J. (2010). Cellulose nanocrystals: chemistry, self-assembly, and applications. Chemical reviews, 110(6), 3479-3500.

Hadrup, N., & Lam, H. R. (2014). Oral toxicity of silver ions, silver nanoparticles and colloidal silver–a review. Regulatory Toxicology and Pharmacology, 68(1), 1-7.

Hajipour, M., Fromm, K., Ashkarran, A., de Aberasturi, D., de Larramendi, I., Rojo, T., . . . Mahmoudi, M. (2012). Antibacterial properties of nanoparticles. Trends in Biotechnology, 30(10), 499-511. doi:10.1016/j.tibtech.2012.06.004

Hajipour, M., Fromm, K., Ashkarran, A., de Aberasturi, D., de Larramendi, I., Rojo, T., . . .

He, C., Hu, Y., Yin, L., Tang, C., & Yin, C. (2010). Effects of particle size and surface charge on cellular uptake and biodistribution of polymeric nanoparticles. Biomaterials, 31(13), 3657-3666.

He, D., A. M. Jones, S. Garg, A. N. Pham and T. D. Waite (2011). "Silver nanoparticle− reactive oxygen species interactions: application of a charging− discharging model." The Journal of Physical Chemistry C 115(13): 5461-5468.

He, D., S. Garg and T. D. Waite (2012). "H2O2-mediated oxidation of zero-valent silver and resultant interactions among silver nanoparticles, silver ions, and reactive oxygen species." Langmuir 28(27): 10266-10275.

He, Y., Murphy, M. B., Richard, M., Lam, M. H., Hecker, M., Giesy, J. P., . . . Lam, P. K. (2008). Effects of 20 PBDE metabolites on steroidogenesis in the H295R cell line. Toxicology Letters, 176(3), 230-238.

He, Y., Wiseman, S. B., Zhang, X., Hecker, M., Jones, P. D., El-Din, M. G., . . . Giesy, J. P. (2010). Ozonation attenuates the steroidogenic disruptive effects of sediment free oil sands process water in the H295R cell line. Chemosphere, 80(5), 578-584.

Hecker, M., Newsted, J. L., Murphy, M. B., Higley, E. B., Jones, P. D., Wu, R., & Giesy, J. P. (2006). Human adrenocarcinoma (H295R) cells for rapid in vitro determination of effects on steroidogenesis: hormone production. Toxicology and applied pharmacology, 217(1), 114-124.

Hedberg, J., E. Blomberg and I. Odnevall Wallinder (2019). "In the search for nanospecific effects of dissolution of metallic nanoparticles at freshwater-like conditions: A critical review." Environmental science & technology 53(8): 4030-4044.

Hedrich, W. D., Panzica-Kelly, J. M., Chen, S.-J., Strassle, B., Hasson, C., Lecureux, L., . . . Gan, J. (2020). Development and characterization of rat duodenal organoids for ADME and toxicology applications. Toxicology, 446, 152614.

Hilscherova, K., Jones, P. D., Gracia, T., Newsted, J. L., Zhang, X., Sanderson, J., . . . Giesy, J. P. (2004). Assessment of the effects of chemicals on the expression of ten steroidogenic genes in the H295R cell line using real-time PCR. Toxicological Sciences, 81(1), 78-89.

Hirn, S., Semmler-Behnke, M., Schleh, C., Wenk, A., Lipka, J., Schäffler, M., . . . Kreyling, W. G. (2011). Particle size-dependent and surface charge-dependent biodistribution of gold nanoparticles after intravenous administration. European Journal of Pharmaceutics and Biopharmaceutics, 77(3), 407-416. doi:10.1016/j.ejpb.2010.12.029

Hou, W.-C., B. Stuart, R. Howes and R. G. Zepp (2013). "Sunlight-driven reduction of silver ions by natural organic matter: formation and transformation of silver nanoparticles." Environmental science & technology 47(14): 7713-7721.

Huang, Y.-N., T.-T. Qian, F. Dang, Y.-G. Yin, M. Li and D.-M. Zhou (2019). "Significant contribution of metastable particulate organic matter to natural formation of silver nanoparticles in soils." Nature communications 10(1): 1-8.

Huk, A., Izak-Nau, E., Reidy, B., Boyles, M., Duschl, A., Lynch, I., & Dušinska, M. (2014). Is the toxic potential of nanosilver dependent on its size? Particle and fibre toxicology, 11(1), 1-16.

Iijima, S. (1980). High-Resolution Electron-Microscopy of Some Carbonaceous Materials. Journal of Microscopy-Oxford, 119(May), 99-111. Doi:10.1111/J.1365-2818.1980.Tb04081.X

Irandost, M., R. Akbarzadeh, M. Pirsaheb, A. Asadi, P. Mohammadi and M. Sillanpää (2019). "Fabrication of highly visible active N, S co-doped TiO2@ MoS2 heterojunction with synergistic effect for photocatalytic degradation of diclofenac: Mechanisms, modeling and degradation pathway." Journal of Molecular Liquids 291: 111342.

Joo, S. H. and D. Zhao (2017). "Environmental dynamics of metal oxide nanoparticles in heterogeneous systems: a review." Journal of hazardous materials 322: 29-47.

Joseph, P., Umbright, C. M., Roberts, J. R., Cumpston, J. L., Orandle, M. S., McKinney, W. G., & Sager, T. M. (2021). Lung toxicity and gene expression changes in response to whole-body inhalation exposure to cellulose nanocrystal in rats. Inhalation Toxicology, 1-15.

Kaminskas, L. M., Boyd, B. J., Karellas, P., Krippner, G. Y., Lessene, R., Kelly, B., & Porter, C. J. (2008). The impact of molecular weight and PEG chain length on the systemic pharmacokinetics of PEGylated poly l-lysine dendrimers. Molecular pharmaceutics, 5(3), 449-463.

Kamp, D. W., & Weitzman, S. A. (1999). The molecular basis of asbestos induced lung injury. Thorax, 54(7), 638-652.

Kane, A. B., Hurt, R. H., & Gao, H. (2018). The asbestos-carbon nanotube analogy: an update. Toxicology and applied pharmacology, 361, 68-80.

Kang, S. W., Char, K., & Kang, Y. S. (2008). Novel application of partially positively charged silver nanoparticles for facilitated transport in olefin/paraffin separation membranes. Chemistry of Materials, 20(4), 1308-1311.

Kang, S. W., Hong, J., Park, J. H., Mun, S. H., Kim, J. H., Cho, J., . . . Kang, Y. S. (2008). Nanocomposite membranes containing positively polarized gold nanoparticles for facilitated olefin transport. Journal of Membrane Science, 321(1), 90-93.

Karakoti, A., Hench, L., & Seal, S. (2006). The potential toxicity of nanomaterials—the role of surfaces. Jom, 58(7), 77-82.

Kaur, M., M. Kaur and V. K. Sharma (2018). "Nitrogen-doped graphene and graphene quantum dots: A review onsynthesis and applications in energy, sensors and environment." Advances in colloid and interface science 259: 44-64.

Keller, A. A. and A. Lazareva (2014). "Predicted releases of engineered nanomaterials: from global to regional to local." Environmental Science & Technology Letters 1(1): 65-70.

Kim, Y., J. G. Smith and P. K. Jain (2018). "Harvesting multiple electron–hole pairs generated through plasmonic excitation of Au nanoparticles." Nature chemistry 10(7): 763-769.

Kobayashi, N., Naya, M., Endoh, S., Maru, J., Yamamoto, K., & Nakanishi, J. (2009). Comparative pulmonary toxicity study of nano-TiO2 particles of different sizes and agglomerations in rats: different short-and long-term post-instillation results. Toxicology, 264(1-2), 110-118.

Lai, A., Caloz, C., & Itoh, T. (2004). Composite right/left-handed transmission line metamaterials. Ieee Microwave Magazine, 5(3), 34-50. doi:10.1109/MMW.2004.1337766

Lewinski, N., V. Colvin and R. Drezek (2008). "Cytotoxicity of nanoparticles." small 4(1): 26-49.

Li, H., Yu, Y., Faraji Dana, S., Li, B., Lee, C.-Y., & Kang, L. (2013). Novel engineered systems for oral, mucosal and transdermal drug delivery. Journal of drug targeting, 21(7), 611-629.

Li, K., J. Qian, P. Wang, C. Wang, X. Fan, B. Lu, X. Tian, W. Jin, X. He and W. Guo (2019). "Toxicity of three crystalline TiO2 nanoparticles in activated sludge: bacterial cell death modes differentially weaken sludge dewaterability." Environmental science & technology 53(8): 4542-4555.

Li, Y., Zhang, W., Niu, J., & Chen, Y. (2013). Surface-coating-dependent dissolution, aggregation, and reactive oxygen species (ROS) generation of silver nanoparticles under different irradiation conditions. Environmental Science and Technology, 47(18), 10293-10301. doi:10.1021/es400945v

Lin, Y. M., Poon, S. L., Choi, J. H., Lin, J. S. N., Leung, P. C., & Huang, B. M. (2008). Transcripts of testicular gonadotropin-releasing hormone, steroidogenic enzymes, and intratesticular testosterone levels in infertile men. Fertility and sterility, 90(5), 1761-1768.

Lindroth, M., Bell, P. B., & Fredriksson, B. A. (1987). TEM-, SEM- and STEM- Studies of Sputter-Coated Cytoskeletons. Scanning, 9, 47-56.

Liu, J. and R. H. Hurt (2010). "Ion release kinetics and particle persistence in aqueous nano-silver colloids." Environmental science & technology 44(6): 2169-2175.

Liu, J., Wang, Z., Liu, F. D., Kane, A. B., & Hurt, R. H. (2012). Chemical transformations of nanosilver in biological environments. ACS nano, 6(11), 9887-9899.

Lowry, G. V., B. P. Espinasse, A. R. Badireddy, C. J. Richardson, B. C. Reinsch, L. D. Bryant, A. J. Bone, A. Deonarine, S. Chae and M. Therezien (2012). "Long-term transformation and fate of manufactured Ag nanoparticles in a simulated large scale freshwater emergent wetland." Environmental science & technology 46(13): 7027-7036.

Lowry, G. V., Gregory, K. B., Apte, S. C., & Lead, J. R. (2012). Transformations of nanomaterials in the environment. In: ACS Publications.

Lu, Q., Yin, H., Grant, M. P., & Elisseeff, J. H. (2017). An in vitro model for the ocular surface and tear film system. Scientific reports, 7(1), 1-11.

Lujan, H., Griffin, W. C., Taube, J. H., & Sayes, C. M. (2019). Synthesis and characterization of nanometer-sized liposomes for encapsulation and microRNA transfer to breast cancer cells. International journal of nanomedicine, 14, 5159.

Lundqvist, M., Stigler, J., Elia, G., Lynch, I., Cedervall, T., & Dawson, K. A. (2008). Nanoparticle size and surface properties determine the protein corona with possible implications for biological impacts. Proceedings of the National Academy of Sciences, 105(38), 14265-14270.

Maiolo, D., Del Pino, P., Metrangolo, P., Parak, W. J., & Baldelli Bombelli, F. (2015). Nanomedicine delivery: does protein corona route to the target or off road? Nanomedicine, 10(21), 3231-3247.

Martinez, K. F., Eastlake, A., Rudie, A., & Geraci, C. (2013). Occupational exposure characterization during the manufacture of cellulose nanomaterials. In: Production and applications of Cellulose Nanomaterials, TAPPI Press, Chapter 1.2, 2013; pp. 61-64., 1, 61-64.

Medici, S., Peana, M., Nurchi, V. M., & Zoroddu, M. A. (2019). Medical uses of silver: history, myths, and scientific evidence. Journal of medicinal chemistry, 62(13), 5923-5943.

Mendes, B. B., Gómez-Florit, M., Osório, H., Vilaça, A., Domingues, R. M., Reis, R. L., & Gomes, M. E. (2020). Cellulose nanocrystals of variable sulfation degrees can sequester specific platelet lysate-derived biomolecules to modulate stem cell response. Chemical Communications, 56(50), 6882-6885.

Michen, B., Geers, C., Vanhecke, D., Endes, C., Rothen-Rutishauser, B., Balog, S., & Petri-Fink, A. (2015). Avoiding drying-artifacts in transmission electron microscopy: Characterizing the size and colloidal state of nanoparticles. Scientific reports, 5, 9793.

Moghimi, S. M., Hunter, A. C., & Murray, J. C. (2001). Long-circulating and target-specific nanoparticles: theory to practice. Pharmacological reviews, 53(2), 283-318.

Moon, R. J., Martini, A., Nairn, J., Simonsen, J., & Youngblood, J. (2011). Cellulose nanomaterials review: structure, properties and nanocomposites. Chemical Society Reviews, 40(7): 3941-3994.

Morrison, H. G., Tao, W., Trieu, W., Walker, S. D., Cui, S., Huggins, S., & Nagapudi, K. (2015). Correlation of Drug Substance Particle Size Distribution with Other Bulk Properties to Predict Critical Quality Attributes. Organic Process Research & Development, 19(9), 1076-1081.

Mortimer, M., Gogos, A., Bartolomé, N., Kahru, A., Bucheli, T. D., & Slaveykova, V. I. (2014). Potential of hyperspectral imaging microscopy for semi-quantitative analysis of nanoparticle uptake by protozoa. Environmental science & technology, 48(15), 8760-8767.

Mulenos, M. R., Liu, J., Lujan, H., Guo, B., Lichtfouse, E., Sharma, V. K., & Sayes, C. M. (2020). Copper, silver, and titania nanoparticles do not release ions under anoxic conditions and release only minute ion levels under oxic conditions in water: Evidence for the low toxicity of nanoparticles. Environmental Chemistry Letters, 1-10.

Nasseri, S., M. O. Borna, A. Esrafili, R. R. Kalantary, B. Kakavandi, M. Sillanpää and A. Asadi (2018). "Photocatalytic degradation of malathion using Zn 2+-doped TiO 2 nanoparticles: statistical analysis and optimization of operating parameters." Applied Physics A 124(2): 175.

Nel, A., Xia, T., Mädler, L., & Li, N. (2006). Toxic potential of materials at the nanolevel. science, 311(5761), 622-627.

Niska, K., Knap, N., Kędzia, A., Jaskiewicz, M., Kamysz, W., & Inkielewicz-Stepniak, I. (2016). Capping agent-dependent toxicity and antimicrobial activity of silver nanoparticles: an in vitro study. Concerns about potential application in dental practice. International journal of medical sciences, 13(10), 772.

Njar, V., & Brodie, A. (1999). Inhibitors of 170-Hydroxylase/17, 20-Lyase (CYP17): Potential Agents for. Current pharmaceutical design, 5(3), 163.

Oh, J. Y., Kim, H. S., Palanikumar, L., Go, E. M., Jana, B., Park, S. A., . . . Kwak, S. K. (2018). Cloaking nanoparticles with protein corona shield for targeted drug delivery. Nature communications, 9(1), 1-9.

Ortelli, S., A. L. Costa, M. Blosi, A. Brunelli, E. Badetti, A. Bonetto, D. Hristozov and A. Marcomini (2017). "Colloidal characterization of CuO nanoparticles in biological and environmental media." Environmental Science: Nano 4(6): 1264-1272.

Palotas, A., Rainey, L., Feldermann, C., Sarofim, A., & VanderSande, J. (1996). Soot morphology: An application of image analysis in high-resolution transmission electron microscopy. Microscopy Research and Technique, 33(3), 266-278. doi:10.1002/(SICI)1097-0029(19960215)33:3<266::AID-JEMT4>3.0.CO;2-O

Paradise, M., & Goswami, T. (2007). Carbon nanotubes–production and industrial applications. Materials & design, 28(5), 1477-1489.

Pati, S. S., L. H. Singh, E. M. Guimarães, J. Mantilla, J. A. H. Coaquira, A. C. Oliveira, V. K. Sharma and V. K. Garg (2016). "Magnetic chitosan-functionalized Fe3O4@ Au nanoparticles: Synthesis and characterization." Journal of Alloys and Compounds 684: 68-74.

Pham, T. D., T. T. Bui, V. T. Nguyen, T. K. V. Bui, T. T. Tran, Q. C. Phan, T. D. Pham and T. H. Hoang (2018). "Adsorption of polyelectrolyte onto nanosilica synthesized from rice husk: characteristics, mechanisms, and application for antibiotic removal." Polymers 10(2): 220.

Poliakoff, M., & Licence, P. (2007). Green chemistry. Nature, 450(7171), 810-812.

Powers, K. W., Palazuelos, M., Moudgil, B. M., & Roberts, S. M. (2007). Characterization of the size, shape, and state of dispersion of nanoparticles for toxicological studies. Nanotoxicology, 1(1), 42-51.

Qin, X., Sufi, J., Vlckova, P., Kyriakidou, P., Acton, S. E., Li, V. S., . . . Tape, C. J. (2020). Cell-type-specific signaling networks in heterocellular organoids. Nature methods, 17(3), 335-342.

Quigg, A., W.-C. Chin, C.-S. Chen, S. Zhang, Y. Jiang, A.-J. Miao, K. A. Schwehr, C. Xu and P. H. Santschi (2013). "Direct and indirect toxic effects of engineered nanoparticles on algae: role of natural organic matter." ACS Sustainable Chemistry & Engineering 1(7): 686-702.

Rai, P. K., V. Kumar, S. Lee, N. Raza, K.-H. Kim, Y. S. Ok and D. C. W. Tsang (2018). "Nanoparticle-plant interaction: Implications in energy, environment, and agriculture." Environment international 119: 1-19.

Ranjan, S. and C. Ramalingam (2016). "Titanium dioxide nanoparticles induce bacterial membrane rupture by reactive oxygen species generation." Environmental Chemistry Letters 14(4): 487-494.

Reynolds, e. (1963). Use of lead citrate at high ph as an electron-opaque stain in electron microscopy. Journal of cell biology, 17(1), 208-&. Doi:10.1083/jcb.17.1.208

Riediker, M., Zink, D., Kreyling, W., Oberdörster, G., Elder, A., Graham, U., . . . Ichihara, S. (2019). Particle toxicology and health-where are we? Particle and fibre toxicology, 16(1), 19.

Rizvi, S. A., & Saleh, A. M. (2018). Applications of nanoparticle systems in drug delivery technology. Saudi Pharmaceutical Journal, 26(1), 64-70.

Romoser, A., D. Ritter, R. Majitha, K. E. Meissner, M. McShane and C. M. Sayes (2011). "Mitigation of quantum dot cytotoxicity by microencapsulation." PLoS One 6(7): e22079.

Rong, H., S. Garg and T. D. Waite (2019). "Impact of light and Suwanee River Fulvic Acid on O2 and H2O2 Mediated Oxidation of Silver Nanoparticles in Simulated Natural Waters." Environmental science & technology 53(12): 6688-6698.

Sabella, S., Carney, R. P., Brunetti, V., Malvindi, M. A., Al-Juffali, N., Vecchio, G., . . . Stellacci, F. (2014). A general mechanism for intracellular toxicity of metal-containing nanoparticles. Nanoscale, 6(12), 7052-7061.

Sani-Kast, N., J. Labille, P. Ollivier, D. Slomberg, K. Hungerbühler and M. Scheringer (2017). "A network perspective reveals decreasing material diversity in studies on nanoparticle interactions with dissolved organic matter." Proceedings of the National Academy of Sciences 114(10): E1756-E1765.

Sayes, C. M., & Warheit, D. B. (2009). Characterization of nanomaterials for toxicity assessment. Wiley Interdisciplinary Reviews: Nanomedicine and Nanobiotechnology, 1(6), 660-670.

Sayes, C. M., Wahi, R., Kurian, P. A., Liu, Y., West, J. L., Ausman, K. D., . . . Colvin, V. L. (2006). Correlating nanoscale titania structure with toxicity: a cytotoxicity and inflammatory response study with human dermal fibroblasts and human lung epithelial cells. Toxicological Sciences, 92(1), 174-185.

SCOGS. (1973). Select Committee on GRAS Substances (SCOGS) Report-25: Evaluation of the health aspects of cellulose and certain cellulose derivatives as food ingredients. Report Number: NTIS #PB274667; SCOGS-25.

Scott, J. L., Gabrielides, C., Davidson, R. K., Swingler, T. E., Clark, I. M., Wallis, G. A., . . . Young, D. A. (2010). Superoxide dismutase downregulation in osteoarthritis progression and end-stage disease. Annals of the rheumatic diseases, 69(8), 1502-1510.

Selikoff, I. J., Churg, J., & Hammond, E. C. (1964). Asbestos exposure and neoplasia. Jama, 188(1), 22-26.

Selvaraj, V., S. Bodapati, E. Murray, K. M. Rice, N. Winston, T. Shokuhfar, Y. Zhao and E. Blough (2014). "Cytotoxicity and genotoxicity caused by yttrium oxide nanoparticles in HEK293 cells." International journal of nanomedicine 9:1379.

Shafiei-Sabet, S., Hamad, W., & Hatzikiriakos, S. (2014). Ionic strength effects on the microstructure and shear rheology of cellulose nanocrystal suspensions. Cellulose, 21(5), 3347-3359.

Shao, Q., & Jiang, S. (2015). Molecular understanding and design of zwitterionic materials. Adv Mater, 27(1), 15-26. doi:10.1002/adma.201404059

Sharma, V. K. (2009). "Aggregation and toxicity of titanium dioxide nanoparticles in aquatic environment—a review." Journal of Environmental Science and Health Part A 44(14): 1485-1495.

Sharma, V. K. and R. Zboril (2017). Silver Nanoparticles in Natural Environment: Formation, Fate, and Toxicity. Bioactivity of Engineered Nanoparticles, Springer: 239-258.

Sharma, V. K., C. M. Sayes, B. Guo, S. Pillai, J. G. Parsons, C. Wang, B. Yan and X. Ma (2019). "Interactions between silver nanoparticles and other metal nanoparticles under environmentally relevant conditions: A review." Science of The Total Environment 653: 1042-1051.

Sharma, V. K., J. Filip, R. Zboril and R. S. Varma (2015). "Natural inorganic nanoparticles–formation, fate, and toxicity in the environment." Chemical Society Reviews 44(23): 8410-8423.

Sharma, V. K., Sayes, C. M., Guo, B., Pillai, S., Parsons, J. G., Wang, C., . . . Ma, X. (2019). Interactions between silver nanoparticles and other metal nanoparticles under environmentally relevant conditions: A review. Science of the Total Environment, 653, 1042-1051.

Shatkin, J.A., & Kim, B. (2015). Cellulose nanomaterials: life cycle risk assessment, and environmental health and safety roadmap. Environmental Science: Nano, 2(5):477-499.

Shatkin, J.A., Wegner, T., Bilek, E., & Cowie, J. (2014). Market projections of cellulose nanomaterial-enabled products - Part 1: Applications. TAPPI Journal, 13(5):9-16.

Shevlin, D., N. O'Brien and E. Cummins (2018). "Silver engineered nanoparticles in freshwater systems–Likely fate and behaviour through natural attenuation processes." Science of the total environment 621: 1033-1046.

Shi, J. H., Axson, J. L., Bergin, I. L., & Ault, A. P. (2020). Nanoparticle Digestion Simulator Reveals pH-dependent Aggregation in the Gastrointestinal Tract. Analytical Chemistry.

Shvedova, A. A., Kisin, E. R., Yanamala, N., Farcas, M. T., Menas, A. L., Williams, A., . . . Star, A. (2015). Gender differences in murine pulmonary responses elicited by cellulose nanocrystals. Particle and fibre toxicology, 13(1), 1-20.

Silva, T., Pokhrel, L. R., Dubey, B., Tolaymat, T. M., Maier, K. J., & Liu, X. (2014). Particle size, surface charge and concentration dependent ecotoxicity of three organo-coated silver nanoparticles: comparison between general linear model-predicted and observed toxicity. Science of the total Environment, 468, 968-976.

Simeone, F. C., M. Blosi, S. Ortelli and A. L. Costa (2019). "Assessing occupational risk in designs of production processes of nano-materials." NanoImpact 14: 100149.

Stebounova, L. V., E. Guio and V. H. Grassian (2011). "Silver nanoparticles in simulated biological media: a study of aggregation, sedimentation, and dissolution." Journal of Nanoparticle Research 13(1): 233-244.

Subramanian, S., Ganapathy, S., Rajaram, M., & Ayyaswamy, A. (2020). Tuning the optical properties of colloidal Quantum Dots using thiol group capping agents and its comparison. Materials Chemistry and Physics, 249, 123127.

Subramoney, S. (1998). Novel nanocarbons - Structure, properties, and potential applications. Advanced Materials, 10(15), 1157-+. doi:10.1002/(SICI)1521

Tao, A., Habas, S., & Yang, P. (2008). Shape control of colloidal metal nanocrystals. Small, 4(3), 310-325. doi:10.1002/smll.200701295

Teeguarden, J. G., Hinderliter, P. M., Orr, G., Thrall, B. D., & Pounds, J. G. (2007). Particokinetics in vitro: dosimetry considerations for in vitro nanoparticle toxicity assessments. Toxicol Sci, 95(2), 300-312. doi:10.1093/toxsci/kfl165

Tenzer, S., Docter, D., Kuharev, J., Musyanovych, A., Fetz, V., Hecht, R., . . . Reinhardt, C. (2013a). Rapid formation of plasma protein corona critically affects nanoparticle pathophysiology. Nature nanotechnology, 8(10), 772-781.

Tenzer, S., Docter, D., Kuharev, J., Musyanovych, A., Fetz, V., Hecht, R., Reinhardt, C. (2013b). Rapid formation of plasma protein corona critically affects nanoparticle pathophysiology. Nature nanotechnology, 8(10), 772.

Teo, H. L., & Wahab, R. A. (2020). Towards an eco-friendly deconstruction of agro-industrial biomass and preparation of renewable cellulose nanomaterials: A review. International journal of biological macromolecules.

Thomas, R.T, Paules, R.S, Simeonov, A, Fitzpatrick, S, Crofton, K, Casey, W and Mendrick, D. The US Federal Tox21 Program: A Strategic and Operational Plan for Continued Leadership. ALTEX. (2018). doi:10.14573/altex.1803011

Trickler, W. J., Lantz, S. M., Murdock, R. C., Schrand, A. M., Robinson, B. L., Newport, G. D., . . . Slikker Jr, W. (2010). Silver nanoparticle induced blood-brain barrier inflammation and increased permeability in primary rat brain microvessel endothelial cells. Toxicological Sciences, 118(1), 160-170.

Troy, C. M., Derossi, D., Prochiantz, A., Greene, L. A., & Shelanski, M. L. (1996). Downregulation of Cu/Zn superoxide dismutase leads to cell death via the nitric oxide-peroxynitrite pathway. Journal of Neuroscience, 16(1), 253-261.

Ubaid, K. A., X. Zhang, V. K. Sharma and L. Li (2019). "Fate and risk of metal sulfide nanoparticles in the environment." Environmental Chemistry Letters: 1-15.

Vincent, A. E., Ng, Y. S., White, K., Davey, T., Mannella, C., Falkous, G., . . . Gorman, G. S. (2016). The spectrum of mitochondrial ultrastructural defects in mitochondrial myopathy. Scientific reports, 6(1), 1-12.

Vishnuvarthanan, M. and N. Rajeswari (2019). "Food packaging: pectin–laponite–Ag nanoparticle bionanocomposite coated on polypropylene shows low O 2 transmission, low Ag migration and high antimicrobial activity." Environmental Chemistry Letters 17(1): 439-445.

Vrček, I. V., Žuntar, I., Petlevski, R., Pavičić, I., Dutour Sikirić, M., Ćurlin, M., & Goessler, W. (2016). Comparison of in vitro toxicity of silver ions and silver nanoparticles on human hepatoma cells. Environmental toxicology, 31(6), 679-692.

Wan, D., V. K. Sharma, L. Liu, Y. Zuo and Y. Chen (2019). "Mechanistic insight into the effect of metal ions on photogeneration of reactive species from dissolved organic matter." Environmental science & technology 53(10): 5778-5786.

Wang, K., S. Garg and T. D. Waite (2017). "Light-mediated reactive oxygen species generation and iron redox transformations in the presence of exudate from the cyanobacterium Microcystis aeruginosa." Environmental science & technology 51(15): 8384-8395.

Wang, P., N. W. Menzies, H. Chen, X. Yang, S. P. McGrath, F.-J. Zhao and P. M. Kopittke (2018). "Risk of silver transfer from soil to the food chain is low after long-term (20 years) field applications of sewage sludge." Environmental science & technology 52(8): 4901-4909.

Wang, Q., Li, H., Chen, L., & Huang, X. (2001). Monodispersed hard carbon spherules with uniform nanopores. Carbon, 39(14), 2211-2214. doi:10.1016/S0008-6223(01)00040-9

Warheit, D. B. (2008). How meaningful are the results of nanotoxicity studies in the absence of adequate material characterization? Toxicol Sci, 101(2), 183-185.

Warheit, D. B., Webb, T. R., Colvin, V. L., Reed, K. L., & Sayes, C. M. (2007). Pulmonary bioassay studies with nanoscale and fine-quartz particles in rats: toxicity is not dependent upon particle size but on surface characteristics. Toxicological Sciences, 95(1), 270-280.

Warheit, D. B., Webb, T. R., Reed, K. L., Frerichs, S., & Sayes, C. M. (2007). Pulmonary toxicity study in rats with three forms of ultrafine-TiO2 particles: differential responses related to surface properties. Toxicology, 230(1), 90-104.

Warheit, D. B., Webb, T. R., Reed, K. L., Frerichs, S., & Sayes, C. M. (2007). Pulmonary toxicity study in rats with three forms of ultrafine-TiO2 particles: differential responses related to surface properties. Toxicology, 230(1), 90-104.

Warheit, D. B., Webb, T. R., Sayes, C. M., Colvin, V. L., & Reed, K. L. (2006). Pulmonary instillation studies with nanoscale TiO2 rods and dots in rats: toxicity is not dependent upon particle size and surface area. Toxicological Sciences, 91(1), 227-236.

Watson, M. (1958). Staining of Tissue Sections for Electron Microscopy with Heavy Metals. Journal of Biophysical and Biochemical Cytology, 4(4), 475-&. Doi:10.1083/Jcb.4.4.475

Weber, J. A., Baxter, D. H., Zhang, S., Huang, D. Y., How Huang, K., Jen Lee, M., . . . Wang, K. (2010). The microRNA spectrum in 12 body fluids. Clinical chemistry, 56(11), 1733-1741.

Weeber, F., Ooft, S. N., Dijkstra, K. K., & Voest, E. E. (2017). Tumor organoids as a pre-clinical cancer model for drug discovery. Cell chemical biology, 24(9), 1092-1100.

Westerhoff, P., A. Atkinson, J. Fortner, M. S. Wong, J. Zimmerman, J. Gardea-Torresdey, J. Ranville and P. Herckes (2018). "Low risk posed by engineered and incidental nanoparticles in drinking water." Nature nanotechnology 13(8): 661-669.

Westesen, K., H. Bunjes and M. H. J. Koch (1997). "Physicochemical characterization of lipid nanoparticles and evaluation of their drug loading capacity and sustained release potential." Journal of controlled release 48(2-3): 223-236.

Wustenberg, T. 2015. Cellulose and cellulose derivatives in the food industry, fundamentals and applications. Wiley-VCH Verlag GmbH & Co. KGaA, Weinheim, Germany

Xie, S., Zhang, X., Walcott, M.P., & Lin, H. (2018). Cellulose nanocrystals (CNCs) applications: a review. Eng. Sci, 2:4-16

Xu, J., J. Li, R. Zhang, J. He, Y. Chen, N. Bi, Y. Song, L. Wang, Q. Zhan and Z. Abliz (2019). "Development of a metabolic pathway-based pseudo-targeted metabolomics method using liquid chromatography coupled with mass spectrometry." Talanta 192: 160-168.

Yih, T., & Al-Fandi, M. (2006). Engineered nanoparticles as precise drug delivery systems. Journal of cellular biochemistry, 97(6), 1184-1190.

Yin, W., Shi, T., & Yan, Y. (2014). Unique Properties of Halide Perovskites as Possible Origins of the Superior Solar Cell Performance. Advanced Materials, 26(27), 4653-+. doi:10.1002/adma.201306281

Yin, Y., D. Han, C. Tai, Z. Tan, X. Zhou, S. Yu, J. Liu and G. Jiang (2017). "Catalytic role of iron in the formation of silver nanoparticles in photo-irradiated Ag+-dissolved organic matter solution." Environmental Pollution 225: 66-73.

Yin, Y., J. Liu and G. Jiang (2012). "Sunlight-induced reduction of ionic Ag and Au to metallic nanoparticles by dissolved organic matter." ACS nano 6(9): 7910-7919.

Yin, Y., W. Xu, Z. Tan, Y. Li, W. Wang, X. Guo, S. Yu, J. Liu and G. Jiang (2017). "Photo-and thermo-chemical transformation of AgCl and Ag2S in environmental matrices and its implication." Environmental Pollution 220: 955-962.

Youle, R. J., & Van Der Bliek, A. M. (2012). Mitochondrial fission, fusion, and stress. Science, 337(6098), 1062-1065.

Zhang, D., S. Yan and W. Song (2014). "Photochemically induced formation of reactive oxygen species (ROS) from effluent organic matter." Environmental science & technology 48(21): 12645-12653.

Zhang, X., Chang, H., Wiseman, S., He, Y., Higley, E., Jones, P., . . . Hecker, M. (2011). Bisphenol A disrupts steroidogenesis in human H295R cells. Toxicological Sciences, 121(2), 320-327.

Zhang, X., Yu, R. M., Jones, P. D., Lam, G. K., Newsted, J. L., Gracia, T., . . . Wu, R. S. (2005). Quantitative RT-PCR methods for evaluating toxicant-induced effects on steroidogenesis using the H295R cell line. Environmental science & technology, 39(8), 2777-2785.

Zhang, X., Z. Xu, A. Wimmer, H. Zhang, J. Wang, Q. Bao, Z. Gu, M. Zhu, L. Zeng and L. Li (2018). "Mechanism for sulfidation of silver nanoparticles by copper sulfide in water under aerobic conditions." Environmental Science: Nano 5(12): 2819-2829.

Zheng, N., Sun, D. D., Zou, P., & Jiang, W. (2017). Scientific and regulatory considerations for generic complex drug products containing nanomaterials. The AAPS journal, 19(3), 619-631.

Zhou, H., L. Lian, S. Yan and W. Song (2017). "Insights into the photo-induced formation of reactive intermediates from effluent organic matter: the role of chemical constituents." Water research 112: 120-128.

Zhou, W., Ling, L., Du, Y., He, W., Xia, Q., Yao, C., & Li, X. (2019). Thiol-Mediated Multidentate Phosphorylcholine as a Zwitterionic Ligand for Stabilizing Biocompatible Gold Nanoparticles. Langmuir, 35(40), 13031-13039.

Zhu, X., Chang, Y., & Chen, Y. (2010). Toxicity and bioaccumulation of TiO2 nanoparticle aggregates in Daphnia magna. Chemosphere, 78(3), 209-215.

Zucker, R. M., Ortenzio, J., Degn, L. L., Lerner, J. M., & Boyes, W. K. (2019). Biophysical comparison of four silver nanoparticles coatings using microscopy, hyperspectral imaging and flow cytometry. PloS one, 14(7), e0219078.